TIME-RESOLVED OPTO-ACOUSTIC SPECTROSCOPY

By

JOSEPH J. WRODEL

A DISSERTATION PRESENTED TO THE GRADUATE COUNCIL OF THE
UNIVERSITY OF FLORIDA
IN PARTIAL FULFILLMENT OF THE REQUIREMENTS FOR THE
DEGREE OF DOCTOR OF PHILOSOPHY

UNIVERSITY OF FLORIDA

1976

To my parents

...The investigations of chemistry have about them all the fluctuating fortunes of a deep and subtle game. There are the same vacillations of good and bad luck; the same tides of hope and fear; the almost certain prospect of success dashed and darkened by failure; the grief and disappointment of failure dispelled by glimpses of bright hope. So many are the disturbing influences, so subtle the causes that derange experiments, where some infinitesmal excess or deficiency, some minute accession of heat or cold, some chance adulteration in this or that ingredient, can vitiate a whole course of enquiry, requiring the labour of weeks to be all begun again, that the pursuit at length assumes many of the features of a game, and a game only to be won by securing every imaginable condition of success.

Charles Lever in his novel,
"One of Them," written
in the middle of the 19th
Century.

ACKNOWLEDGMENTS

I would like to acknowledge Dr. Martin Vala for the guidance, encouragement and assistance he provided throughout the course of this work. His confidence in me and the remarkable understanding he displayed over the long period of our association made the completion of this work possible.

I would like to acknowledge my wife Margaret, whose peanut butter, jelly, patience and love kept my body and soul together, and my daughter Jennifer, whose welcome-home smile could make the world go away.

I would also like to acknowledge those fellow graduate students, with whom I worked and with whom I played, for helping to lighten the burden and, likewise, the staff of the Department of Chemistry both in the offices and in the shops for their essential contributions.

TABLE OF CONTENTS

ACKNOWLEDGMENTS iv

LIST OF TABLES vii

LIST OF FIGURES viii

KEY TO SYMBOLS x

ABSTRACT xiii

CHAPTER ONE. INTRODUCTION 1

CHAPTER TWO. THEORETICAL CONSIDERATIONS 10
Introduction and Direction 10
The Solution of the Heat-Flow Equations 13
Simple Two-State Model 13
Multi-State Model 17
Neglect of density fluctuations 21
Neglect of thermal conductivity 22
The Extraction of Molecular Parameters from the Gross Pressure Signal 32
Excitation into the First Excited Triplet State 33
Excitation into the First Excited Singlet State 38
Consideration of the Total Disturbance: Pressure Wave Plus Acoustic Harmonics 47
Evaluation of the Expansion Coefficients 47
Computer Simulation of Opto-acoustic Signal 50
Limitations and Extensions of the Theory 57
Limitations on Experimental Design 62
Cell construction 62
Pressure transducer 64
Illumination source 66
Extensions of Theory to Additional Effects 67
Effect of window absorption 67
Effect of luminescence heating 67
Effect of a second gas 68
Effect of photochemistry 69

CHAPTER THREE. EXPERIMENTAL SYSTEM 72
Equipment 72
Opto-acoustic Cell and Vacuum System 72
Excitation Source 76
Pressure Detection System 115

Data Gathering and Processing System 125
Operating Procedure 132

CHAPTER FOUR. OBSERVATIONS 136
Flashlamp Experiments 136
Laser Experiments 138
Choice of Sample 138
Pyridazine 138
Oxalyl chloride 140
Results 151

CHAPTER FIVE. COMMENTS 160

LIST OF REFERENCES 164

BIOGRAPHICAL SKETCH 169

LIST OF TABLES

Table	Description	Page
1.	Triplet a_{uj} and b_u.	36
2.	Singlet a_{uj} and b_u.	44
3.	$J(s_i,\beta)$.	54
4.	Characteristics of laser system.	113

LIST OF FIGURES

Figure	Description	Page
1.	Experimental pressure signal of O_2.	12
2.	Diagram of two-state model.	15
3.	Diagram of triplet state processes.	35
4.	Form of pressure rise for triplet excitation.	40
5.	Diagram of singlet state processes.	41
6.	Plot of expression (18), high absorptivity.	56
7.	Plot of expression (18), moderate absorptivity.	59
8.	Plot of expression (18), low absorptivity.	61
9.	Diagram of opto-acoustic cell.	74
10.	Plot of calculated pulse energy versus wavelength.	80
11.	Spectra of dye No. 386.	83
12.	Reflectivity of R1 reflector.	85
13.	Diagram of laser alignment.	87
14.	Diagram of laser-monochromator alignment.	90
15.	Plot of nitrogen emission lines versus distance on photograph.	93
16.	Plot of wavelength of laser output versus micrometer setting.	98
17.	Schematic of photodiode circuit.	100
18.	Effect of intercavity reflector.	103
19.	Absorption spectrum of optical filter.	109
20.	Oscilloscope tracing of phototube signal from laser pulse.	112

Figure	Description	Page
21.	Schematic of standard Pitran circuit.	117
22.	Cross-section of Pitran mounted in cell.	120
23.	Block diagram of Pitran circuit.	123
24.	Plots of channel count versus dwell time.	129
25.	Block diagram of elements of opto-acoustic experiments.	134
26.	Absorption spectrum of pyridazine vapor, 4.6m path.	142
27.	Absorption spectrum of oxalyl chloride vapor, 10cm path.	145
28.	Absorption spectrum of oxalyl chloride vapor, 6.4m path.	148
29.	Plot of absorbance of $S_0 \rightarrow T_1$ band of oxalyl chloride versus path length.	150
30.	Plot of pressure rise due to oxalyl chloride decomposition.	155
31.	Signal generated by laser firing.	158

KEY TO SYMBOLS

Symbol	Definition	Units
a_{uj}	Expansion coefficient of n_j	mol cm^{-3}
A	Absorptivity; $A = \varepsilon C$	none
b_u	$\sum_j^u a_{uj} W_j$	erg cm^{-3} s^{-1}
B	Beam size correction factor	none
c	Speed of sound; $c^2 = \gamma p/\rho$	cm s^{-1}
c_v	Heat capacity at constant volume	erg g^{-1} deg^{-1}
C	Concentration	mole l^{-1}
$\bar{C}_p, \bar{C}_v$	Molar heat capacity at constant pressure, volume	erg $mole^{-1}$ deg^{-1}
E	Energy	erg
f	Oscillator frequency	s^{-1}
h	Planck's constant	erg s mol^{-1}
H(x)	Heaviside function	none
I	Energy flux	erg cm^{-2} s^{-1}
J_o, J_1, J_2	Zero, first and second order Bessel functions	none
k	First-order rate constant	s^{-1}
K	Thermal conductivity	erg cm^{-1} deg^{-1} s^{-1}
L	Length of sample cell	cm
M	Molecular weight	g $mole^{-1}$
n_j	Number density of molecules in state j	mol cm^{-3}
N	Number of moles	mole

Symbol	Definition	Units
N_A	Avogadro's number	mol $mole^{-1}$
OD	Optical density; OD=AL	none
p	Pressure	erg cm^{-3}
$p_{m,i}$	Expansion coefficients of p	erg cm^{-3}
q(r,z)	Spatial dependence of Q	none
$q_{m,i}$	Expansion coefficients of q(r,z)	none
Q	Source term	erg cm^{-3} s^{-1}
r	Radial coordinate	cm
r_b	Beam radius	cm
r_c	Cell radius	cm
R	Molar gas constant	erg $mole^{-1}$ deg^{-1}
S_o, S_1, S_2	Ground, first and second singlet states	none
t	Time	s
T	Temperature	deg
T_1	First excited triplet state	none
U	Internal energy	erg g^{-1}
$\vec{v}$	Flow velocity	cm s^{-1}
V	Sample cell volume	cm^3
W	Power	erg s^{-1}
W_j	Rate of heat release from molecule in state j	erg s^{-1} mol^{-1}
x_i	Root i of J_1	none
y_i	x_i/r_c	cm^{-1}
z	Axial coordinate	cm

Symbol	Definition	Units
α	Absorption coefficient; $\alpha = \tilde{\varepsilon}C$	cm^{-1}
β	Ratio of beam to cell radii; $\beta = r_b/r_c$	none
γ	Heat capacity ratio; $\gamma = \bar{C}_p/\bar{C}_v$	none
$\delta(t)$	Delta function	none
ε	Molar extinction coefficient	$cm^2\ mole^{-1}$
$\tilde{\varepsilon}$	Molar coefficient of absorption; $\tilde{\varepsilon} = \varepsilon \ln 10$	$cm^2\ mole^{-1}$
θ	Angular coordinate	rad
κ	Thermal diffusivity; $\kappa = K/\rho c_v$	$cm^2\ s^{-1}$
$\lambda_{m,i}$	Acoustic resonance frequency; $\lambda^2_{m,i} = c^2[y_i^2 + (m\pi/L)^2]$	s^{-1}
$\nu_{j,l}$	Frequency of transition from state j to state l	s^{-1}
ξ	Mean free path	cm
ρ	Density	$g\ cm^{-3}$
ϕ_j^X	Yield of process X from state j	none
$\omega_{m,i}$	Acoustic resonance frequency; $\omega^2_{m,i} = c^2[y_i^2 + (2m\pi/L)^2]$	s^{-1}

Abstract of Dissertation Presented to
the Graduate Council of the University of Florida
in Partial Fulfillment of the Requirements for the
Degree of Doctor of Philosophy

TIME-RESOLVED OPTO-ACOUSTIC SPECTROSCOPY

By

Joseph J. Wrobel

August, 1976

Chairman: Martin T. Vala
Major Department: Chemistry

A new approach to the study of excited state radiationless processes of large molecules in the vapor phase is proposed. The basis of the approach is the opto-acoustic effect, the generation of temperature and pressure fluctuations in a sample upon absorption of optical energy. The set of heat flow equations governing this effect are constructed and solved, under certain restrictions, for a sample in an isothermal cylindrical cell acted on by a short pulse of light. Computer simulations of the expected pressure signals are presented, and it is shown how molecular parameters can be extracted from experimental measurements.

Limitations on experimental design imposed by theoretical assumptions are discussed and applied to the construction of an experimental system for performing time-resolved opto-acoustic spectroscopy. The properties of oxalyl chloride are examined, and it is chosen as the object of experimental study. An attempt to verify the theoretically

predicted opto-acoustic signals using oxalyl chloride is made but is unsuccessful due to insufficient pulse energy from the excitation source employed. Improvements of the experimental system are suggested, and areas for future work are designated.

CHAPTER ONE
INTRODUCTION

In the past several years a great deal of work has been done exploring the theory of radiationless processes in polyatomic molecules [1-7]. Although differing theories have posed the problem in different frameworks, they all have in common the goal of explaining and anticipating the influence of temperature [8,9], isotopic substitution [10,11], excitation energy [12,13], singlet-triplet energy gap [14,15] or vibrational state of the molecule [16,17], on the nonradiative decay rate.

As in all branches of science, previous experimental work led to current theoretical interest which now demands more experiments on which to judge the merit of the theory. In this case, since all the theories of radiationless transitions deal with "isolated" molecules, the need grew for experimental studies of vapor phase molecules at pressures low enough so as to preclude collisions of an excited molecule during the lifetime of its excitation. Also, since the deactivation rates were known to be dependent upon the excitation wavelength at these low pressures [18-20], restrictions had to be made on the band width of the incident light thus decreasing its available intensity.

Although the advent of the tunable laser [21] will serve to compensate for the diminished intensity of irradiation at first caused by the second restriction, experimentalists studying excited states by their light emission must still reckon with the small number of photons which are emitted from the low density vapor. The sensitive light detection required in these cases initiated the use of photon counting techniques to measure lifetimes and yields. However, photon counting has its share of pitfalls [22] which add to the already difficult problem of measuring accurate radiative yields from which the non-radiative yields are derived [23].

There is a somewhat separate problem associated with studying molecular de-excitation solely by light emission. Even if one can accurately measure the lifetime and radiative yield of the monitored state and thus derive the overall non-radiative yield, the distribution of the excitation energy among the available non-radiative pathways remains unknown. Even if photochemical reactions are excluded, one cannot tell, for example, upon excitation into an upper singlet state, what portion of the non-radiative yield is due to intersystem crossing to the triplet manifold and what portion derives from internal conversion to the ground electronic state.

It is because of the need for more information on excited state properties in the low pressure vapor and because of the problems associated with the usual spectro-

scopic methods for getting this information that we sought an alternative approach. The most appealing approach, of course, would be some course of experimentation that would allow us to examine the radiationless behavior of a molecule directly, rather than through its radiative properties. At the same time, it would have to be sensitive enough to pick up the small amounts of heat given off during non-radiative decay. This line of thinking led us to investigate the application of the opto-acoustic effect to this area of research.

Initial investigations of the opto-acoustic effect date back almost a century. Following the invention of the telephone, Alexander Graham Bell continued his investigation in the area of voice transmission. Specifically, in 1880, he was involved with the production and reproduction of sound by light, i.e. transmitting sound not through wires but through air using an undulatory beam of light [24]. Taking advantage of the then recently discovered effect of light on selenium's electrical resistance, Bell constructed a receiving circuit comprised of a telephone, a battery and a piece of selenium. Using such a device and a proper transmitter, he found he could communicate over long distances.

Bell then questioned whether the molecular disturbance causing the effect required the telephone and battery to be heard, and, further, whether the sound generation was specifically a property of selenium or rather one which would occur in a variety of substances. After a series of

experiments using samples in the form of thin diaphragms, he concluded that sound could indeed be produced by substances of all kinds. Further experiments by Bell [25] and others [26-30] established that the effect was a general phenomenon as long as the substance was irradiated with a source whose radiation it could absorb. They reasoned, and correctly so, that the absorbed energy was degraded in the sample to heat pulses which caused pressure pulses to occur in the surrounding gas. Thus if the incident light were chopped at a frequency in the sound region, the sample could be heard to emit sound of the same frequency.

In 1881 Bell [25] introduced a device by which one could examine the absorption spectrum of a sample by noting the intensity of the sound produced when the sample was irradiated by chopped radiation from different regions of the spectrum. This device Bell called the spectrophone. Although Bell noted the promise of the spectrophone in his 1881 paper, especially in examining infrared absorption, it was not until 1938 that the device was rediscovered by Veingerov [31], and later by others [32-34], who sought to exploit the opto-acoustic effect for both qualitative and quantitative analyses of gases based on their infrared absorptivity. Several types of radiation detectors were built at this time incorporating the effect as an integral part of the detection scheme [35]. As the spectrophone technique was established for vapor analysis in the infrared, the application of the method broadened. The spectro-

phone was used to measure absorptivities in the microwave region of the spectrum [36], and its use in the visible and untraviolet regions was investigated [37]. More recently, the use of the spectrophone technique for detection and analysis has brought high sensitivity to mm and cm spectroscopy of gases [38-39]. It has also proven to be a very sensitive method for detection of air pollutants [40-42]. Further, since this type of spectroscopy does not require that samples be translucent, it has opened the door to the study of absorption spectra of solids, biological materials and other opaque substances [43].

As the use of the spectrophone for analyses grew, a second use for this technique was discovered and investigated. In 1946 Gorelik [44] proposed that the spectrophone could be used to measure vibrational relaxation times of gases. Slobodskaya [45] did the first work along these lines on carbon dioxide and his results were subsequently given a theoretical analysis by Stepanov and Girrin [46]. Two methods of determining vibrational relaxation times using the spectrophone were investigated both theoretically and experimentally [47]. The phase shift method relates the vibrational relaxation time to the phase shift between the sinusoidal excitation and the resultant sinusoidal pressure changes. The amplitude- or frequency-response method measure the amplitude of the pressure response as a function of the frequency of the excitation which theory shows is related to the vibrational relaxation rate.

Both methods have the advantage over previous methods in that they can be made specific to a particular molecular vibration by using incident radiation limited to a single spectral band.

Interest in opto-acoustic effect has been revived again in recent years [48] as a tool for studying molecules under the action of visible and ultraviolet radiation. The interest here lies in the fact that while polyatomic molecules which are vibrationally excited relax almost totally by nonradiative pathways, electronically excited molecules typically deactivate along numerous pathways including those which lead to light emission as well as photoreaction. Since the response of an opto-acoustic cell is only to that protion of the absorbed energy which is released as heat, opto-acoustic spectroscopy allows one to measure the yield of nonradiative pathways directly, and in this way it complements the standard method of stydying molecular excited states by light emission alone.

In 1967, employing broadband excitation Hey [49] applied the standard spectrophone amplitude-response technique to the measurement of relaxation rates of dye molecules in solution with some success. In 1969, two studies were performed on similar compounds in solution. In the first, Seybold et al. used steady-state illumination and detected pressure increases by a capillary rise technique [50]. In the second Callis et al. employed broadband flashlamp excitation and a cell equipped with a capacitance

microphone to detect the resultant pressure pulse [51]. In the latter study, the quantum yield of triplet formation was calculated by comparing the fast heating due to singlet state deactivation with the slow heating resulting from the triplet state decay.

Since the inception of the present work, investigations of excited state kinetics employing the opto-acoustic effect have been extended to the gas phase. deGroot et al. uncovered details of aldehyde photochemistry which could not have been easily detected if standard photochemical methods had been employed [52]. Other photochemical studies were later carried out by Harshbarger and Robin on NO_2 and SO_2 [48]. Quenching of iodine atoms has also been studied opto-acoustically by these same authors [53]. Another quenching study was carried out by Parker and Ritke who concerned themselves with deactivation of the first vibrational level of the lowest electronic singlet state of O_2 [54-56].

Recently, Kaya et al. have examined the opto-acoustic spectra of biacetyl [57] and the azabenzenes [58] using a spectrophone technique. Their qualitive interpretation of these spectra provides new insight into the radiationless processes which affect the excited state kinetics of these molecules.

Also recently, Hunter and Stock began a series of papers on photophysical processes in the vapor-phase measured by the opto-acoustic effect. The first of these

papers [59] developed a multi-state relaxation model to be used as a basis for the study of radiationless processes from excited electronic states. This model essentially incorporates the complex deactivation schemes available to electronically excited polyatomic molecules into the basic spectrophone theory. Later papers by the same authors applied this model to the study of excited benzene [60] and biacetyl [61]. Although each compound was studied at only one particular wavelength of excitation, the results show the usefulness of the opto-acoustic approach. Using both phase shift and amplitude-response data, the lifetime and yield of formation of the triplet state of both compounds were determined in agreement with previously reported values where available for comparison.

In this work it is our intention to further explore the application of the opto-acoustic effect to the examination of photophysical processes. Our approach, however, differs from that of previous workers who used the standard spectrophone technique to study indirectly the course of energy flow in the sample. In the present work, a pulsed excitation source will be employed in conjunction with suitable transient recording instrumentation to study directly the time-evolution of the resultant pressure wave which appears in the gaseous sample upon irradiation. As will be shown in the following chapter, such an approach should allow us to gain both lifetime and yield information in what we consider to be a more convenient

manner than the traditional spectrophone technique. Further, by utilizing a tunable dye laser as the source of the incident radiation, the manner in which these quantities vary as a function of excitation wavelength may be explored.

CHAPTER TWO
THEORETICAL CONSIDERATIONS

Introduction and Direction

Although no formal theory describing the pulsed opto-acoustic effect has previously been reported, the effect has been observed in molecular oxygen by Parker and Ritke [54]. They used a Nd: glass laser to pulse-excite molecular oxygen in a high-pressure cell and monitored the pressure changes using a capacitance type microphone. The pressure response to the optical pulse (reproduced in Figure 1) was found to be fundamentally an exponential rise to a limiting value followed by a slow return to the initial value. The rise time of the pressure signal was found to correspond to the lifetime of the initially excited O_2 vibronic level as determined by Parker and Ritke from a frequency-response opto-acoustic approach [54]. Superimposed upon this rise was an oscillatory component corresponding to an acoustic resonance of the cell. This secondary signal was ascribed to absorption of the excitation beam by the cell windows.

In this chapter, these observations will be given a theoretical foundation by constructing a model describing the pressure disturbance which occurs in a vapor upon the

Figure 1. Experimental pressure signal obtained upon pulse excitation of 18 atmospheres of O_2 by a Nd: glass laser. From Parker and Ritke [54].

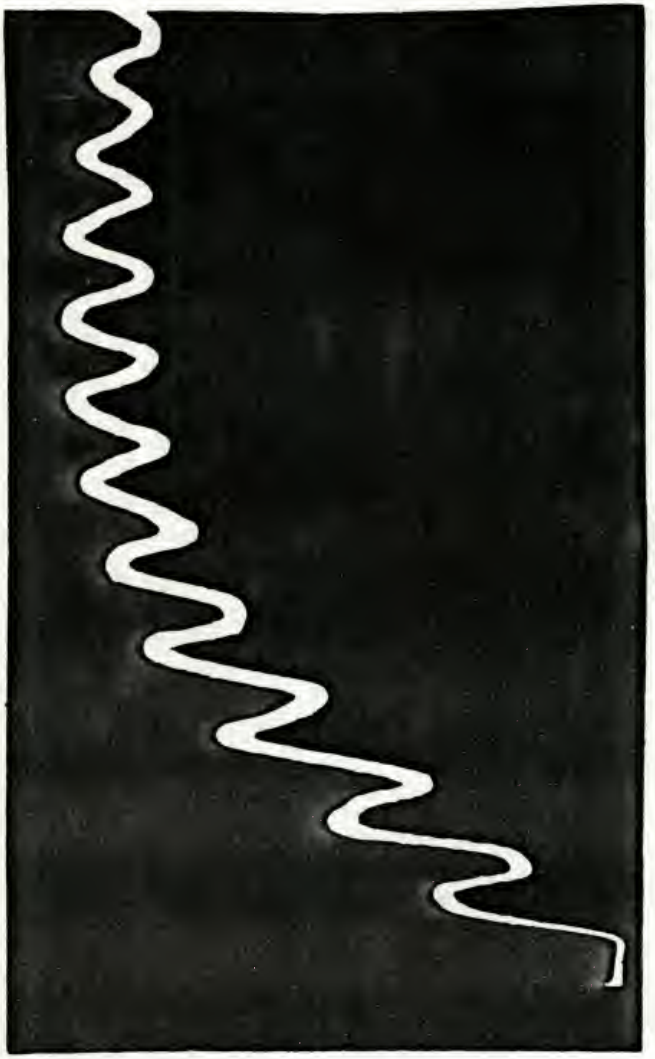
1.0 V/div
1.0 ms/div

absorption of a pulse of optical energy. Also, the dependence of the magnitude and time-evolution of this pressure fluctuation upon the molecular parameters of the sample will be examined. Further, the effects of the solution on experimental design will also be discussed.

The Solution of the Heat-Flow Equations

Simple Two-State Model

To prepare for dealing with the complexities of the model for a real experimental system, a simplified model is first considered. In it, it is assumed that the molecules of the sample vapor possess only two energy states (see Figure 2) a ground state and an excited state which can be populated from the ground state by absorption of a photon with energy $h\nu$. Further, it is assumed that a molecule in the excited state can lose energy and relax back to the ground state in two ways, either by radiation of the absorbed photon with first-order rate constant k^r or by nonradiative loss with first-order rate constant k^{nr}. What we wish to predict is how the pressure in the sample vapor will change with time if it is allowed to absorb an amount of radiative energy E_a.

Let us start by examining the rate at which heat energy is given up by the excited molecules. If we let E = heat energy released and $n_{exc}(t)$ = number density of excited molecules at time t, then

Figure 2. Diagram of molecular energy states in simple two-state model.

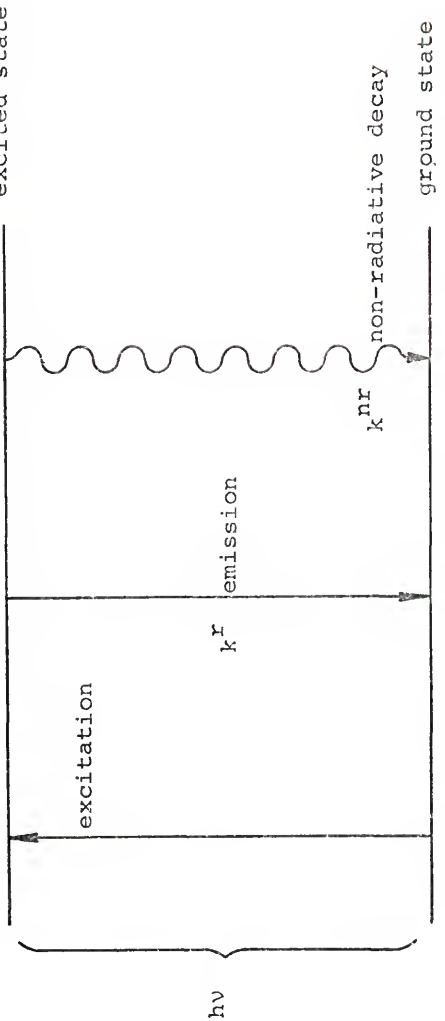
excited state
ground state
non-radiative decay
k^{nr}
emission
k^{r}
excitation
$h\nu$

$$dE/dt = k^{nr} n_{exc}(t) h\nu \, V,$$

where V is the sample volume. Since the excited state decays by first-order processes only, it is a simple matter to show that

$$n_{exc}(t) = n_{exc}(0)\exp(-(k^{nr}+k^{r})t) = \frac{(E_a/h\nu)\exp(-kt)}{V}$$

by which we obtain $dE/dt = k^{nr}E_a\exp(-kt)$, where $k = k^{r}+k^{nr}$. Integrating this expression, we find that the heat released as a function of time is given by

$$E = k^{nr}E_a(1-\exp(-kt))/k = \phi^{nr}E_a(1-\exp(-kt)),$$

where $\phi^{nr} = k^{nr}/k$ is the nonradiative yield of the state initially excited.

The change in pressure p' produced in the sample can be related to E through the ideal gas law and the relation between E and the resultant temperature change T' brought about in a constant volume system. Thus

$$p' = NRT'/V = (NR/V)(E/N\bar{C}_v) = (\gamma-1)\phi^{nr}E_a(1-\exp(-kt))/V \quad (1)$$

where N is the number of moles of the sample, γ is the heat capacity ratio $\bar{C}_p/\bar{C}_v$, $\bar{C}_p$ is the molar heat capacity at constant pressure, $\bar{C}_v$ is the molar heat capacity at constant volume and R is the gas constant which is equal to $\bar{C}_p-\bar{C}_v$ for an ideal gas.

Equation (1) shows how, in this simple model, the pressure change in a sample upon absorption of a pulse of optical energy is related to parameters of the excited state.

It makes clear that the lifetime of the excited state (k^{-1}) can be determined directly from the rise time of the pressure jump. Further, if V, E_a and γ can be evaluated independently, it shows that the value of ϕ^{nr} can be determined from the amplitude of the pressure jump.

This is the basic result of time-resolved opto-acoustic spectroscopy; it relates the time-evolution of the radiation-induced pressure signal to an excited state lifetime and provides from the pressure amplitude information relating to yields of radiationless processes. In the next section the theory of the opto-acoustic effect will be treated more rigorously. It will be shown that the multiplicity of states in real molecules and the spatial nonuniformities of the absorbed radiation cause the form of the pressure signal to become somewhat more complex than that given in equation (1). However, the method of extracting excited state parameters from this signal will not differ significantly from that used on the simple model examined above.

Multi-State Model

Let us consider a molecular vapor at equilibrium contained in a cylindrical cavity of length L and radius r_c. Let the initial state of the gas be defined by the density ρ_o, the pressure p_o and the temperature T_o. If the vapor is now pulsed with optical energy in an absorption region, the resultant heating brought about by the molecular relaxation will cause the gas to undergo local variations in pressure, density and temperature and to assume the new

values of these parameters p, ρ and T respectively. Also, in response to these local variations, the gas will assume a flow velocity $\vec{v}$ *.

All these changes must occur under the constraints imposed by the equation of state of the gas ** as well as the following three partial differential equations which reflect the quantities conserved in molecular collisions in the absence of external forces [62, p. 698]:

1. conservation of mass

$$D\rho/Dt = -\rho(\partial/\partial\vec{r}\cdot\vec{v})$$

2. conservation of momentum

$$D\vec{v}/Dt = -(d/d\vec{r}\cdot\vec{p})/\rho$$

3. conservation of energy

$$DU_{tot}/Dt = -(\partial/\partial\vec{r}\cdot(\vec{I}+\vec{I}_R))/\rho - (\overleftrightarrow{p}:\partial\vec{v}/\partial\vec{r})/\rho.$$

In the above equations, t = time, $\overleftrightarrow{p}$ = pressure tensor, U_{tot} = total molecular energy per gram, $\vec{I}$ = energy flux vector, $\vec{I}_R$ = radiative energy flux vector and D/Dt = $\partial/\partial t + \vec{v}\cdot\partial/\partial\vec{r}$.

In the general case, this system of equations is not solvable; thus, some simplification through reasonable

---

* The dependence of the functions v, p, ρ and T on time and position will be in general not written explicitly.

** The assumption of gas ideality will be accepted throughout and justified by restricting our considerations to sufficiently low pressures.

assumptions is in order. First, we ignore the dissipation of energy due to viscous effects. This action is rigorously justified only if the product of the shear viscosity times the divergence of the flow velocity is much less than the pressure [62, p. 521;63]. If the divergence of $\vec{v}$ is approximated by v/r_c and the simple kinetic theory definition of the coefficient of viscosity as one-third the product of density, average molecular speed and mean free path is adopted [62, p. 13], then an equivalent requirement for ignoring viscous effects can be stated. This requirement is that the flow velocity be less than or comparable to the speed of sound in the gas while at the same time the mean free path in the gas be much smaller than the cell radius. The restriction on the flow velocity should be easily met since the effect of the pressure pulse will be slight. As for the other condition, for a molecule the size of biacetyl, at a pressure of one torr, the mean free path is calculated as 2×10^{-3}cm [58]. Since the cell to be used in this work has a radius almost three orders of magnitude greater than this value, we are justified in ignoring viscous effects. This allows the replacement of the pressure tensor $\overleftrightarrow{p}$ with the scalar pressure p times the unit tensor.

Next, we assume that the disturbances caused by the optical pulse will be very small. That is, we let $p = p_o + p'$, $\rho = \rho_o + \rho'$ and $T = T_o + T'$ where the primed terms represent small local changes from the initial bulk values which occur upon absorption of the optical pulse. Upon

insertion of these expressions for p, ρ and T in the general conservation equations and subsequent deletion of terms second-order in p', ρ', T' or $\vec{v}$, we arrive at the following set of equations;

$$\partial\rho'/\partial t = -\rho_o \vec{\nabla}\cdot\vec{v} \tag{2}$$

$$\partial\vec{v}/\partial t = -\vec{\nabla}p'/\rho_o \tag{3}$$

and

$$DU_{elec}/Dt + c_v \partial T'/\partial t = -\vec{\nabla}\cdot(\vec{I}+\vec{I}_R)\rho_o - p_o\vec{\nabla}\cdot\vec{v}/\rho_o \tag{4}.$$

U_{tot} has been divided into a sum of two terms; U_{elec} represents the energy per gram stored in electronically excited molecules, and $c_v T'$ represents the internal energy per gram expended in translation motion and the population of electronic ground state rovibrational levels.

Recognizing that $\vec{I} = -K\vec{\nabla}T'$ [62, p. 717] where K is the gas thermal conductivity and, from equation (2), that $\vec{\nabla}\cdot\vec{v} = -(d\rho'/dt)/\rho_o$, we can rearrange equation (4) to obtain:

$$\rho_o c_v(\partial T'/\partial t) - K\nabla^2 T' - p_o(d\rho'/dt)/\rho_o = -\vec{\nabla}\cdot\vec{I}_R - \rho_o(DU_{elec}/Dt) \tag{5}$$

The series of equations (2), (3) and (5) still, in general, do not yield to analytical solution because the left side of equation (5) cannot be reduced to a function of one variable. For this reason, one further assumption must be made, namely, that either the $d\rho'/dt$ term or the $\nabla^2 T'$ term in equation (5) can be ignored. We will examine both alternatives.

Neglect of density fluctuations

Kerr and Atwood [40] based their theoretical consideration of the opto-acoustic phenomenon on an equation similar to equation (5), but with the $d\rho'/dr$ term deleted. They omitted this term without explanation, thus leaving it unclear as to whether this was done by design or by oversight. The latter is possible since most texts on heat conduction delete the $d\rho'/dt$ term from the equation in question without stating the fact that it is truely insignificant only in solids. Regardless of the reason, however, removal of the $d\rho'/dt$ term from the problem allows for solution of (5) in terms of T', and Kerr and Atwood arrive at such a solution for the case of a time-independent source.

Their solution predicts that upon illumination the average cell pressure undergoes a more-or-less exponential rise to a steady-state pressure, $p(\infty)$, given by $p(\infty) = (1 + AWB/4\pi KT)p_o$ where A is the absorptivity of the sample at the exciting wavelength, W is the beam power and B is a correction factor dependent upon beam size. The rate of the pressure rise, as that of the decay upon cessation of illumination, is related to the thermal time constant r_c^2/κ, where κ is the thermal diffusivity given by $K/\rho c_v$.

Although the observations of Kerr and Atwood agree reasonably with the theoretical predictions for $p(\infty)$, there are some drawbacks to their solution. For example, their solution does not predict the acoustic disturbances which have been found to occur upon pulsed excitation. Further,

due to their choice of boundary conditions, their theory predicts that T', and hence p' since ρ is taken as a constant, is zero at the cell walls. This clearly contradicts the pressure behavior which has been observed [54,64,65]. Incorporating a time-dependent source into their theoretical framework does not remove the major problems.

Neglect of thermal conductivity

Deletion of the thermal conductivity term of equation (5) has been considered by Longaker and Litvak [63]. They conclude that omission of this term is justified for short times after excitation, explicitly when $\kappa t/r_c^2 \ll 1$. In physical terms, the solution is limited to times which are small compared to the time it would take to cool the excited gas by thermal diffusion. For benzene vapor at a pressure of one torr, this limits the solution to times much less than 20 msec. At longer times thermal damping due to diffusion becomes important and the assumption becomes invalid. Accepting this time limitation, this approach to the problem has shown to be most satisfactory in explaining infrared spectrophone phenomena [66], and so it will be applied to the case at hand. The following method of solution follows closely that of Bates et al. [64] but differs significantly in the time-dependence and complexity of the source terms (those on the right of equation (5)).

After deleting the $\nabla^2 T'$ term from equation (5), the relation $\partial T = (dT/d\rho)_p \partial\rho + (dT/dp)_\rho \partial p$ is used to eliminate

the remaining T' dependence yielding

$$\partial p'/\partial t - (\gamma p_o/\rho_o)(\partial p'/\partial t) = \partial p'/\partial t - c^2(\partial p'/\partial t) = (\gamma-1)Q \quad (6)$$

where c is the speed of sound in the sample gas and Q represents the source term:

$$- \vec{\nabla}\cdot\vec{I}_R - \rho_o DU_{elec}/Dt.$$

Differentiating (2) with respect to time, we have

$$\partial^2\rho'/\partial t^2 = -\rho\ \vec{\nabla}\cdot\partial\vec{v}/\partial t \quad (7)$$

and upon substitution of equation (3) into equation (7), we obtain

$$\partial^2\rho'/\partial t^2 = \nabla^2 p'.$$

Differentiating equation (6) with respect to time and substituting the above relation, the following equation is obtained solely as a function of p':

$$\partial^2 p'/\partial t^2 - c^2\nabla^2 p' = (\gamma-1)\partial Q/\partial t. \quad (8)$$

The solution to equation (8) for a particular form of Q will yield the spatial and temporal dependence of p' which we seek.

First let us consider the spatial dependence of p'. In our experiments an illumination beam will be employed which reflects the cylindrical symmetry of the excitation cell, and logically p' is expected to do so also. Because of this, p' will have no dependence on the angular

cylindrical coordinate θ. The dependence of p' on the radial coordinate r may be expanded in terms of the Bessel functions $J_o(y_i r)$ where $r_c y_i = x_i$, the roots of the first-order Bessel function. The expansion of p' in terms of Bessel functions of zero order only is due to the absence of θ dependence in p'. The presence of the roots of J_1 in the argument of the expansion functions reflects the boundary condition of the radial component of the flow velocity v_r, i.e. $v_r(r=r_c)=0$. Thus equation (3) requires that

$$-(\partial p'/\partial r)_{r=r_c}/\rho_o = (\partial v_r/\partial t)_{r=r_c} = 0,$$

and since

$$(\partial J_o(y_i r)/\partial r)_{r=r_c} = (-y_i J_1(y_i r))_{r=r_c} = -y_i J_1(x_i) = 0$$

the boundary condition is satisfied.

Likewise, boundary conditions on the longitudinal component of $\vec{v}$ fix the set of functions in which p' can be expanded to express its z-dependence. The two boundary conditions of importance here are $v_z(z=0)=v_z(z=L) = 0$. That these boundary conditions are satisfied by the set of expansion functions given by

$$\cos(m\pi z/L) \; ; \; m = 0, 1, 2, \ldots$$

will now be shown. Again using equation (3) it is found that it requires of p' that

$$-(\partial p'/\partial z)_{z=0,L}/\rho_o = (\partial v_z/\partial t)_{z=0,L} = 0.$$

The above relation is satisfied by expanding p' in cos $(m\pi z/L)$ since

$$(\partial(\cos(m\pi z/L))/\partial z)_{z=0,L} = (-m\pi\sin(m\pi z/L)/L)_{z=0,L} = 0.$$

Thus, p' can be written as the expansion

$$p' = \sum_{m,i} p'_{m,i}(t) J_o(y_i r)\cos(m\pi z/L),$$

where the coefficients $p'_{m,i}(t)$ must be determined so as to solve equation (8). Substituting the above expression for p' into equation (8), we see that this requires solving the following equation given a particular form for the source term:

$$\sum_{m,i} J_o(y\ r)\ \cos(m\pi z/L)\,[\ddot{p}'_{m,i}(t) + \lambda^2_{m,i} p'_{m,i}(t)] =$$

$$(\gamma-1)\,\partial Q/\partial t \qquad (9)$$

where

$$\lambda^2_{m,i} = c^2(y_i^2 + (m\pi/L)^2).$$

The solution of equation (9) requires that $\partial Q/\partial t$ be expressed as an expansion over the same set of eigenfunctions as used for p'. Since, in general, the temporal and spatial portions of $\partial Q/\partial t$ are spearable, $\partial Q/\partial t$ may be written as the product $q(r,z)\dot{\bar{Q}}(t)$, where $\dot{\bar{Q}}(t)$ is defined as the volume-averaged time derivative of Q, i.e.

$$\bar{\dot{Q}}(t) = \int^{cell} (\partial Q/\partial t)\, dV/V.$$

The term $q(r,z)$ represents the spatial dependence of $\partial Q/\partial t$ deriving from that of the excitation source. From the above two equations, it follows that

$$\int^{cell} q(r,z)\, dV = V. \tag{10}$$

Separation of variables allows the expansion of dQ/dt to be of the form

$$\partial Q/\partial t = \sum_{m,i} q_{m,i} \bar{\dot{Q}}(t) J_o(y_i r) \cos(m\pi z/L)$$

where the $q_{m,i}$ are determined such that

$$q(r,z) = \sum_{m,i} q_{m,i} J_o(y_i r) \cos(m\pi z/L). \tag{11}$$

The expression in brackets in equation (9) can now be set equal to the coefficients of the source term expansion, and the resulting differential equation solved for the $p'_{m,i}(t)$. Before this can be done, of course, an expression for Q must be derived. We will now examine individually the two terms which comprise Q.

The divergence of the radiative energy flux vector is given by [62, p. 721]

$$\vec{\nabla} \cdot \vec{I}_R = Q_e - Q_a$$

where Q_e is the rate of radiation energy emission per unit volume and Q_a is the rate of radiation energy absorption per unit volume. In general Q_e can be written as a sum-

mation over all the emitting levels of the molecule. For the jth level, the contribution to Q_e will be dependent on the number density of molecules in the jth level, n_j, the rate of radiative emission from state j to some lower state l, k^r_{jl}, and the energy of the emitted photon, $h\nu_{jl}$. Hence

$$Q_e = \sum_j^s n_j \sum_{l<j} k^r_{jl} h\nu_{jl}$$

where the upper limit on the first summation refers to the level s which is the uppermost level initially populated by the excitation source.

As regards to Q_a a similar summation could be written:

$$Q_a = 10^3 \sum_j^s n_j \sum_{u>j} (I_{ju} \tilde{\varepsilon}_{ju})/N_A$$

where $\tilde{\varepsilon}_{ju}$ is the molar coefficient of absorption for the transition from level j to an upper level u, I_{ju} is the source radiation energy flux at the frequency of the j→u transition and N_A is Avogadro's number.* In the case of the proposed experiments, we will attempt to excite only a single transition, that being from the ground state to state s. If we let $\tilde{\varepsilon}$ be the molar extinction coefficient for this transition and define the absorption coefficient α by $\alpha = \tilde{\varepsilon}C$ where C is the bulk concentration, then $Q_a = \alpha I$, where I is the intensity of the excitation source.

We now turn our attention to an expression for

---

* $\tilde{\varepsilon}$ is related to the molar extinction coefficient ε by the equation $\tilde{\varepsilon} = \varepsilon \ln 10$.

DU_{elec}/Dt. Quite simply,

$$U_{elec} = \sum_{j=0}^{s} n_j h\nu_{j0}/\rho_o$$

so that

$$DU_{elec}/Dt = \sum_{j}^{s} \dot{n}_j h\nu_{j0}/\rho_o + \sum_{j}^{s} (\vec{v}\cdot\vec{\nabla}n_j) h\nu_{j0}/\rho_o.$$

The second summation in the above equation is second-order in two small quantities and can be ignored, allowing us to write

$$\rho_o DU_{elec}/Dt = \sum_{j}^{s} n_j h\nu_{j0}.$$

Thus, for the case in question, the source term is

$$Q = \alpha I - \sum_{j}^{s} (\dot{n}_j h\nu_{j0} + n_j \sum_{l<j} k^r_{jl}\, h\nu_{jl}).$$

At low pressures second-order decay processes of excited electronic states are negligible. Thus we can write as the rate equation for state s

$$\dot{n}_s = \alpha I/h\nu_s - n_s \sum_{l<s} k_{sl}$$

and in general

$$\dot{n}_j = \sum_{u>j} k_{uj} n_u - n_j \sum_{l<j} k_{jl} \qquad (12)$$

where $k_{jl} = k^{nr}_{jl} + k^r_{jl}$ is the sum of both the radiative and nonradiative first-order rate constants for the transition from state j to state l. After substitution of equation (12) into the expression for Q and simplification, the source term is given by

$$Q = \sum_{j}^{s} n_j \sum_{l<j} k_{jl}^{nr} h\nu_{jl} = \sum_{j}^{s} n_j W_j \qquad (13)$$

The W_j defined by equation (13) represent the total heat energy per unit time being released per molecule residing in state j via all nonradiative pathways and is a constant. The sought-after time-dependence of $\partial Q/\partial t$ thus could be written explicitly if it were known for the n_j.

When only first-order processes are operative and $n_j(t=0) = 0$ for all $j \neq 0$, the n_j take the form of solutions to a system of linear differential equations which reflects the various transitions between different energy levels occurring during molecular relaxation. Assuming pulsed excitation of the sample the general form for these solutions is

$$n_j = \left(\sum_{u=j}^{s} a_{uj} e^{-k_u t} \right) q(r,z).$$

The spatial dependence of the n_j has been withheld from inclusion in the a_{uj} for convenience. If the time derivative of equation (13) is now taken, we have that

$$\partial Q/\partial t = \sum_{j}^{s} (\partial n_j/\partial t) W_j$$

$$= -q(r,z) \sum_{j}^{s} W_j \sum_{u=j}^{s} a_{uj} k_u e^{-k_u t}$$

$$= -q(r,z) \sum_{u}^{s} \left(\sum_{j}^{u} a_{uj} W_j \right) k_u e^{-k_u t}$$

$$= -q(r,z) \sum_{u}^{s} b_u k_u e^{-k_u t}$$

where we have defined for convenience

$$b_u = \sum_j^u a_{uj} W_j .$$

Using the last expression for $\partial Q/\partial t$, the bracketed part of (9) can be rewritten as

$$\ddot{p}'_{m,i}(t) + \lambda^2_{m,i} p'_{m,i}(t) = -(\gamma-1) q_{m,i} \sum_u^s b_u k_u e^{-k_u t} .$$

Solving this second-order differential equation will give a form for the $p'_{m,i}$ which will provide a general expression for p'.

Applying the standard methods of solving differential equations to the bracketed equation, one can solve for the $p'_{m,i}$ and obtain for p':

$$p' = (\gamma-1) \sum_{m,i} q_{m,i} \{\sum_u^s [b_u k_u/(k_u^2 + \lambda^2_{m,i})] \times$$

$$[\cos(\lambda_{m,i} t) - \exp(-k_u t) - (\lambda_{m,i}/k_u)\sin(\lambda_{m,i} t)]\} \times$$

$$J_o(y_i r) \cos(m\pi z/L) \qquad (14)$$

Before applying this equation to specific cases of molecular excitation in which the b_u will be evaluated in terms of actual excited state parameters, it will prove informative to examine the general expression for p'. Note that for all terms of the summation except the $m = i = 0$ term, the long-term time-dependence is periodic in nature, with a frequency of oscillation for a particular i and m dependent on the speed of sound in the sample gas

and the cell dimensions. What these terms represent is, in fact, not a true "pressure" wave since their long-term time-average amplitude is zero. Rather, what they describe is the infinite set of resonances available in the cell for radial and transverse acoustic wave propagation. The amplitude of these acoustical disturbance terms and their relative contribution to the total sum, as we shall see later when the $q_{m,i}$ are evaluated, are very sensitive to the degree of uniformity of absorption of the exciting illumination throughout the cell, becoming increasingly large as the absorption becomes less uniform.

The $i = m = 0$ term of the summation in equation (14) thus carries the body of the "pressure" information. One can write for the contribution of this term to the p' summation the expression

$$p'_{o,o} = (\gamma-1)q_{o,o} \sum_{u}^{s} b_u (1-e^{-k_u t})/k_u \qquad (15)$$

There is a noteworthy resemblance of an individual term of this summation to the form of p' derived in the simple two-state nodel. See equation (1). The terms of the sum merely represent the individual contributions to p' from each of the molecular levels. As in the simple solution for p', equation (15) predicts that p' increases asymptotically to a nonzero value, thus implying that the sample pressure does not return to its preexcitation equilibrium value. This is, of course, not true; the cell is not adiabatic and heat transfer through its walls quickly

returns the sample vapor to its original pressure. The reason the solution does not reflect this physical reality is the neglect of the thermal diffusion term of equation (5) on which the derivation of this section is based.

The Extraction of Molecular Parameters from the Gross Pressure Signal

To this point, the derivation of the theory of time-resolved opto-acoustic spectroscopy has been kept as general as possible. Now, to calculate the actual form of the a_{uj} (and from them the b_u), the set of equations which define the time-evolution of the states which participate in the electronic excitation and relaxation of polyatomic molecules must be solved. To do so, a specific model must be constructed and necessarily generality is lost. The important point is, though, that just as this model is constructed assuming certain characteristics of excited state kinetics, so others might be constructed based on other assumptions. Thus, the following model, though applicable to a great number of actual cases, should be considered as just an example of how time-resolved opto-acoustic spectroscopy may be applied to the study of molecular excited states. Only two electronic states besides the electronic ground state will be considered explicitly, these being the first excited singlet S_1 and the first excited triplet T_1. In general, population of higher excited states leads only to rapid nonradiative decay to the vibrational manifolds of these lowest states. Thus, for our purposes, excitation

to more highly excited electronic states is equivalent to excitation of higher vibrational levels of S_1 and T_1; deactivation of these vibronic levels is considered in the discussion below. Because the form of the a_{uj} will depend on that level which is initially populated, two cases will be treated which encompass the two possible choices for the initially populated level (level s) in our narrowed scheme.

Excitation into the First Excited Triplet State

The electronic states and their first-order decay constants which are typically of importance in this case are shown in Figure 3. T_1^v represents the initially populated vibronic level of the lowest triplet state T_1, T_1^o represents the vibrationless level of T_1 and S_o represents the molecular state before excitation. For this case equation (12) takes the form:

$$\dot{n}_{T_1^v} = \alpha I/h\nu_{T_1^v} - n_{T_1^v}(k_2+k_3)$$

$$\dot{n}_{T_1^o} = k_2 n_{T_1^v} - k_1 n_{T_1^o}$$

where

$$k_1 = k_1^r + k_1^{nr}.$$

To solve this coupled set of equations, a form for I must be chosen which expresses explicitly the time-dependence of the source illumination. Since the excitation will consist of a very short duration laser pulse, a valid and convenient approximation to its temporal form

is the delta function, $\delta(t)$. This function assumes a value of unity when its argument is zero and equals zero for all other values of t. Allowing I to assume this functional dependence on t, the above set of differential equations can be solved in the standard manner to yield:

$$n_{T_1^v} = n^o_{T_1^v} e^{-(k_2 + k_3)t}$$

$$n_{T_1^o} = [n^o_{T_1^v} k_2/(k_3+k_2-k_1)]. \ (e^{-k_1 t} - e^{-(k_2+k_3)t}).$$

$n^o_{T_1^v}$ is the initial population of T_1^v equal to $\bar{n}^o_{T_1^v} q\ (r,z)$ where $\bar{n}^o_{T_1^v}$ is the cell-averaged initial number density of molecules excited into T_1^v given by $E(1-e^{-\alpha l})/h\nu_{T_1^v} V$, where E is the laser pulse energy.

The forms for the a_{uj} and the b_u can now be derived in a straightforward manner and are listed in Table 1. Using these values, the gross time-dependence of the pressure pulse expected to occur upon excitation into T_1^v can be determined by expanding equation (15) to obtain

$$p'_{o,o} = (\gamma-1) q_{o,o} \bar{n}^0_{T_1 v} [k_1^{nr} k_2 h\nu_{T_1^o} (1-e^{-k_1 t})/(k_3+k_2-k_1)k_1$$

$$+(k_2 h\nu_{T_1^v, T_1^o}/(k_2+k_3) - k_1^{nr} h\nu_{T_1^o}/(k_3+k_2-k_1))(1-e^{-(k_2+k_3)t})].$$

Since the vibrational relaxation time of T_1^v is ordinarily much shorter than the spin-forbidden deactivation of T_1^o, k_1 can be assumed to be much less than k_2, and the above equation can be simplified to the form:

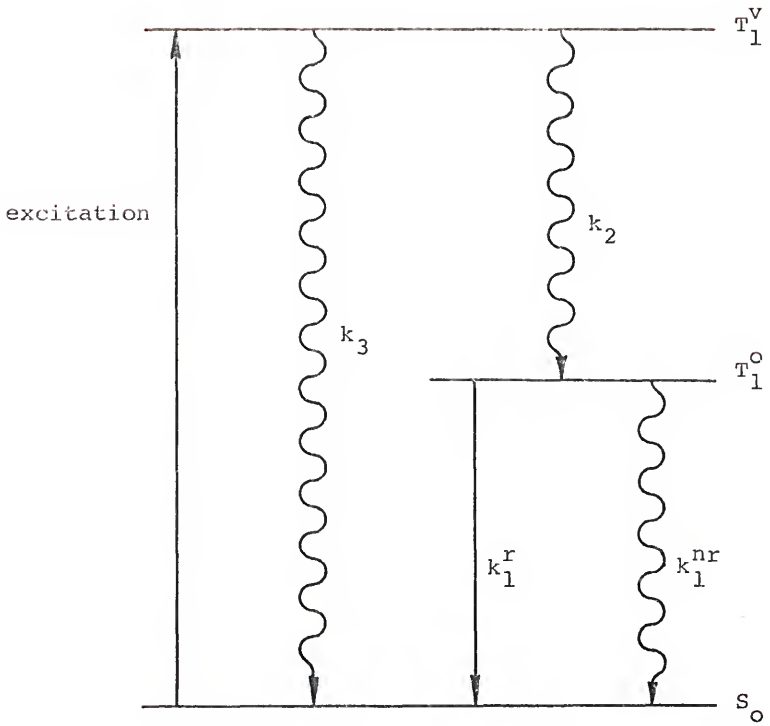

Figure 3. Diagram of energy levels typically of importance for first excited triplet state excitation and decay.

Table 1. Triplet a_{uj} and b_u.

$a_{uj}/\overline{n}^{\,o}_{T_1 v}$

j \ u	$T_1^{\,o}$	$T_1^{\,v}$	W_j
$T_1^{\,o}$	$\dfrac{k_2}{k_3+k_2-k_1}$	$-\dfrac{k_2}{k_3+k_2-k_1}$	$k_1^{nr}{}_{h\nu_{T_1}{}^o}$
$T_1^{\,v}$		1	$k_2{}_{h\nu_{T_1}{}^v,T_1{}^o}$
$b_u/\overline{n}^{\,o}_{T_1 v}$	$\dfrac{k_2}{k_3+k_2-k_1} k_1^{nr}{}_{h\nu T_1{}^o}$	$k_2{}_{h\nu_{T_1}{}^v,T_1{}^o} - \dfrac{k_2}{k_3+k_2-k_1} k_1^{nr}{}_{h\nu_{T_1}{}^o}$	——

$$p'_{o,o} = (\gamma-1)q_{o,o}\bar{n}^{o}_{T_1 v}\ [\phi^{ISC}_{T_1 v} h\nu_{T_1 v, T_1 o}(1-e^{-(k_2+k_3)t}) + \phi^{IC}_{T_1 v}\ \phi^{ISC}_{T_1 o}\ h\nu_{T_1 o}\ (1-e^{-k_1 t})]$$

where k_1^{nr}/k_1 has been recognized to be $\phi^{ISC}_{T_1^o}$, the intersystem crossing yield of T_1^o, and $k_2/(k_2+k_3)$ is represented by $\phi^{IC}_{T_1^v}$, the internal conversion yield of T_1^v. One should note that this equation applies equally well to direct excitation of the vibrationless level of T_1, in which case $\nu_{T_1 v}$ is replaced by $\nu_{T_1 o}$, $\phi^{IC}_{T_1^v}$ goes to unity and $h\nu_{T_1 v, T_1 o}$ goes to zero. These changes cause the first term in the brackets to be deleted and the second to be somewhat simplified.

The above equation predicts the main pressure signal to be a sum of two exponentially rising components, each of different amplitude. In general a response of this type would be difficult to deconvolute. However, because of the large difference in the magnitudes of k_1 and k_2, the two exponential rises should be well separated temporally. In fact, the first term in the brackets above will most likely appear as a step-rise in pressure at t=0 with the second exponential rise building with time on top of it, as pictured in Figure 4.

The figure indicates that $\phi^{IC}_{T_1^v}$ can be evaluated only if the true magnitude of the pressure rise is known, as well as the values of γ, α, E and $q_{o,o}$. However, if $h\nu_{T_1 v, T_1 o}$ is known as is usually the case, $\phi^{ISC}_{T_1^o}$ can be determined in a

more straightforward manner. If we let p'_f be the amplitude of the fast rise and p'_s be that of the slow rise, then

$$\phi_{T_1^o}^{ISC} = (h\nu_{T_1^v, T_1^o}/h\nu_{T_1^o})\ p'_s/p'_f.$$

Since k_1 can be extracted solely from the time-evolution of the pressure rise, this indicates that k_1^r and k_1^{nr} can be evaluated individually without critical measurement of either intensity of the beam or absorption and specific heat of the sample vapor.

Figure 4, is, to be sure, an idealized version of the pressure response of the sample vapor; built upon this signal will be the acoustic "bumps" discussed earlier. The presence of these periodic disturbances is not solely deleterious, however, and they can in fact provide needed information about the vapor under study.

Excitation into the First Excited Singlet State

The molecular levels and decay channels which are generally of importance in this case are displayed in Figure 5. S_1^v is the initially populated vibrational level of S_1, S_1^o the vibrationless level of S_1, T_1^o the vibrationless level of T_1 and S_o represents the molecular state before excitation. For this case, equation (12) takes the form

$$\dot{n}_{S_1^v} = \alpha I/h\nu_{S_1^v} - n_{S_1^v} k_{S_1^v}$$

Figure 4. Form of gross pressure rise for triplet state excitation.

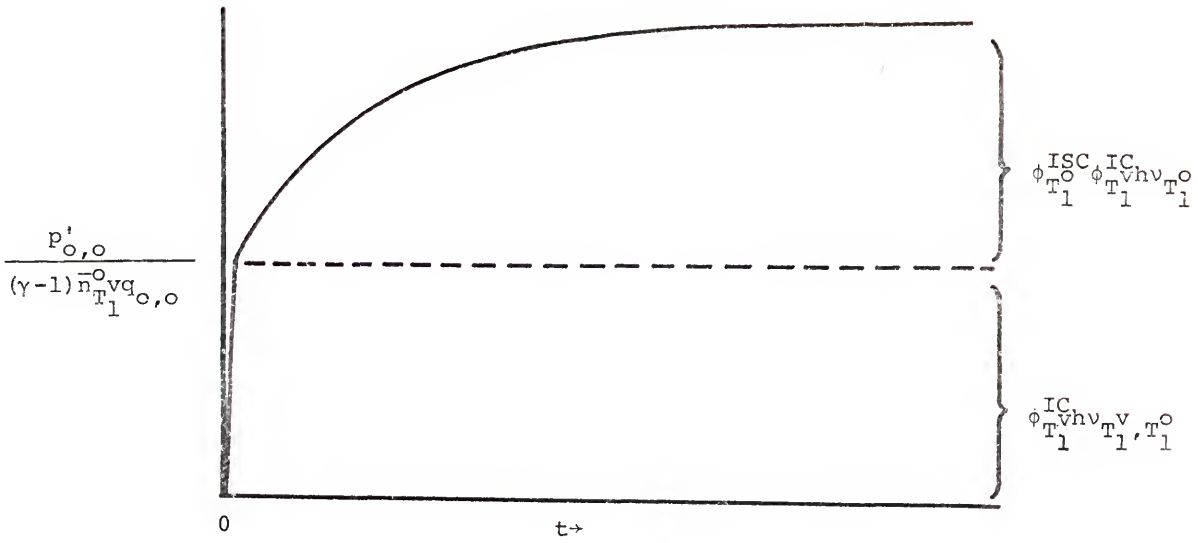
$\frac{p'_{o,o}}{(\gamma-1)\bar{n}^{o}_{T_1} v q_{o,o}}$
$\phi^{ISC}_{T_1^o}\phi^{IC}_{T_1 \bar{\nu} h\nu_{T_1^o}}$
$\phi^{IC}_{T_1 \bar{\nu} h\nu_{T_1^v, T_1^o}}$
0
t→

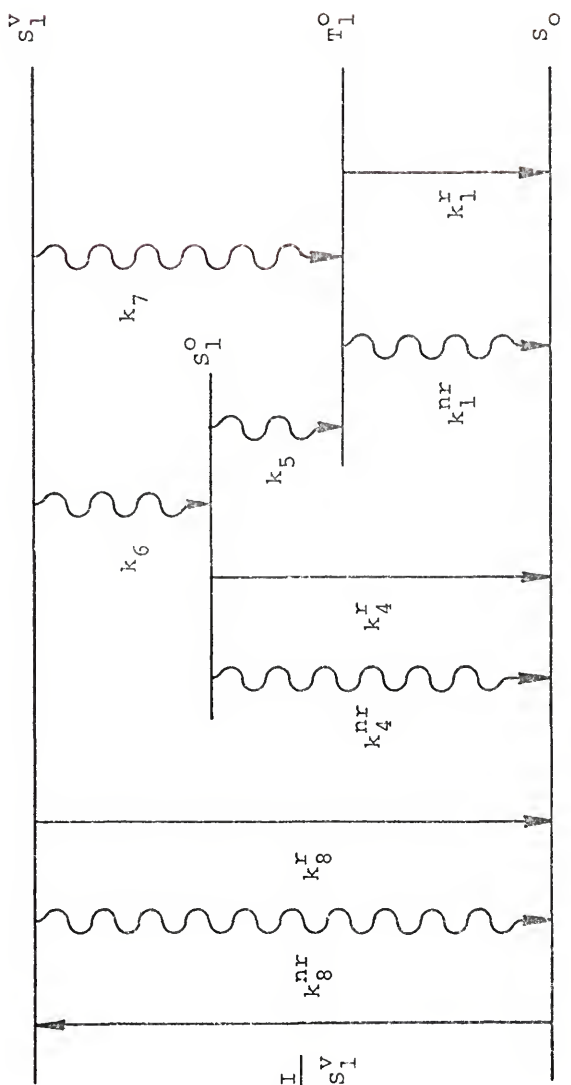

Figure 5. Diagram of energy levels typically of importance for first excited singlet state excitation and decay.

$$\dot{n}_{S_1}^{o} = k_6 n_{S_1}^{v} - k_{S_1}^{o} n_{S_1}^{o}$$

$$\dot{n}_{T_1}^{o} = k_5 n_{S_1}^{o} + k_7 n_{S_1}^{v} - k_{T_1}^{o} n_{T_1}^{o}$$

where

$$k_{S_1}^{v} = k_6 + k_7 + k_8^{r} + k_8^{nr}$$

$$k_{S_1}^{o} = k_4^{r} + k_4^{nr} + k_5$$

and

$$k_{T_1}^{o} = k_1^{r} + k_1^{nr}.$$

Again approximating the time dependence of I by a delta function, the above set of differential equations can be solved in the standard manner to obtain:

$$n_{S_1}^{v} = n_{S_1}^{o v} e^{-k_{S_1}^{v} t}$$

$$n_{S_1}^{o} = k_6 n_{S_1}^{o v} (e^{-k_{S_1}^{o} t} - e^{-k_{S_1}^{v} t})/(k_{S_1}^{v} - k_{S_1}^{o})$$

$$n_{T_1}^{o} = n_{S_1}^{o v}(k_7 - k_5 k_6/(k_{S_1}^{v} - k_{S_1}^{o}))(e^{-k_{T_1}^{o} t} - e^{-k_{S_1}^{v} t})/(k_{S_1}^{v} - k_{T_1}^{o})$$

$$+ k_5 k_6 n_{S_1}^{o v}(e^{-k_{T_1}^{o} t} - e^{-k_{S_1}^{o} t})/(k_{S_1}^{v} - k_{S_1}^{o})(k_{S_1}^{o} - k_{T_1}^{o})$$

where $n_{S_1}^{o v} = \bar{n}_{S_1}^{o v}\, q(r,z)$ and $\bar{n}_{S_1}^{o v}$ is defined similarily to the analogous term in the triplet case.

As in the previous case, the forms of the $a_{u,j}$ and b_u

are listed in tabular form in Table 2. Equation (15) can now be expanded using these values in order to obtain an idea of the gross form of the pressure pulse expected upon excitation into S_1^v. Before this is done, however, let us take advantage of the fact that k_1^{nr} and k_1^r are extremely small with respect to the remainder of the rate constants under consideration. This circumstance allows the deletion of terms in equation (15) which because of it become insignificant. Further, the $e^{-k_{S_1^v} t}$ and $e^{-k_{S_1^o} t}$ terms are discarded to reflect the "step" nature of the pressure rise due to the fast processes. By doing this, $p'_{o,o}$ for the case considered here takes the form

$$p'_{o,o} = (\gamma-1)\bar{n}^o_{S_1^v} q_{o,o} [\phi^{VD}_{S_1^v} h\nu_{S_1^v,S_1^o} + \phi^{ISC}_{S_1^v} h\nu_{S_1^v,T_1^o}$$

$$+ \phi^{IC}_{S_1^v} h\nu_{S_1^v} + \phi^{VD}_{S_1^v} (\phi^{ISC}_{S_1^o} h\nu_{S_1^o,T_1^o} + \phi^{IC}_{S_1^o} h\nu_{S_1^o})$$

$$+\phi^{ISC}_{T_1^o} h\nu_{T_1^o} (\phi^{VD}_{S_1^v} \phi^{ISC}_{S_1^o} + \phi^{ISC}_{S_1^v})(1-e^{-k_{T_1^o} t})]$$

where

$$\phi^{VD}_{S_1^v} = k_6/k_{S_1^v}$$

is the vibrational deactivation yield of S_1^v to S_1^o,

$$\phi^{ISC}_{S_1^v} = k_7/k_{S_1^v}$$

is the intersystem crossing yield of S_1^v to T_1^o,

$$\phi^{IC}_{S_1^v} = k_8^{nr}/k_{S_1^v}$$

TABLE 2. SINGLET a_{uj} AND b_u

j \ u	T_1^o	S_1^o
T_1^o	$\frac{1}{(k_{S_1}{}^v - k_{T_1}{}^o)}[k_7 + \frac{k_5 k_6}{k_{S_1}{}^o + k_{T_1}{}^o}]$	$\frac{-k_5 k_6}{(k_{S_1}{}^v - k_{S_1}{}^o)(k_{S_1}{}^o - k_{T_1}{}^o)}$
S_1^o		$\frac{k_6}{k_{S_1}{}^v - k_{S_1}{}^o}$
S_1^v		
$b_u/\bar{n}_{S_1}^o{}^v$	$\frac{k_1^{nr} h\nu_{T_1}{}^o}{(k_{S_1}{}^v - k_{T_1}{}^o)}[k_7 + \frac{k_5 k_6}{k_{S_1}{}^o - k_{T_1}{}^o}]$	$\frac{k_6}{(k_{S_1}{}^v - k_{S_1}{}^o)}[k_4^{nr} h\nu_{S_1}{}^o + k_5 h\nu_{S_1}{}^o, T_1{}^o] - \frac{k_5 k_6 k_1^{nr} h\nu_{T_1}{}^o}{(k_{S_1}{}^v - k_{S_1}{}^o)(k_{S_1}{}^o - k_{T_1}{}^o)}$

TABLE 2. - extended

S_1^v	W_j
$\frac{-1}{(k_{S_1^v} - k_{T_1^o})} [k_7 - \frac{k_5 k_6}{k_{S_1^v} - k_{S_1^o}}]$	$k_1^{nr} h\nu_{T_1^o}$
$\frac{-k_6}{k_{S_1^v} - k_{S_1^o}}$	$k_4^{nr} h\nu_{S_1^o} + k_5 h\nu_{S_1^o, T_1^o}$
1	$k_6 h\nu_{S_1^v, S_1^o} + k_7 h\nu_{S_1^v, T_1^o}$ $+ k_8 h\nu_{S_1^v}$
$k_6 h\nu_{S_1^v, S_1^o} + k_7 h\nu_{S_1^v, T_1^o}$ $+ k_8 h\nu_{S_1^v}$ $- \frac{k_6}{(k_{S_1^v} - k_{S_1^o})} (k_4^{nr} h\nu_{S_1^o} +$ $k_5 h\nu_{S_1^o, T_1^o})$ $\frac{k_1^{nr} h\nu_{T_1^o}}{k_{S_1^v} - k_{T_1^o}} (k_7 - \frac{k_5 k_6}{k_{S_1^v} - k_{S_1^o}})$	

is the internal conversion yield of S_1^v to S_o,

$$\phi_{S_1^o}^{IC} = k_4^{nr}/k_{S_1^o}$$

are the internal conversion yield of S_1^o to S_o and

$$\phi_{T_1^o}^{ISC} = k_1^{nr}/k_{T_1^o} \qquad \text{and} \qquad \phi_{S_1^o}^{ISC} = k_5/k_{S_1^o}$$

is the intersystem crossing yields of T_1^o to S_o and of S_1^o to T_1^o, respectively.

The expression above for $p'_{o,o}$ is quite a bit more complex than that derived in the previous case and the reason for the added complexity is simply the greater number of states and decay channels involved. Obviously, for a molecular system in which all the deactivation paths considered here play a significant role, none of the radiationless yields included in the expression for $p'_{o,o}$ can be uniquely determined by the sole opto-acoustic experiment involving excitation into S_1^v. Some of these yields may be evaluated by other (optical) methods or may be deemed insignificant based on previous work on molecules having similar excited state characteristics to the sample being investigated. It is more interesting in the present context that some may also be evaluated by further opto-acoustic experiments involving excitation into T_1^o, T_1^v or S_1^o. In the previous case for example, we have shown how $\phi_{T_1^o}^{ISC}$ could be evaluated by excitation into T_1^v. Note that if S_1^o is excited directly instead of S_1^v

$$p'_{o,o} = (\gamma-1)\bar{n}^{o}_{S_1} q_{o,o} \left[\phi^{ISC}_{S_1^o} h\nu_{S_1^o} \tau^{o}_{1} + \phi^{IC}_{S_1^o} h\nu_{S_1^o}\right.$$

$$\left. + \phi^{ISC}_{S_1^o} \phi^{ISC}_{T_1^o} h\nu_{T_1^o} (1-e^{-k_{T_1^o} t}) \right].$$

This equation indicates that both $\phi^{ISC}_{S_1^o}$ and $\phi^{IC}_{S_1^o}$ can be evaluated with an accuracy determined by the accuracy to which $p'_{o,o}$, γ, α, E and $q_{o,o}$ are known. Since these parameters can be determined with reasonably good accuracy, this avenue of approach promises significant insight into the dominant processes in excited states.

Consideration of the Total Disturbance: Pressure Wave Plus Acoustic Harmonics

In the last section we limited our view to the gross pressure change in the cell in order to examine how important molecular parameters might be extracted from its behavior. In this section we will investigate the total summation of equation (14). To do so, we must derive a form for the $q_{m,i}$ which, in turn, requires that a spatial dependence for the n_j be specified. Essentially, an explicit form must be determined for q(r,z).

Evaluation of the Expansion Coefficients

As was noted in a previous section, q(r,z) represents the spatial distribution of the initially excited molecules. The radial part of this distribution will be determined by the radial shape of the illumination beam. For simplicity we shall assume a uniform intensity to exist over the beam cross-section which drops to zero outside the beam. For a

dye laser such as employed in this work which operates in many high order modes, this is a quite good approximation of its shape [64]. This dependence can be expressed in mathematical form using the Heaviside function, H(x), which is zero for negative values of its argument and unity otherwise. Hence, for a beam of radius r_b, the spatial distribution to be used here can be written as $H((r_b-r)/r_c)$. Alternative beam distribution functions may be used, e.g. gaussian, but in general the small variations they introduce into the calculated form of p' is not worth the added complexity which they introduce in the $q_{m,i}$.

The longitudinal, or z-axis, dependence of beam intensity is due to attenuation of the beam by the sample vapor. For low to moderate power lasers where saturation or two-photon absorption effects are not important, the diminution of the excitation beam as it travels through the sample vapor can be expressed according to the familiar Beer-Lambert expression, 10^{-Az}. In this expression, A is the absorptivity and is related to the absorption coefficient α by the equation $A = \alpha/\ln 10$.

An expression for q(r,z) is thus of the form

$$q(o,o)\ H((r_b-r)/r_c)\ e^{-\alpha z},$$

where q(o,o) is a normalization constant. The normalization integral (equation (10)) can be easily evaluated yielding

$$q\ (o,o) = r_c^2\ \alpha L/r_b^2\ (1-e^{-\alpha L}).$$

Having now given explicit form to $q(r,z)$, we must determine the set of $q_{m,i}$ which will solve equation (11). Multiplying both sides of that equation by $\cos(m\pi z/L)\,dz$ and integrating over the length of the cell, we obtain

$$q(o,o)\,\frac{H((r_b-r)/r_c)}{\alpha}\,\frac{1-(-1)^m e^{-\alpha L}}{1+(m\pi/\alpha L)^2} = \frac{L(1+\delta(m))}{2}\,\Sigma_i q_{m,i} J_o(y_i r)$$

Letting

$$q_m = 2q(o,o)(1-(-1)^m e^{-\alpha L})/\,\alpha L(1+\delta(m))(1+m\pi/\alpha L)^2),$$

we now have

$$q_m\,H((r_b-r)/r_c) = \Sigma_i q_{m,i} J_o(y_i r).$$

If we now take the derivative of both sides with respect to r, then multiply both sides by $rJ_1(y_i r)dr$ and integrate over the cell radius we have

$$q_m \int_o^{r_c} rJ_1(y_i r)\,dH((r_b-r)/r_c)dr = -\Sigma q_{m,i} y_i \int_o^{r_c} rJ_1(y_i r)J_1(y_i r)dr.$$

Integrating the left side of the above equation by parts and applying the appropriate Bessel function relations [67] to the integral on the right, we obtain

$$q_m[rJ_1(y_i r)H((r_b-r)/r_c)\,|_o^{r_c} - \int_o^{r_c} H((r_b-r)/r_c)\,y_i r\,J_o(y_i r)dr]$$

$$= -q_{m,i} y_i r_c^2\,J_2^2\,(y_i r_c)/2 \quad .$$

The first term on the left of the above equation equals zero; the second term can be evaluated from standard

Bessel function relations [67]. This allows us to write the following general expression for the

$$q_{m,i} = \frac{1-(-1)^m e^{-\alpha L}}{1+(m\pi/\alpha L)^2} \quad \frac{2q(0,0)}{\alpha L\ (1+\delta(m))} \quad \frac{r_b^2}{r_c^2} \quad \frac{J(x_i,\beta)}{J_o(y_i r_c)}$$

where we define

$$J(x_i,\beta) = \frac{J_o(y_i r_b) + J_2(y_i r_b)}{J_o(y_i r_c)} = \frac{J_o(x_i\beta) + J_2(x_i\beta)}{J_o(x_i)}$$

with $\beta = r_b/r_c$.

Computer Simulation of Opto-acoustic Signal

With the form of the $q_{m,i}$ now determined, an expression for the pressure change in the sample cell upon optical illumination can now be written which contains the explicit dependence of p' on cell coordinates and time.

$$p' = \frac{r_b^2}{r_c^2} \quad \frac{\gamma-1}{\alpha L} \quad \sum_{m,i} \frac{2q(0,0)}{1+\delta(m)} \quad \frac{1-(-1)^m e^{-\alpha L}}{1+(m\pi/\alpha L)^2} \quad \frac{J(x_i,\beta)}{J_o(y_i r_c)} J_o(y_i r) \times$$

$$\sum_u^s b_u k_u \quad \frac{\cos\lambda_{m,i}t - e^{-k_u t} - (\lambda_{m,i}/k_u)\sin\lambda_{m,i}t}{k_u^2 + \lambda_{m,i}^2} \cos(m\pi z/L). \qquad (16)$$

To test the degree of correspondence between equation (16) and the actual pressure response in an opto-acoustic cell, a computer simulation of the equation was undertaken. The objective of the simulation was to provide a theoretical form for p' which could be subsequently checked by experimental observation. In practice, this meant that the

simulation should calculate the predicted temporal evolution of p' at a particular point chosen on the cell surface where a suitable detector might be placed.

Examination of equation (16) suggests two unique choices of r and z coordinates which might be of special interest with regards to simplifying the simulation.* Placement of the detector at the end of the cell and on the cell axis ($z = L$; $r = 0$) would reduce the $J_o(y_i r)$ term to unity for all i and allow the replacement of $\cos(m\pi z/L)$ with $(-1)^m$. However, placement of the detector in the light path would certainly rule out measurement of beam energy directly and might cause secondary problems such as reflecting the beam back down the cell. The alternative choice of detector placement is at the cell wall midway down the length of the cell ($r = r_c$, $z = L/2$). There are no experimental problems with placing the detector in the cell wall, although some nonuniformity in cell wall curvature may be introduced depending on the relative size of the detector surface and wall cross-section. As shall be discussed later, however, the small dimensions of the detector employed cause these deviations to be minor. Insertion of this set of coordinates into equation (16) brings about a significant simplification in the expression;

---

* A third choice, $r = 0$ and $z = 0$, would certainly provide simplification but would just as certainly dramatically increase the problem of getting light into the cell.

most notably, for all odd values of m, the summation is zero. The summation can be rewritten taking this effect into account, leaving the following equation:

$$p'(r_c,L/2,t) = (\gamma-1)\sum_i J(x_i,\beta) \sum_m \frac{2}{1+\delta(m)} \frac{(-1)^m}{1+(2m\pi/\alpha L)^2} \quad x$$

$$\sum_u^s b_u k_u (\cos\omega_{m,i}t - e^{-k_u t} - (\omega_{m,i}/k_u)\sin\omega_{m,i}t)/(k_u^2+\omega_{m,i}^2), \qquad (17)$$

where

$$\omega_{m,i}^2 = c^2 \left[y_i^2 + \left(\frac{2m\pi}{L}\right)^2\right].$$

For the simulation, only a single term in the bracketed summation in equation (17) is kept. This simple two-state model would correspond in practice to excitation into T_1^o. Higher states were not included since their effect on the form of p', besides the initial step rise, would be only to alter slightly the appearance of the acoustic bumps and add to their peak-to-peak amplitude. The actual expression evaluated in the simulation, then is

$$\Sigma J(x_i,\beta) \sum_m \frac{2}{1+\delta(m)} \frac{(-1)^m}{1+\left(\frac{2m\pi}{\alpha L}\right)^2} \frac{\cos\omega_{m,i}t - e^{-kt} - (\omega_{m,i}/k_u)\sin\omega_{m,i}t}{1+(\omega_{m,i}/k)^2} \qquad (18)$$

which is the temporal form of $p'(r_c,L/2,t)$ normalized to the long-time amplitude of the pressure rise,

$$(\gamma-1)\,\phi^{nr}E(1-e^{-\alpha L})/V.$$

A simple Fortran program was written to evaluate the

$J(x_i,\beta)$ on an IBM (360/75) computer. Representative values of this parameter for i = 1 to 20 and β = 0.25, 0.50 and 0.75 are listed in Table 3. The $J(x_i,\beta)$ values for a chosen value of β were incorporated into a program written for execution on a WANG 700c Programmable calculator. This program is capable of calculating the expression of interest for i running from 0 to 20. It was found, however, that in all the cases investigated, only the first few partial sums were significant, and the sum could be truncated at much smaller values of i. The number of significant terms in the m summation is found to vary considerably with the choice of α. Because of this, the summation over m was terminated at no set value of m, but rather when a particular term caused a change in the current i sum of less than 0.1%. As the values of expression (18) are calculated at time increments Δt, they are plotted, point-by-point, by a WANG 702 Output Plotter.

A typical plot is shown in Figure 6. This plot displays the signal calculated for excitation of a sample in the opto-acoustic cell used in this work (to be described later) with β=0.5, k=1 ms, c=L/k and $\alpha=2\pi/L$. As expected, it shows the gross exponential rise and the periodic acoustical undulations which have been observed in pulsed excitation experiments. On close observation, one notes that the acoustic signal appears to be a sum of two waves with different amplitude and frequency. The higher frequency smaller amplitude oscillation is due to the radial modes of

Table 3. $J(x_i, \beta)$.

i \ β	0.25	0.50	0.75
1	-2.209	-1.505	-0.664
2	2.205	0.255	-0.437
3	-1.531	0.529	-0.174
4	0.572	-0.147	0.041
5	0.271	-0.323	0.154
6	-0.714	0.103	0.154
7	0.684	0.232	0.076
8	-0.317	-0.079	-0.022
9	-0.134	-0.182	-0.088
10	0.426	0.064	-0.094
11	-0.441	0.149	-0.049
12	0.219	-0.054	0.015
13	0.088	-0.126	0.061
14	-0.304	0.047	0.068
15	0.326	0.110	0.036
16	-0.167	-0.041	-0.011
17	-0.065	-0.097	-0.047
18	0.236	0.037	-0.053
19	-0.258	0.087	-0.028
20	0.135	-0.033	0.009

Figure 6. Plot of expression (18) versus kt for $\beta = 0.5$, $k = 1$ ms, $c = L/k$ and $\alpha = 2\pi/L$.

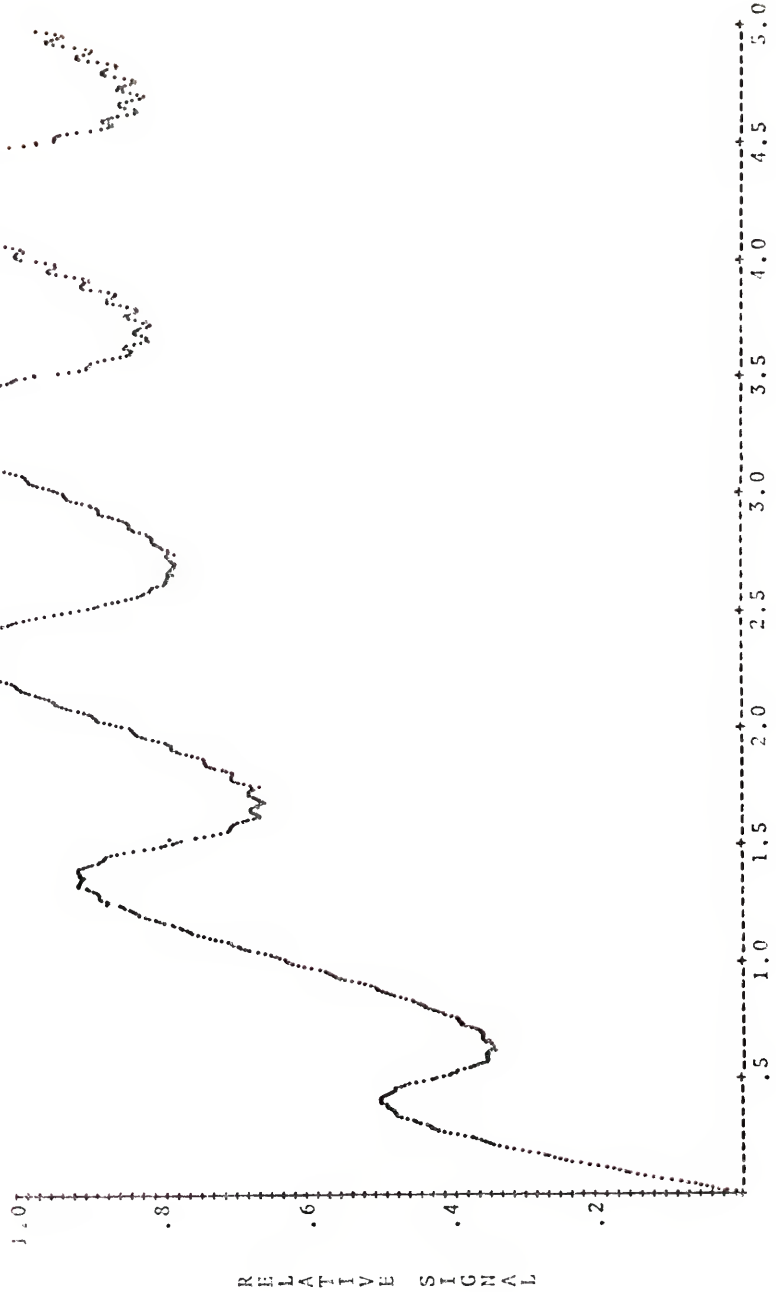
1.0
.8
.6
.4
.2
RELATIVE SIGNAL
.5
1.0
1.5
2.0
2.5
3.0
3.5
4.0
4.5
5.0
kt

standing wave formation. The larger amplitude component is formed by the action of the longitudinal standing waves. The frequency ratio of the two waves is $\sim L/r_c$, and their absolute frequencies are determined by both the cell dimensions and the speed of sound in the gas. Because of this, the speed of sound in the sample gas can be determined rather accurately by measuring the period of the acoustic "bumps." This is a very convenient happenstance because it allows a simultaneous determination of the heat capacity ratio since

$$\gamma = c^2\rho/p = Mc^2/RT \tag{19}$$

where M is the molecular weight of the sample [68].

Figures 7 and 8 are two further plots derived from expression (18). The parameters chosen are identical to those used to generate Figure 6 except for the value of α which is $2\pi/\sqrt{10}$ L in Figure 7 and $2\pi/10$L in Figure 8. The most noticeable effect on the plots due to this change is the decrease in amplitude of the longitudinal acoustic waves. This decrease occurs because as α decreases, the distribution of excited molecules down the cell axis becomes more uniform. This results in a reduced longitudinal pressure differential occurring after molecular relaxation, and hence the longitudinal resonances are driven less strongly.

Limitations and Extensions of the Theory

The purpose of this section is to tie together the previous sections with regards to the general applicability of the method therein described. The many assumptions made

Figure 7. Plot of expression (18) versus kt for $\beta = 0.5$, $k = 1$ ms, $c = L/k$ and $\alpha = 2\pi/\sqrt{10L}$.

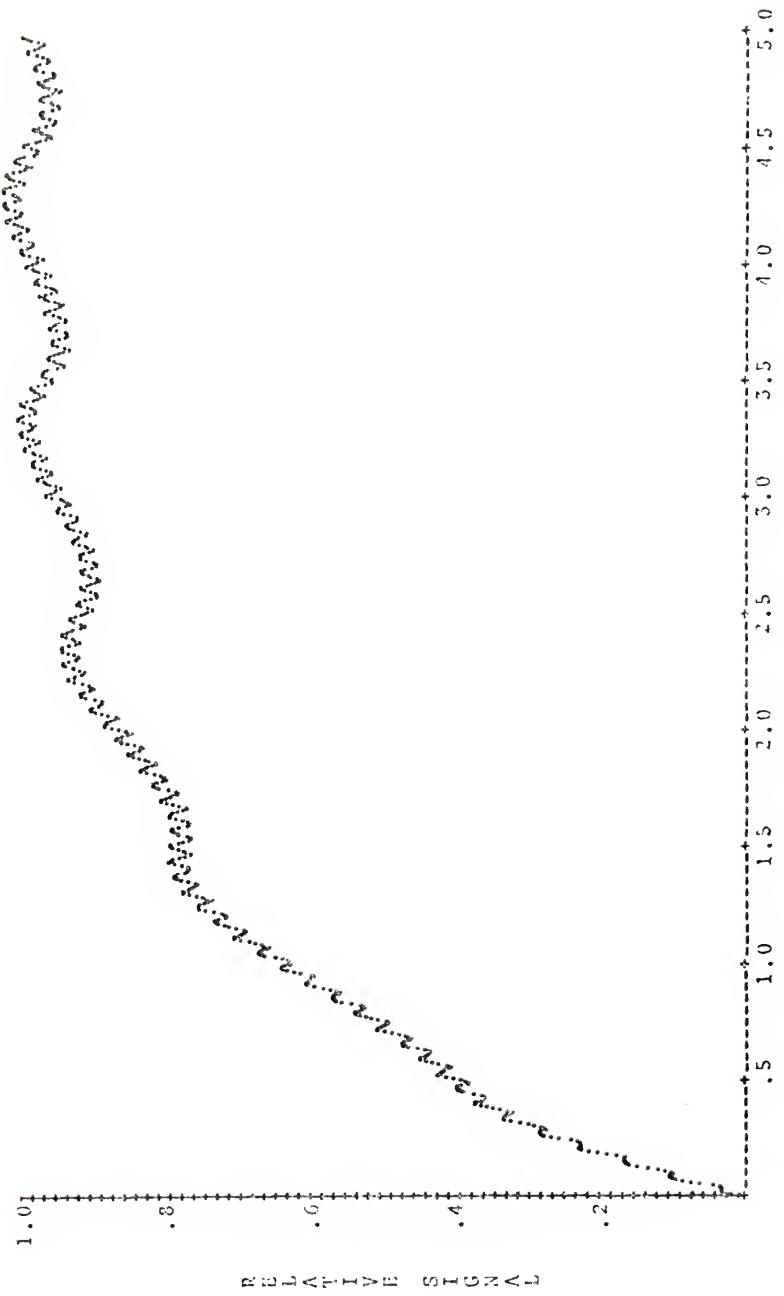
RELATIVE SIGNAL
1.0
.8
.6
.4
.2
.5
1.0
1.5
2.0
2.5
3.0
3.5
4.0
4.5
5.0
kt

Figure 8. Plot of expression (18) versus kt for $\beta = 0.5$, k = 1 ms, c = L/k and $\alpha = 2\pi 10L$.

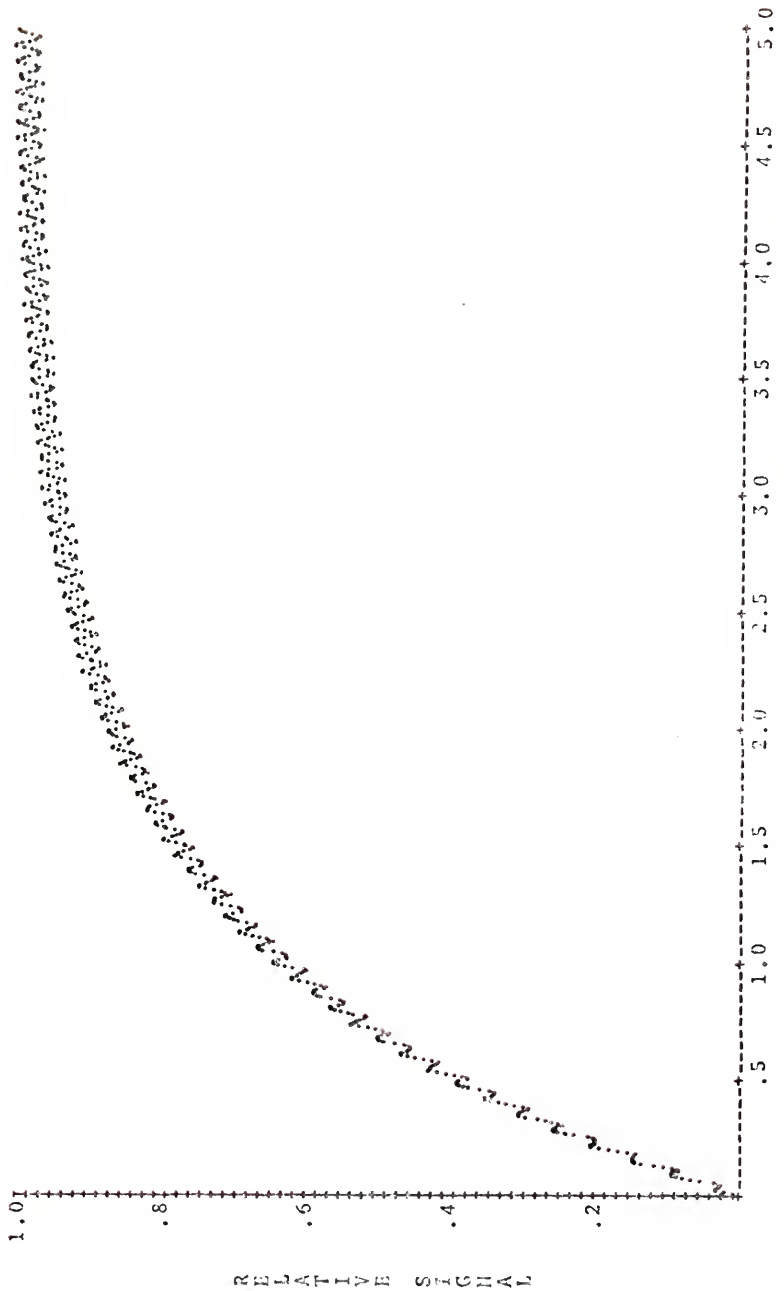
RELATIVE SIGNAL
1.0
.8
.6
.4
.2
.5
1.0
1.5
2.0
2.5
3.0
3.5
4.0
4.5
5.0
kt

set restrictions on the type of experiments which can be performed and the kind of equipment needed to carry them out. These restrictions will be reviewed below and their effect on experimental design will be discussed. Also, many effects were purposefully excluded from previous sections for simplicity. Therefore, a discussion of how the theory might be extended and corrected to include these effects is provided.

Limitations on Experimental Design

Cell construction

In the foregoing sections, the sample was assumed to be contained in an isothermal cell of perfect cylindrical symmetry. In practice, the symmetry of the cell is upset by ports through which the cell can be evacuated and through which the sample can be introduced. Further, a port for the pressure transducer must be provided; a side-viewing port for the attachment of a light detection device is optional. By employing a transducer which is externally translatable, a single port can serve both to connect the cell with the remainder of the sample handling system and provide an access port for the transducer. This arrangement does add considerably to the complexity of cell construction, however. In general, one can approach sufficiently close to the ideal geometry if care is taken to limit cell connections to minimal length and to limit port size to a small fraction of the circumference of the cell. So that the cell has no initial temperature variation, it

should be built from materials of high thermal conductivity and have a high thermal capacity.

The volume of the cell is determined by its length and radius. The length is certainly the less critical of the two dimensions; it will be shown in the next section that the samples of low to moderate absorptivity, the pressure pulse amplitude is independent of cell length. Optimum cell length is thus determined by "second order" effects. Increasing cell length increases the useful cell volume and minimizes the effect of "dead" space in the connectors and ports. The cell must be short enough, however, so beam divergence over the cell length can be disregarded and no significant temperature variations exist at the walls. From these considerations, it is clear that there is much lattitude in the choice of cell length.

This is not the case for the cell radius. Noting the strong dependence of p' on r_c, one might assume that the smaller r_c is chosen, the better. We must, however, recall that two very important assumptions depend on the size of r_c. Sample viscosity was neglected only under the condition that r_c be much greater than the mean free path of the sample. More importantly, the neglect of thermal conductivity, the ultimate basis for equation (5) being solvable, is strictly justifiable only for times less than r_c^2/κ. Thus, choosing a larger r_c increases the upper limit on the available observation time of the experiment. There is a lower limit of observation time

sample pressure will be determined very much by sample volatility and the nature of the investigation, larger pressures tend to relax the restrictions on r_c. Both ξ and κ are inversely proportional to pressure, so at higher pressures lower values of r_c become justifiable.

Pressure transducer

The only explicit restriction placed on the pressure sensing device in previous sections is that it be small with respect to the cell circumference, so as not to interfere significantly with the cylindrical symmetry of the cell. A reasonable interpretation of this restriction would be to require that the diameter of the transducer port be comparable to or smaller than the cell radius. Since the transducer itself must be placed so that its sensor is positioned directly at the cell wall, this will cause only a small amount of nonideality.

Besides the above explicit assumption about the transducer, two implicit ones have been presumed. The first is that the response time of the device is short enough to adequately transduce the rapidly fluctuating pressure level at the cell wall. This requires a response time of about two orders of magnitude smaller than the rise time of the gross pressure signal. For a molecule with a triplet lifetime of 5ms, this translates into a response time on the order of 50μs.

A second implicit requirement on the performance of the pressure transducer is that it is sensitive enough

to respond to the small pressure fluctuations involved. These have been assumed to be very small with respect of p_o. To help determine the sensitivity required of the transducer, an estimate can be made of the magnitude of the opto-acoustic pressure pulse expected. For this purpose, the long-time value of the gross pressure pulse for a simple two-state case can be calculated. The explicit form for this value is obtained by evaluating equation (15) for u = s and t very large

$$\begin{aligned} p'_{o,o}|_{t\to\infty} &= (\gamma-1)q_{o,o}b_s/k_s = (\gamma-1)a_{s,o}W_s/k_s \\ &= (\gamma-1)\bar{n}_s^o k_s^{nr} h\nu_s/k_s \\ &= (\gamma-1)\phi_s^{nr}(1-e^{-\alpha L})E/V \end{aligned} \tag{20}$$

where E = output energy of the excitation beam and V = cell volume. For small values of α, the $1-e^{-\alpha L}$ term is approximately equal to αL; in particular, letting p_o = 1 torr, $\tilde{\varepsilon}$ = 10 liter/mole-cm, L = 10 cm and T = 300K, less than three per cent error is introduced by rewriting the above equation as

$$p'_{o,o}|_{t\to\infty} = (\gamma-1)\phi_s^{nr}E\tilde{\varepsilon}p_o/\pi r_c^2 RT \tag{21}$$

where the relation $\alpha = \tilde{\varepsilon}C = \tilde{\varepsilon}p_o/RT$ has been used. If we now let γ = 1.10, ϕ_s^{nr} = 1.10, r_c = 0.5cm and E = 5 mJ, a value of 26 mtorr is calculated for the longterm pressure rise. This value both verifies the assumption that the experiment causes a small change in pressure and aids in

quantitatively specifying the sensitivity needed in the transducer. It is of further importance that a satisfactory device should not only respond to pressures as small as or smaller than that calculated above but also should do so while limiting its pressure equivalent noise level to a reasonable level.

Illumination source

The illumination source assumed in deriving equation (16) has been fairly well defined. It must deliver a sharply-collimated narrow-bandwidth short-duration pulse of optical energy. In general, the restrictions on beam profile and bandwidth may be relaxed; these would require, however, a redetermination of the $q_{m,i}$ in the former case and in the latter case a change in the deactivation scheme to one involving multiple-level initial population. Deviation of the temporal form of the excitation source from that of a delta pulse can also be accommodated, but this involves a resolution of equation (12) using the new time-dependence. One characteristic of the excitation source which has not been discussed as yet is the pulse energy which it must be capable of delivering. Although the absolute pressure developed in an opto-acoustic experiment depends strongly on the absorption and emission characteristic of the sample, even for large values of $\tilde{\varepsilon}$ and ϕ^{nr} the excitation beam must be relatively energetic ($\geq$1 m J). Ordinary flashlamps can provide this excitation, but when the requirements of narrow-bandwidth and short pulse dur-

ation accompany the energy requirements, it appears that only laser sources will suffice.

Extensions of Theory to Additional Effects

Effect of window absorption

Absorption of the exciting light by the inner surface of either cell window will cause local heating of the sample in the vicinity of the surface [70]. The effect of this heating will be the production of an acoustic wave whose amplitude will depend on the extent of window absorption. The presence of this unwanted absorption is most easily determined by illuminating a gas, such as N_2, which does not absorb in the wavelength region employed. If the window material is satisfactory and no traces of absorbing substances are adhering to its surface, then no signal will occur. In experiments in which the cell is heated to increase the vapor pressure of the sample, special care must be taken to avoid condensation on the windows which can also cause this spurious effect.

Effect of luminescence heating

In our development of the molecular deactivation scheme, decay paths were divided into nonradiative and radiative types with the former ostensibly being the sole heat producers. Radiative decay paths do give off heat, however, because radiative transitions to vibrational levels of the ground state produce a non-Boltzmann distribution of these vibrational levels. Although the amount of heat energy produced by a molecule undergoing a radiative

deactivation is a small fraction of that produced by an initially identical molecule undergoing totally nonradiative decay, the problem is significant when dealing with a molecule possessing a large luminescence yield.

To correct for this effect requires some knowledge of the emission characteristics of the sample. In particular, the average frequency of emission, $\bar{\nu}$, must be determined from the emission spectrum of the sample for the emitting state in question. Then, for a state u which undergoes radiative decay to the ground state, the term $\phi_u^{lum}(h\nu_u - h\bar{\nu})$ is added to the term in p' which accounts for the heat produced by the corresponding nonradiative process. In the above expression, ϕ_u^{lum} is the luminescence yield of the state u. Addition of this further term to p' may cause some difficulties; specifically it may now become impossible to derive the yields of all decay processes for all the states of interest from opto-acoustic measurements. In these cases, the problem will require the use of optical methods to complement the information gained from the opto-acoustic studies.

Effect of a second gas

The effect of a second nonabsorbing or buffer gas on the excited state decay parameters of an absorbing vapor is easily studied using the opto-acoustic method. As noted in the introduction, several quenching studies have already been published. The only direct changes in the theoretical formulation which accompany the study of a gas mixture is

that the heat capacity ratio used in equation (16) and elsewhere must now be that of the mixture, and p_o in equation (21) is now taken to be the equilibrium partial pressure of the absorbing species.

In general, the addition of a buffer gas will affect the rates of the various relaxation processes occurring in the excited sample and may also open new channels for release of excitation energy. These actions will change both the amplitude and time evolution of the opto-acoustic signal relative to that observed in the pure sample. Aside from these changes, the amplitude will also be affected by the change in γ noted above. Further, since the mixture of a buffer gas plus sample may have a significantly different thermal diffusivity than that of the sample gas alone, especially if He, Ne or H_2 are used, the temporal part of the signal will also be affected. Specifically, an increase in thermal diffusivity will cause the sample to cool more rapidly and thus limit the available observation time.

Effect of photochemistry

Inclusion of the possibility of a photo-induced chemical reaction adds another decay path to those already available to the excited state. Predicting the effect on the pressure signal in the cell of a molecule traversing this path is much more difficult, however, than for a standard radiative or nonradiative process. The reason for this difficulty is that a molecule undergoing photo-reaction can contribute to the overall pressure response

in several ways. Firstly, the endo- or exothermicity of the reaction step must be considered. Depending on this value, the products of the reaction will have more or less energy available for heating than the energy of the initially absorbed photon. Secondly, the products of the photoreaction may not be formed in their ground electronic state. Thus, a whole new set of excited state decay kinetics must be investigated to determine how that electronic energy is dissipated. Finally, the initially excited molecule may break up into a number of products. Thus, regardless of the heat released or potentially available, the pressure of the vapor increases solely due to the increase of the number of molecules in the cell.

It is clear, then, that studying photochemically reactive systems via time-resolved opto-acoustic spectroscopy is a complex matter. This is not to say that such a study can not be done, but rather that one must carefully investigate the probable pathways open to a system before such a study is undertaken. If a well-defined model can be constructed for the decay kinetics of a photochemically reactive species which does not involve a change in the number of gaseous molecules in the cell, then this model in conjunction with the theory developed in this chapter can be used to predict the pressure behavior of a sample of this species upon pulsed optical illumination.

If a change in the number of molecules in the vapor phase accompanies photoreaction, then the detailed

prediction of the pressure response of the sample upon optical illumination is beyond the scope of this work. However, one might expect that the overall response should not be greatly different than what might normally be observed in the absence of photoreaction, with one significant exception. Where photoreaction takes place accompanied by a change in the number of gaseous molecules, the long-time pressure in the cell will not return to its initial level. The change in pressure can be written by analogy with equation (20) as

$$p'_{pr|t\to\infty} = \frac{N'RT}{N_a h\nu}\,\phi^{pr}\,(1-e^{-\alpha l})\,\frac{E}{V}$$

where N' is the difference between the number of moles of reactants and the number of moles of products per mole of excited molecules which react, and ϕ^{pr} is the yield of the photoreaction (number molecules reacted/number molecules excited). If one calculates a typical value of $p'_{pr|t\to\infty}$ one finds it is about one order of magnitude smaller than $p'_{o,o|t\to\infty}$ for comparable values of ϕ^{pr} and ϕ^{nr}_s and with N' = 1. In general, this presents no problem, since the device used for the steady-state measurement involved in evaluating $p'_{pr|t\to\infty}$ usually will have a much greater sensitivity than the device required to follow the rapid fluctuation of p' during transient heating.

CHAPTER THREE
EXPERIMENTAL SYSTEM

Equipment

Opto-acoustic Cell and Vacuum System

During the course of this work, several opto-acoustic cells were constructed and used for preliminary studies. As work progressed, design changes were made to increase the ruggedness of the cell and especially to provide better access and shielding for the dynamic pressure sensor. The final result of this refinement process is diagrammed in Figure 9. The cell consists basically of two chambers: the experimental chamber in which the sample is optically excited and a second larger reference chamber. These chambers are mounted together on a height-adjustable aluminum platform which can be leveled.

The experimental chamber is fashioned from a block of aluminum 3" x 4" x 6 1/2" by drilling a 1/2" diameter hole down the center of the long axis of the block. At either end of the chamber are attached 1" diameter Suprasil quartz windows with vacuum-tightness insured by rubber "O"-rings. At the midpoint of the chamber length a 0.1934" diameter hole is drilled perpendicular to the chamber axis on the

Figure 9. Diagram of opto-acoustic cell.

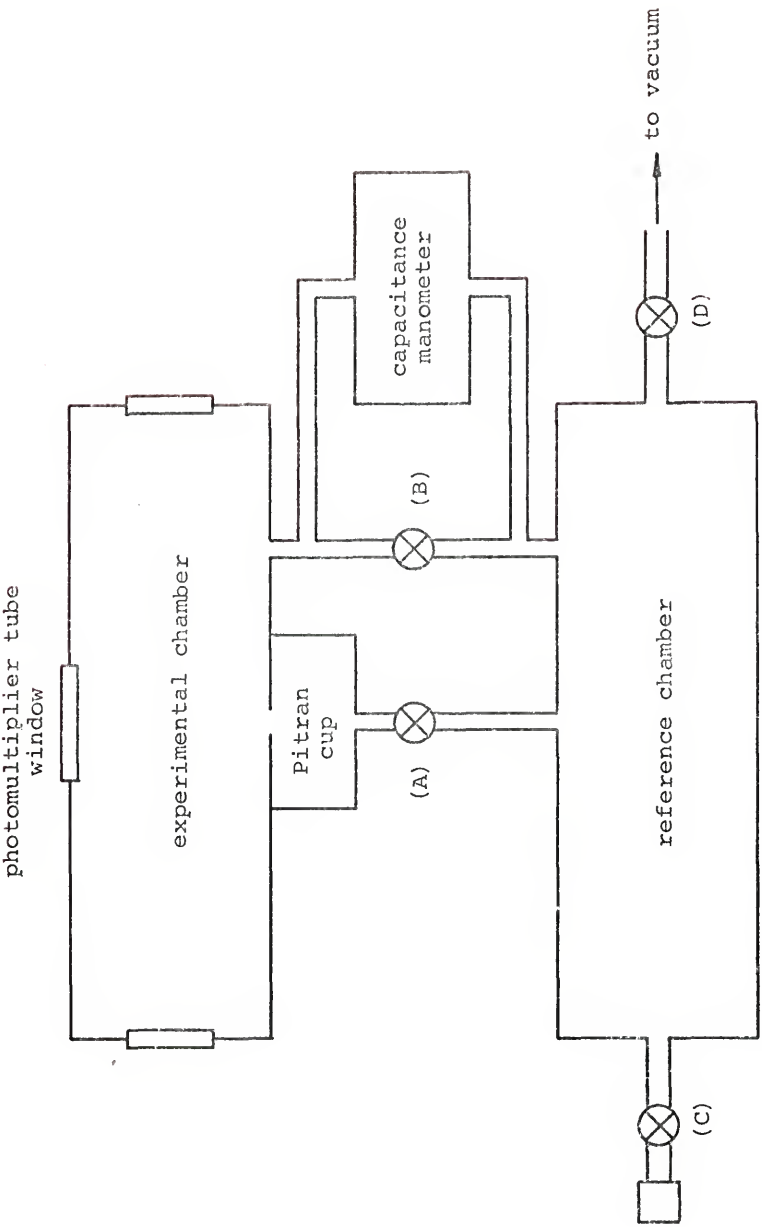
photomultiplier tube
window
experimental chamber
Pitran
cup
(A)
(B)
capacitance
manometer
reference chamber
(C)
(D)
to vacuum

large face of the block to provide a port for the pressure transducer. Provisions for mounting a phototube on the opposite face of the aluminum block are provided and a second 0.1934" diameter hole is drilled diametrically opposite the first to allow light output through a third Suprasil window. A 3/16" diameter port for gas transfer from the reference chamber is placed 3/4" from the cell end on the same side as the transducer port.

The transducer which measures the excitation-induced dynamic pressure fluctuations is attached to the experimental chamber after mounting it in its own special holder. Because the transducer is a differential device, its reference side must be held at the initial pressure of the sample vapor. To accomplish this, the transducer mount is covered by an aluminum cup which, when fastened to the cell wall, provides a vacuum-tight compartment. This cup is then connected by copper tubing through bias vacuum valve (A) to the reference chamber.

Gas flow between the two chambers takes place through 1/4" copper tubing and is regulated by the action of brass vacuum valve (B). A capacitance manometer is connected in parallel with this valve and measures any pressure differential which may exist between the experimental and reference chambers. This manometer also serves to measure the initial pressure of the sample as part of the procedure which shall be discussed later.

The reference chamber is basically a 5" long, 1 3/4" diameter closed cylinder with three radial ports and one port at each end. The uses of the radial ports have already been discussed. One end port is employed for vapor entry of samples and this port is controlled by vacuum valve (C). The valve is connected to a metal "quick-connect" which allows facile attachment and removal of sample containers. Cell evacuation takes place through the reference chamber port controlled by valve (D). Through this valve the opto-acoustic system is connected to a glass vacuum line and gas handling manifold. The vacuum is provided by a mercury diffusion pump used in conjunction with a liquid nitrogen cold trap and mechanical roughing pump. Line pressure is monitored by an ionization gauge, and pressures down to 2×10^{-6} mm of Hg are attainable in the line.

Excitation Source

As discussed in the previous chapter, the requirements for the excitation source for time-resolved opto-acoustic experiments are most fittingly satisfied by a pulsed laser. Especially useful for general work of this type is the tunable laser, which would allow excitation of electronic transitions over a broad range in the visible and ultraviolet spectral regions. In general this type of laser employs a solution of an organic dye which, upon excitation in a

cavity equipped with suitable reflectors, has the ability to lase over a broad band of 10 to 50 nm in the optical spectrum. By replacing the rear reflector of the laser cavity with an element whose reflectivity is sharply peaked at one wavelength in the lasing band, e.g. a grating, lasing will occur only at this particular wavelength with only slight loss of optical energy [71]. Thus, by tuning the cavity's selective reflector to a particular wavelength, monochromatic output can be achieved anywhere within the lasing region of the dye being employed.

The optical energy by which the lasing dye is excited or "pumped" can be supplied either by a fixed frequency pulsed laser, e.g. nitrogen or argon lasers, or by a flashlamp which emits high intensity broad band excitation. A laser pump would allow for very high repetition rates as well as provide very short lasing pulsing. On the other hand, a flashlamp excited device provides much more energetic optical pulses and is considerably less expensive than a laser-pumped system. As was shown in a previous section, the pressure fluctuation produced in an optoacoustic experiment is quite small and linearly dependent on pulse energy. So, primarily on the basis of the pulse energy available, the decision was made to utilize a flashlamp-pumped dye laser system in this work.

The system chosen (Model DL 1200, Phase-R Co.) is a complete dye laser system including flashlamp, power supply,

dye circulation, cavity reflectors, tuning grating and control electronics. This system is primarily designed for use with dyes lasing in the 320 to 420nm region but will also accept dyes lasing throughout the visible if the cavity is fitted with reflectors optimized for the visible region. The rated pulse energy from the system (for Rhodamine 6B at 588nm) is 150mJ, and the manufacturer's literature describes this rating as "conservative." The data presented on ultraviolet dyes indicates output energies in the 330 to 420nm region of from 5 to 15mJ depending on wavelength and dye chosen (see Figure 10). Bandwidth is given as 0.1-0.2nm when the laser cavity is grating tuned. The laser pulses are provided in a beam nominally 5mm in diameter and with a stated pulse width of less than 250 ns (full width at half maximum). The firing mode is either manual or by external trigger pulse, and the maximum repetition rate is given as ten pulses per second.

We elected to purchase this commercial laser system rather than construct one of our own design sc as to minimize time spent on laser research at the expense of the major interest of our investigation. As it occurred, this was not the case. Component failures in the laser system were numerous and continued to occur from time to time throughout the course of this study. These problems aside, however, the laser, under the best conditions, fell far short of expected performance in three citiical areas:

Figure 10. Calculated pulse energy of DL 1200 laser system versus wavelength from data presented by Phase-R Co. for four dye/solvent combinations. DMF = dimethylformamide, PBD = 2-(4-biphenyl)-5-phenyl-1,3,4-oxadiazole, P-386 and X-413 are the code numbers of two laser dyes whose structure is not specified.

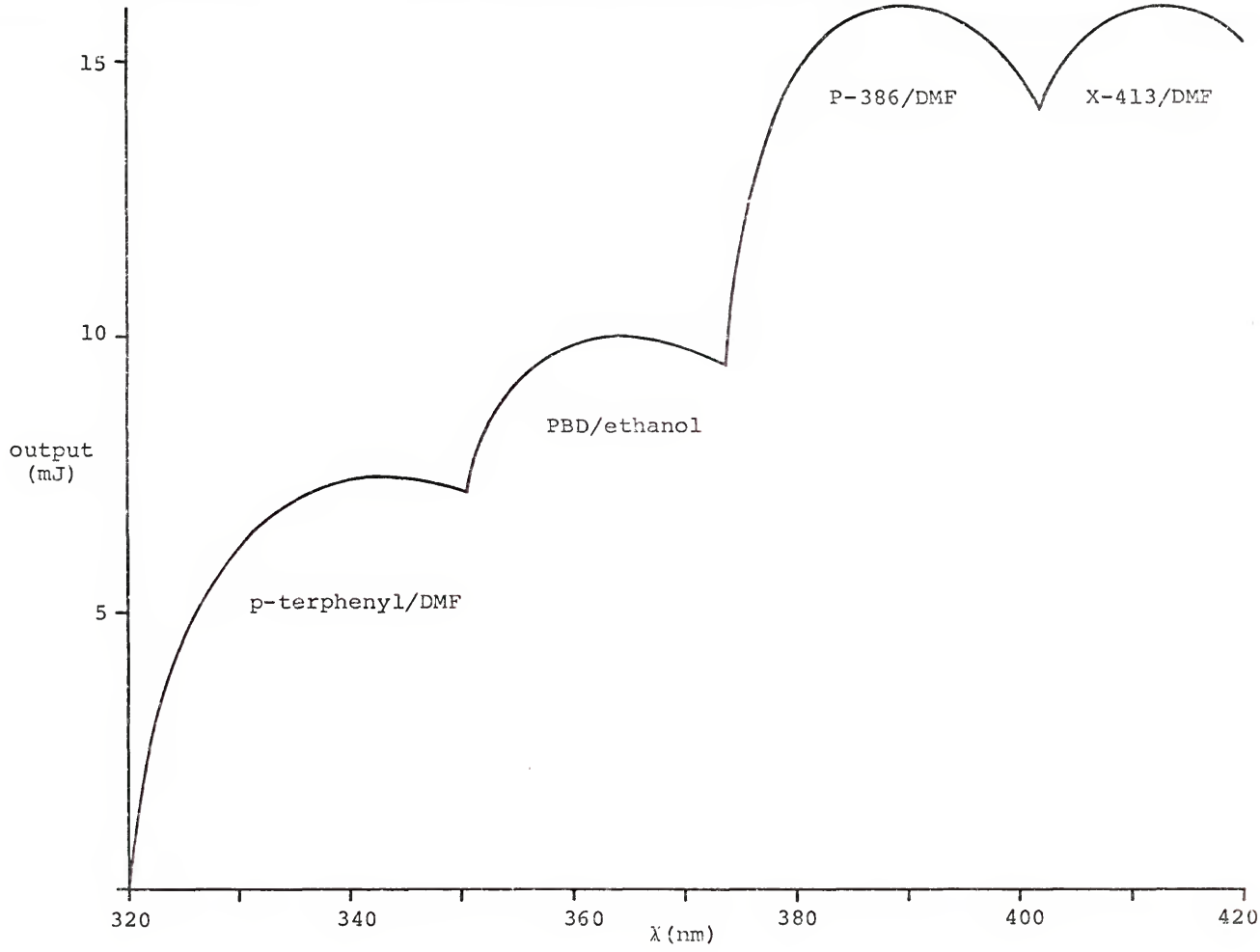
15
10
5
output
(mJ)
p-terphenyl/DMF
PBD/ethanol
P-386/DMF
X-413/DMF
320
340
360
380
400
420
λ (nm)

pulse repetition rate, optical bandwidth and output energy. Because these reduced performance levels so affected the course of this research, we will describe here our efforts to achieve the expected laser operation and report the final performance obtained.

Preliminary work with the laser system was performed using the ultraviolet laser dye No. 386 (New England Nuclear) in dimethyl formamide (DMF) solution, as per manufacturer's suggestion. This dye is supplied as a 10^{-3}M concentrated solution and is diluted to 5×10^{-4}M using Spectroquality DMF (Matheson Coleman and Bell). Absorption and emission spectra of this dye are shown in Figure 11. The front reflector used in conjunction with this dye, hereafter referred to as R1, is matched to the output characteristics of No. 386, having a peak reflectance of 85% at 389nm. The spectral variation of the reflectance of R1 is indicated in Figure 12.

Before lasing can be attempted, the laser cavity must be aligned. This is accomplished with the use of a 1mW He-Ne laser (Metrologic). The He-Ne laser is first adjusted so that its beam is co-linear with the flashlamp using the pin-hole caps provided. When a mirror is used as the rear reflector of the cavity, the front and rear reflectors are then adjusted so that they direct the He-Ne beam back upon itself. See Figure 13. The laser is now roughly aligned. At this point, the He-Ne laser is removed and the dye laser

Figure 11. Absorption and uncorrected emission spectra of dye No. 386 2×10^{-5} M in D.M.F. Ordinate is scaled in optical density units for absorption, relative units for emission.

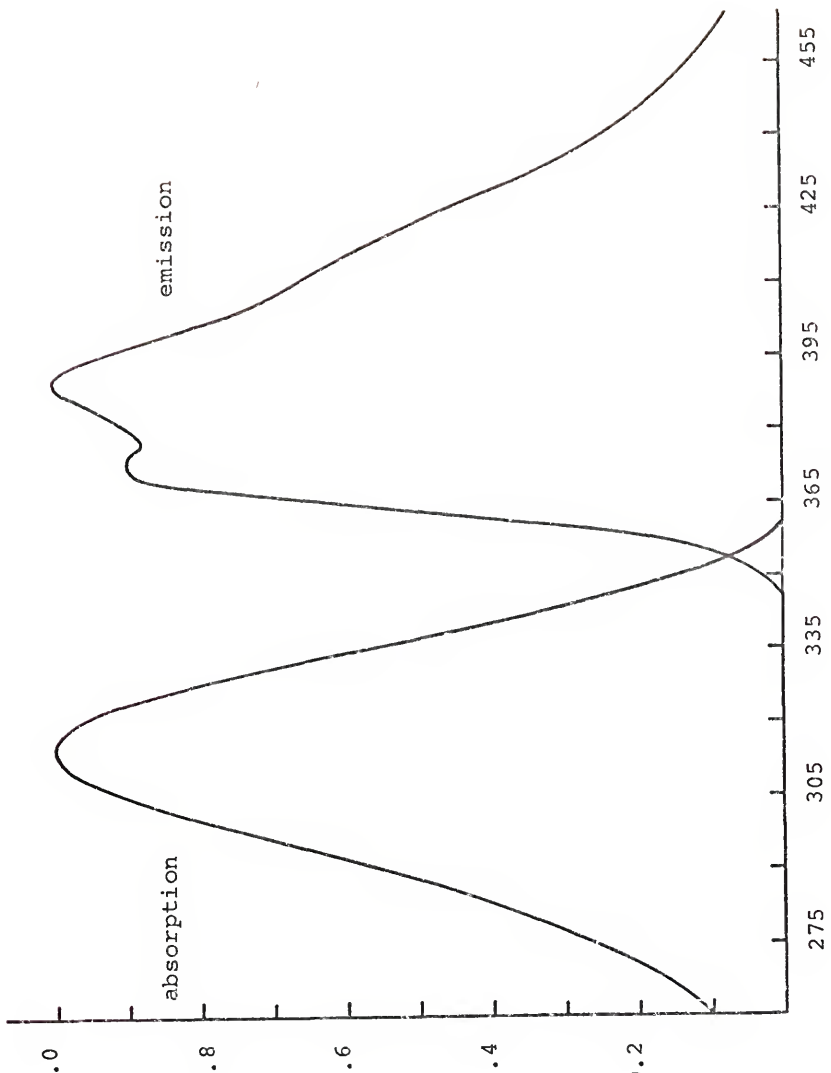
absorption
emission
1.0
0.8
0.6
0.4
0.2
275
305
335
365
395
425
455
λ (nm)

Figure 12. Variation in reflectivity of R1 reflector versus wavelength.

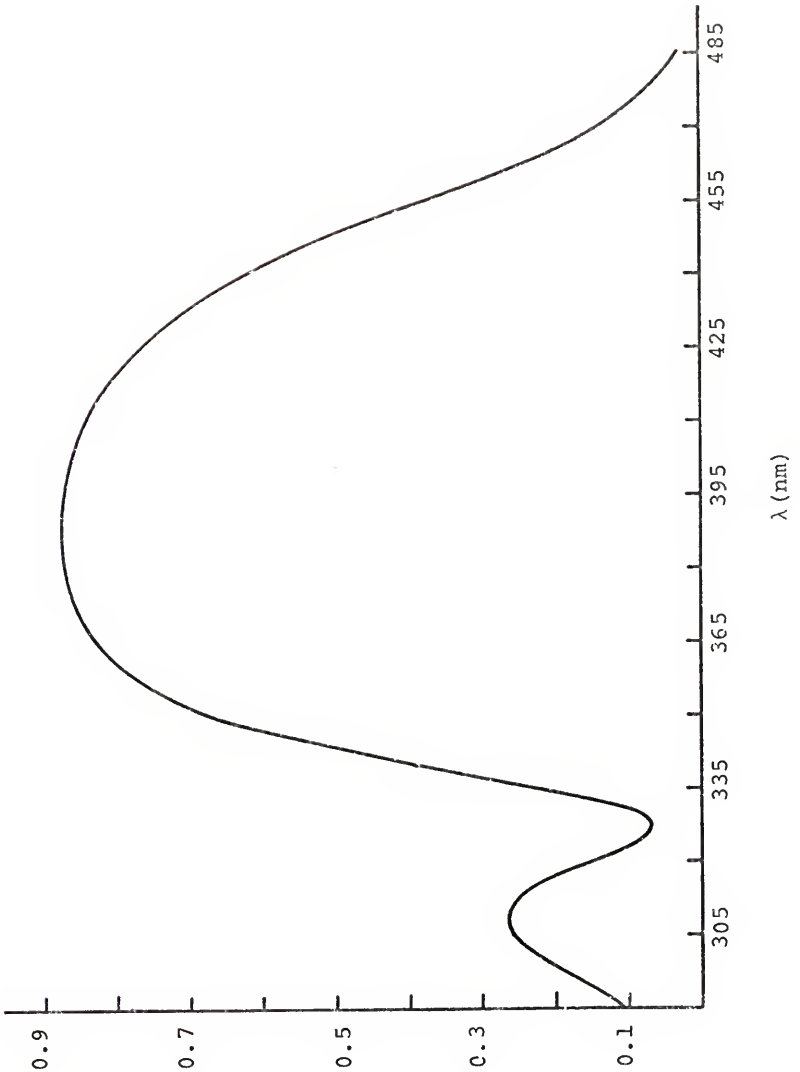
0.9
0.7
0.5
0.3
0.1
305
335
365
395
425
455
485
λ (nm)

Figure 13. Diagram of laser alignment set-up using rear reflector as a mirror.

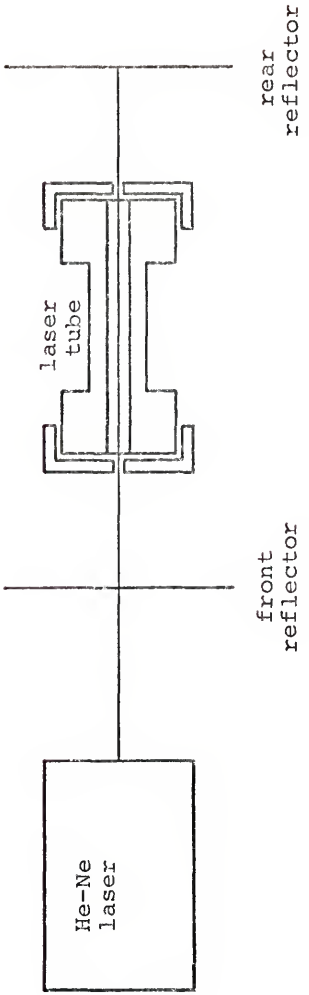
rear
reflector
laser
tube
front
reflector
He-Ne
laser

is turned on. With a solution of dye circulating in the laser, the spark gap is pressurized with dry nitrogen gas, the voltage across the flash capacitor is raised and the flashlamp is manually fired. Fine tuning of laser alignment consists of observing the laser output pulse on a white card and making small adjustments in reflector positions so as to achieve an output beam which is circular in cross-section and uniform in intensity. In the aligned cavity formed by R1 and a total reflector, the onset of lasing of a freshly-prepared circulating solution of dye No. 386 is found to occur at 15kV with a spark gap pressure of 20psi.

To measure the spectral range of this broad band lasing, as well as to monitor tuned output pulses, a 3/4 meter monochromator (Spex) with Polaroid camera attachment was used. See Figure 14. In this mode, dye laser alignment was preceded by alignment of the He-Ne laser to the monochromator. This was accomplished by directing the He-Ne laser into the center of the exit slit of the monochromator, then, with the monochromator wavelength setting at 6328Å, adjusting the He-Ne laser so that its beam exited the monochromator at the center of its entrance slit. This exiting beam is then used (as described previously) to align the dye laser cavity to the monochromator. To photograph the laser output, the monochromator wavelength setting is adjusted to a value close to where lasing is expected and

Figure 14. Diagram of laser-monochromator alignment set-up. Movable mirror is shown swung down into light path, directing dye laser beam to camera.

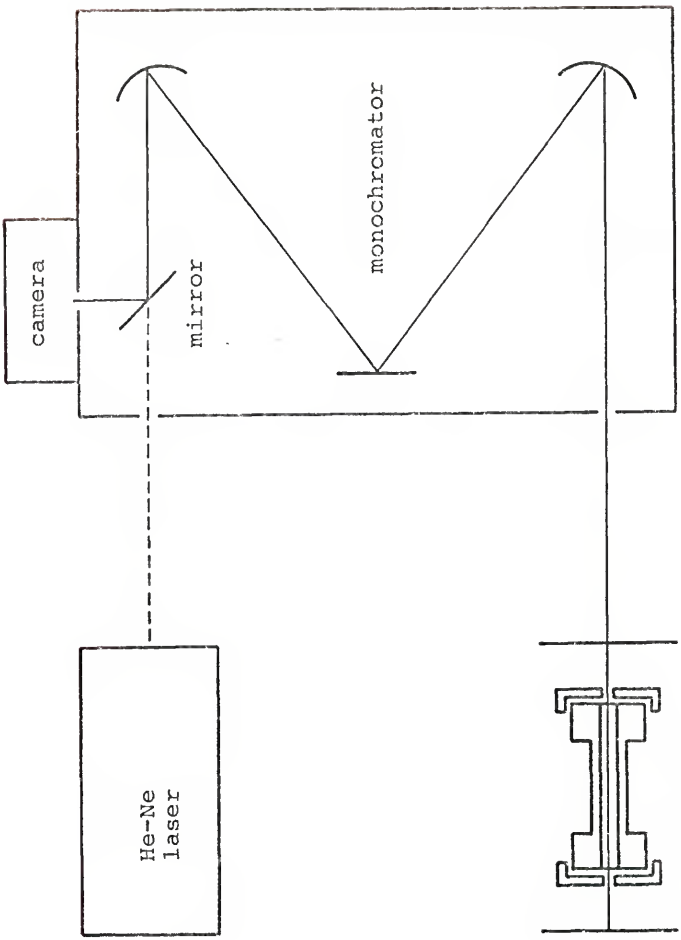
camera
mirror
monochromator
He-Ne
laser
dye laser

a movable mirror is dropped into the light path to direct the beam to the camera.

Spectral position of the laser output is usually determined by comparison to a photograph of a standard source taken in the same manner. Alternatively, it is possible to record the standard spectrum on the same photograph as the laser output. For the region around 390nm, a nitrogen Geissler tube was used to standardize the photographs. Portions of the second positive band of nitrogen lie in this region [72]. With the monochromator set at 387.5nm, a photograph is made of the dispersed nitrogen emission. If one now plots the known wavelength of the transition band vs. the distance of this band in nm from the left edge of the photo, one obtains the plot shown in Figure 15. The plot shows that wavelength is linear with distance across the photo. A least squares fit of the line gives the intercept as 344.04nm and the slope as 1.09nm/mm; this latter value correlates well with the stated dispersion of the instrument. Since distances on the photo can be read to $\pm$0.1mm, wavelengths derived from them are thus good to $\pm$ 0.1nm. Photos taken in this manner of the unfiltered broad band output of dye No. 386 show detectible intensity over a 50nm band from about 320 to 420nm with bright areas centered at 387 and 400nm.

To achieve narrow-band output, the rear reflector assembly is removed and replaced with a grating (1200 l/mm)

Figure 15. Plot of wavelength of nitrogen emission lines versus distance from edge of photograph taken with monochromator mounted camera.

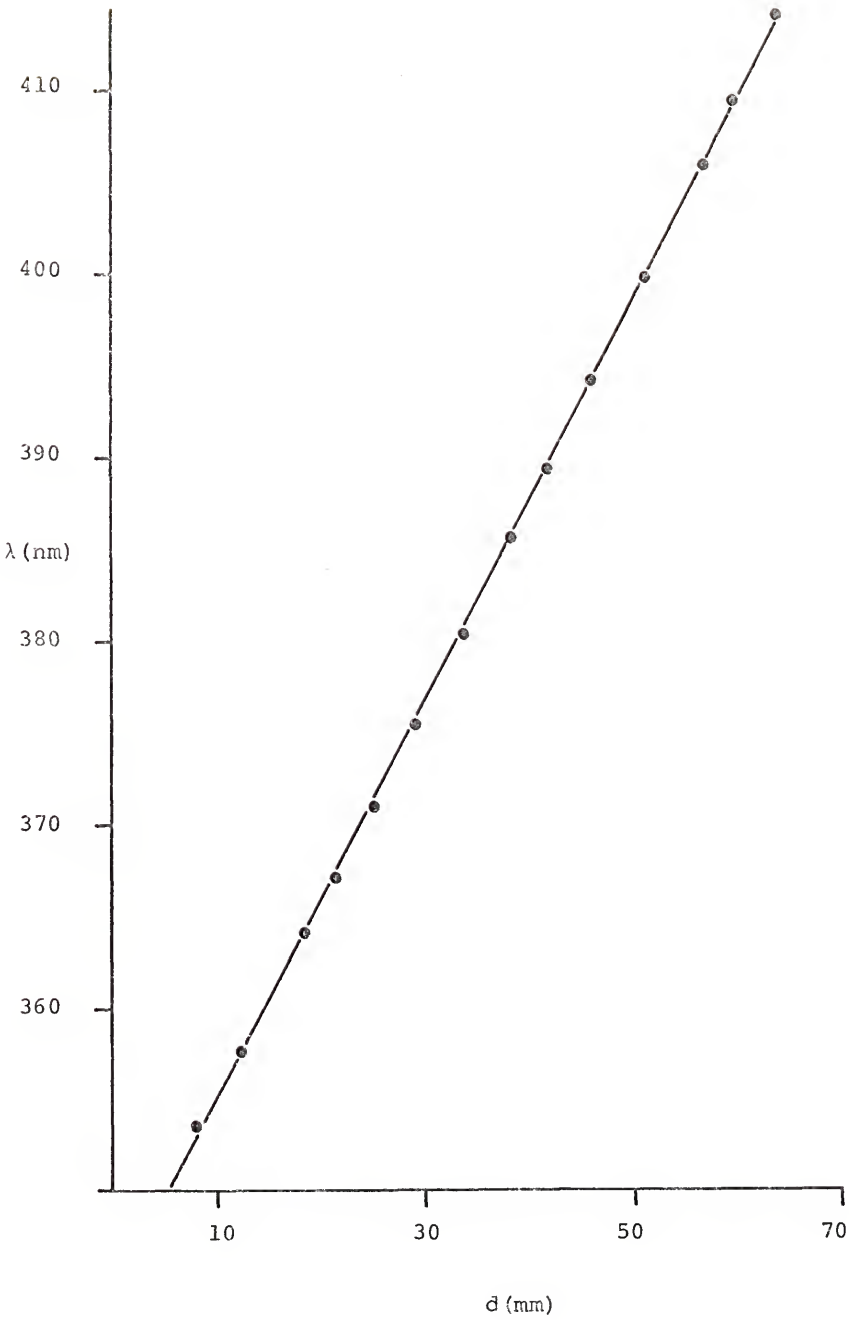
410
400
390
λ (nm)
380
370
360
10
30
50
70
d (mm)

in a gimbal mount. Set screws on the mount are available for adjusting the grating about its horizontal axis and for rotating it in the vertical plane. A micrometer drive is used for rotating the grating about its vertical axis and it is this motion which is used to select the lasing wavelength. The micrometer is calibrated so that one small division represents 0.2nm. A fine adjust micrometer is also available with vernier adjustment to 0.005nm, but it was not used.

Alignment of the laser when using the grating mount is slightly more involved than when using a rear reflector. First, the flashlamp and front reflector are aligned with the He-Ne laser as described previously. A glass microscope slide used as a beamsplitter is now placed in the He-Ne beam in front of the front reflector so as to direct the return beam to the ceiling or a far wall. Using the micrometer drive, the grating is now rotated so as to best align the zeroth order He-Ne beam with the return beam off the front reflector. If exact alignment cannot be achieved solely by micrometer adjustment, the grating is tilted about the horizontal axis through the grating using the appropriate adjustment screws.

Next the micrometer drive is used to select the 1st order beam and align it as well as possible. If exact alignment of this beam cannot be achieved solely by micrometer adjustment, the grating is rotated about the hori-

zontal axis perpendicular to its face by adjusting the appropriate set screws. Alignment of the zero order and first order beams is now repeated until both can be aligned exactly using the wavelength drive only.

The micrometer is now set to select the wavelength of peak lasing for the dye in the laser. In doing so, one must take into account any zero shift in the micrometer drive. If the micrometer scale does not read zero when the zeroth order beam is aligned, this reading must be added to the wavelength desired to determine the appropriate micrometer setting. Lasing is now attempted. Fine adjustment of the alignment involves tilting the grating about its horizontal axis in small, incremental steps and observing the effect on lasing threshhold and spot size.

This procedure was followed using a freshly prepared circulating solution of dye No. 386 (1×10^{-4}M in DMF) to produce very intense lasing over a large spectral region. To calibrate the micrometer readings in terms of actual lasing wavelengths, the monochromator-mounted camera was used. To reduce the amount of scattered flashlamp light entering the monochromator, the laser beam was passed through a visible light filter, a 10% transmitting neutral density filter and a diffuser screen. On a single photo, a series of 16 laser exposures was made with the grating micrometer drive increased one unit after each exposure. The wavelength of each pulse was then determined from the

photograph using the calibration data. A plot of output wavelength vs. micrometer setting is shown in Figure 16; the solid line is the best fit assuming a slope of unity.

The plot in Figure 16 verifies the tunability of the laser system. However, the photograph from which the plot was made, as all the photographs taken of tuned laser pulses, cast doubt on the narrowness of the bandwidth of the individual pulses. All the photographs of laser pulses indicate bandwidths of approximately 2 nm. Although photographs of Geissler tube emissions show that the photographic technique used here is capable of capturing and reproducing much smaller line widths, to completely rule out the possibility of the photographic technique displaying falsely broadened spectra, an alternate measuring procedure was employed. A simple photodiode circuit (see Figure 17.) was placed at the exit slit of the monochromator to monitor pulse intensity. With the laser aligned to the entrance slit, the output of the photo circuit was monitored during laser firings as the monochromator was made to scan across the beam. Large variations in pulse-to-pulse intensity were found and this made accurate determination of bandwidth impossible; however, the accumulated data bears out the photographic data. Both indicate much larger bandwidths than expected.

A technique has been suggested for use with tunable lasers to provide narrower line widths [73]. In a grating

Figure 16. Plot of wavelength of laser output versus grating micrometer setting.

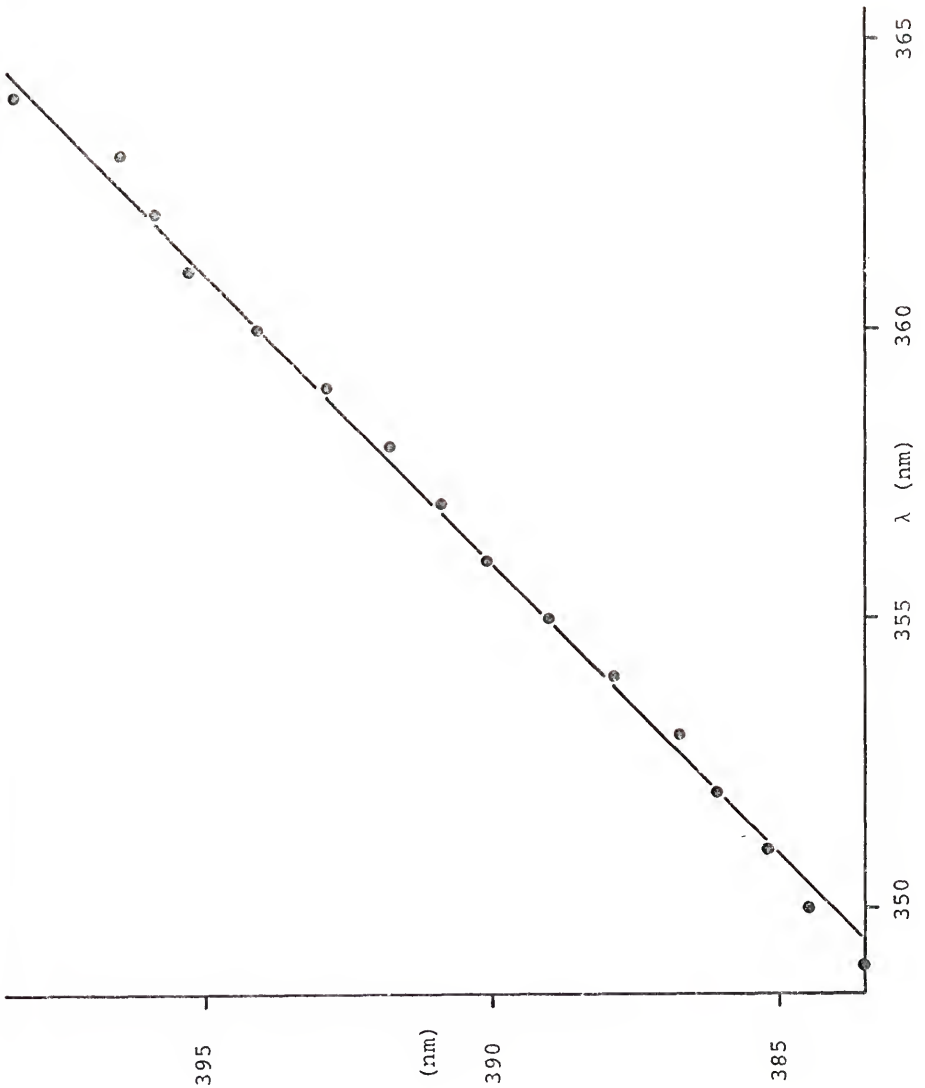
395
390
385
λ (nm)
350
355
360
365
λ (nm)

Figure 17. Schematic of battery-powered photodiode circuit.

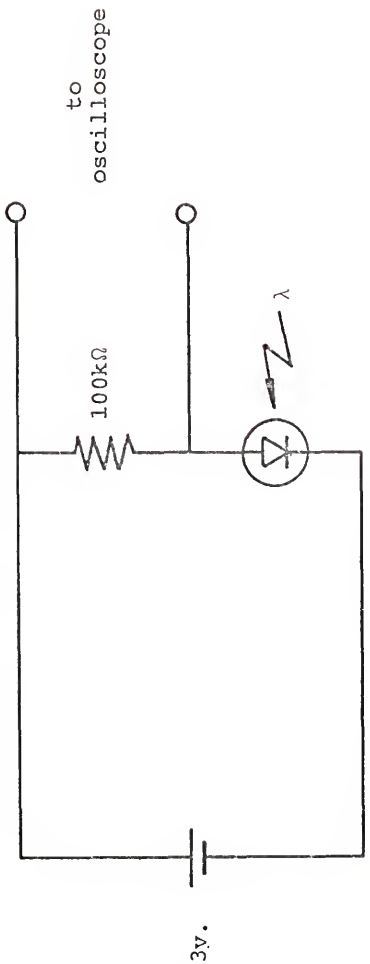
to
oscilloscope
100kΩ
λ
3v.

tuned system, this technique involves placing a mirror of intermediate reflectivity in the laser cavity between the active medium and the grating. The grating-mirror combination now acts similarly to a Fabry-Perot etalon to reduce the bandwidth of the reflected light while at the same time increasing the reflectivity to the tuned wavelength over that of the grating alone. This technique was tried on our system using a variety of reflectors, none of which produced the desired result. Of those which did affect the output, all had the same undesired effect: tunability was lost and lasing occurred at 389nm. It is felt that the cause of this finding is that although addition of the added reflector does fractionally increase the reflectivity of the tuning element at the wavelength of interest, it also introduces a reflective element which acts at all wavelengths as opposed to the narrow band of the grating itself (see Figure 18). Thus, if the lasing system has potentially high gain at a particular wavelength, introduction of the partial reflector will cause lasing at this wavelength rather than the one selected by the grating. As we see from Figures 11 and 12, dye emission and R1 reflection both peak at 389nm. Thus, sufficient gain exists at this wavelength when a reflective element is introduced that lasing is required to occur here. If a sufficiently poor reflector is used so as to overcome the 389nm lasing, its ability to produce bandwidth reduction becomes lost. Because of this situation,

Figure 18. Effect of intercavity reflector on overall reflectivity. Solid line, reflectivity of grating alone. Dotted line, reflectivity of grating-reflector combination.

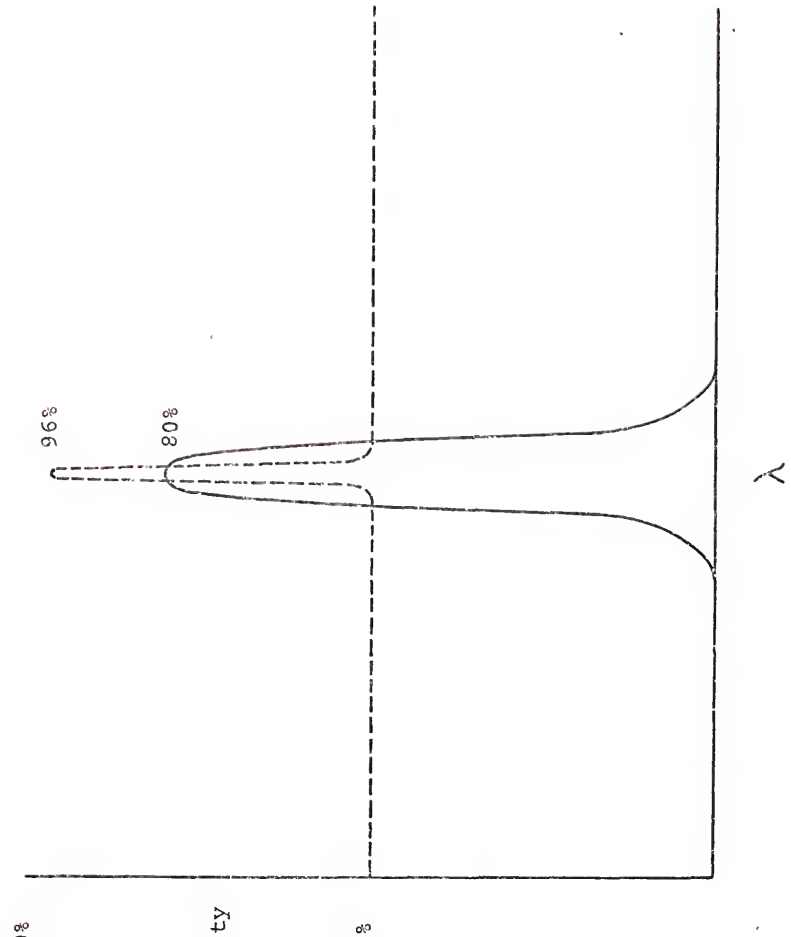
96%
80%
100%
reflectivity
50%
λ

further work was done without an intracavity reflector and with an output bandwidth of ∿2nm.

A simpler approach to bandwidth reduction was also attempted, but without success. It involved merely reducing the flow rate of the laser dye solution through the flashlamp with the rationale that if flow turbulence was at the root of the large bandwidth observed, this would diminish its effect. As noted, this approach was not fruitful, but it is mentioned here because it drew our attention to the repetition rate of the laser. At reduced flow rates it is found that 20 to 30 seconds must be allowed between laser firings for lasing to occur. The reason for this can be observed quite well when aligning the laser using the beamsplitter technique. As mentioned previously, in this technique the He-Ne beam which is reflected off the rear reflector (or grating) is observed on the ceiling or a far wall. This beam is normally very steady. However, when the laser is fired, turbulence in the dye cavity causes the beam to bounce about erratically for ten seconds or so before again becoming steady. If the laser is fired during the turbulent period, lasing will not occur. This is not surprising. However, we did find that even at the highest flow rates, this turbulence followed a laser firing for a period of several seconds. Thus, even though the laser flashlamp could be fired at a rate approaching 10pps, actual lasing could not be repeated at a rate exceeding 0.1pps. Other

investigators [74] have increased the maximum repetition rate for this system to about 1pps but only after considerable alteration and replacement of original equipment. Thus, our laser system is restricted to a very low repetition rate. Although not a crucial restriction in an opto-acoustic system, for experiments which suffer from a high background noise, it becomes difficult to markedly enhance the overall signal-to-noise by increasing the number of observations.

Having characterized the tunability, bandwidth and repetition rate of the laser system, the measurement of pulse energy was next approached. Preliminary measurements were attempted using a ballistic thermopile (Hadron Model 101) connected to a digital multimeter (Keithley Model 150). However, the thermopile was found too insensitive to the laser's output and the multimeter too sensitive to the electromagnetic interference produced by the laser during a flash to be of any use.

The next approach to measuring output pulse energy was by means of a chemical actinometer. This method has the advantages of being quite sensitive to light, totally insensitive to electrical interference and able to integrate a number of pulses to smooth out the observed pulse-to-pulse variation in output energy. This last feature is especially attractive for a multiple shot opto-acoustic experiment. Instead of having to monitor the energy in

each pulse, only a single measurement need be made at the experiment's conclusion to determine the average pulse energy delivered.

The chemical actinometer used is the potassium ferrioxalate system of Hatchard and Parker [75]. Specifically, a 5cm long quartz cell is filled with 14ml of a solution 0.006M in potassium ferrioxalate and 0.005M in sulfuric acid. It is then placed in front of the laser output reflector and the laser is fired a number of times. A 3x5 card held behind the absorption cell gives no indication of any light being transmitted. Equal portions of the exposed solution and an identical unexposed one are then each processed identically. The processing forms the highly absorbing 1,10-phenanthroline complex of the photogenerated ferrous ion.

Using the value of 1.11×10^4 1/mole-cm as the extinction coefficient of the iron-phenanthroline complex at 510nm, the energy per laser pulse can be computed from the formula

$$E = 377J \times \frac{OD}{N_s \times \lambda \times \phi_{\lambda}^{Fe^{+2}}} \qquad (22)$$

where OD is the optical density of the irradiated sample vs. the blank at 510nm in matched 1cm quartz cells, N_s is the number of laser shots absorbed by the actinometer, λ is the lasing wavelength in nanometers and $\phi_{\lambda}^{Fe^{+2}}$ in the quantum

yield of ferrous ion at λ in molecules/photon. With $N_s = 10$, $\lambda_{exc} = 386.4$nm and extrapolating $\phi^{Fe^{+2}}_{386.4nm}$ as 1.16 from reported yields at other wavelengths [76, p. 784], equation (22) reduced to E = 84.1mJ x A. Absorbances were read using a Cary 14 Recording Spectrophotometer (Applied Physics Corporation) fitted with a 0.2 full scale slide-wire permitting a resolution of 0.001 absorbance units. Three separate experiments were run and the absorbance of the exposed solution exceeded that of the blank by an average of only 0.001 absorbance units. This result indicates an average energy per pulse of only 80μJ, more than two orders of magnitude below that expected for dye No. 386 at this wavelength.

Because of the lack of precision available from the actinometer technique and the wide variance of the experimentally determined pulse energy from that expected, another approach was used to accurately determine pulse energy. A biplanar phototube (Model F4000, ITT Electro-Optical Products Division) especially designed for monitoring high intensity radiation was employed. With a rise time less than 5×10^{-10} seconds, the phototube is thus also suited for observing the temporal pulse width of the laser pulse. When monitoring laser pulses with the device, the beam is first passed through a 2.0 neutral density filter and then through a pass-band optical filter (see Figure 19) to reject scattered flashlamp radiation. The output of the phototube is

Figure 19. Absorption spectrum of pass-band optical filter used in laser pulse energy measurements.

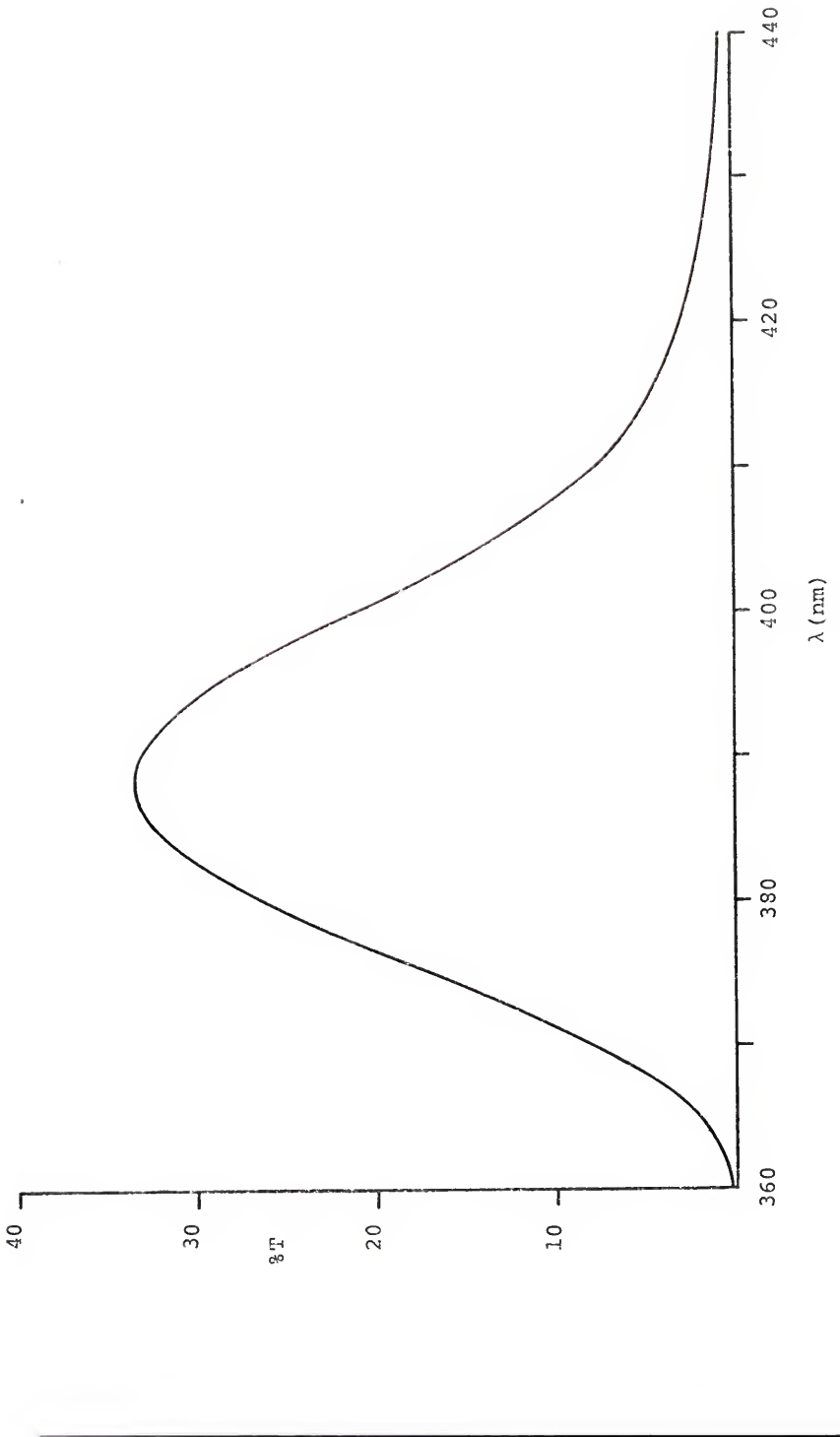
40
30
20
10
%T
360
380
400
420
440
λ (nm)

connected to an oscilloscope (Tetronix Model 535A) through a 50 ohm termination (actual resistance: 51.5Ω). The oscilloscope is triggered by the laser firing unit and the resultant sweep is photographed for analysis.

With the laser tuned to 386.4nm and adjusted for optimum output, a number of shots were made and recorded at a firing voltage of 20kV. A typical scope trace is reproduced in Figure 20. The occurrence of the laser pulse takes place approximately 500 nanoseconds after the sweep is triggered. The full width of the trace at half height is 100 nsec, however this value may be affected somewhat by the rise time (∿20 nsec) of the oscilloscope. There is considerable variation in peak amplitude from pulse to pulse, however, the majority of sweeps showed peaks in the range from 5 to 8 volts. The energy in a single pulse can be estimated as the product of peak power and full width at half-height. Correcting for filter losses and using the calibrated phototube sensitivity at the lasing wavelength, the pulse energy in the most energetic pulse observed can be calculated as

$$E = \left(\frac{15v.}{51.5\Omega}\right) \cdot 100ns \cdot 3.07 \times 10^{2} / (57.5\ mA/watt) = 125\mu J.$$

This finding corroborates the actinometer results and would appear to place the upper limit of pulse energy obtainable from dye No. 386 at around 0.15mJ for our laser operating at 20 kV.

Table 4 summarizes the important parameters of our

Figure 20. Typical oscilloscope tracing of phototube signal resulting from laser pulse.

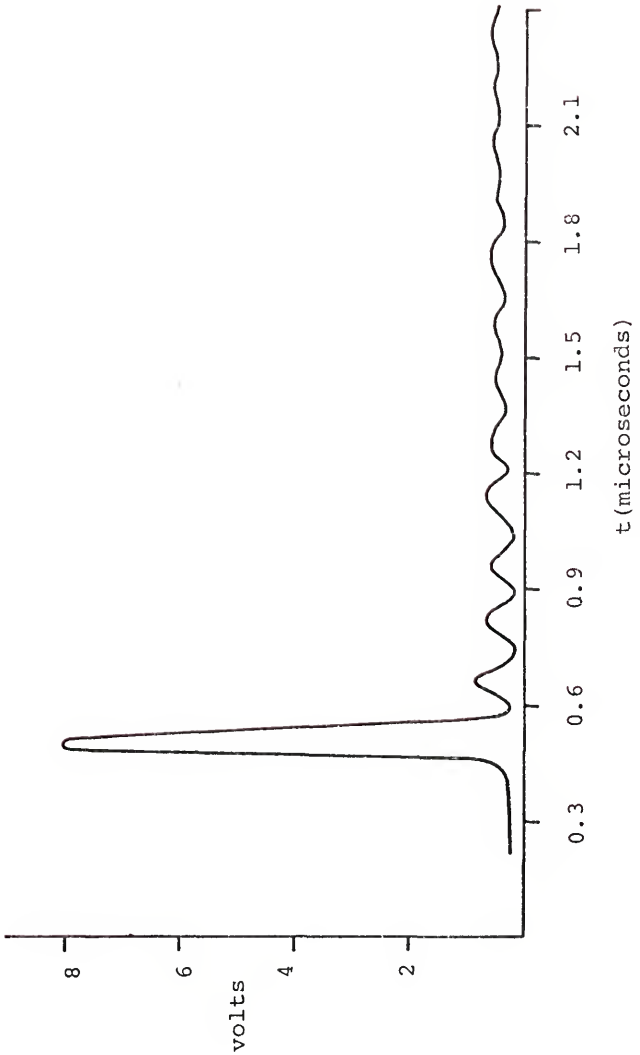
8
6
4
2
volts
0.3
0.6
0.9
1.2
1.5
1.8
2.1
t(microseconds)

Table 4. Characteristics of laser system using laser dye No. 386.

	Expected	Achieved
Pulse width	250 ns	100 ns
Repetition Rate	10 pps	0.1 pps
Tuning Range	375-401 nm	383-399 nm
Bandwidth	0.1-0.2 nm	1.5-2.0 nm
Pulse Energy	10-15 mJ	0.15 mJ

laser system, both expected and achieved, when dye No. 386 is used for lasing in the ultraviolet region. Two other ultraviolet lasing dyes, p-terphenyl (New England Nuclear) and p-quaterphenyl (Eastman Kodak laser grade) were also examined in our system with appropriate reflectors and grating settings, however no lasing could be achieved under a variety of conditions.

With p-terphenyl a dye concentration series was run to determine whether lasing might occur only for solutions within a certain concentration range. In particular, it was questioned whether the suggested lasing concentration of 10^{-3}M was too high. This is indicated when one considers the absorption depth of a 10^{-3}M p-terphenyl solution in dimethylformamide. From a spectrum of this solution, the molar extinction coefficient at the absorption peak (283.2nm) is found to be 3.3×10^{4} lit/mole-cm. In a 10^{-3}M solution, this means that 90% of the flash energy is absorbed in the first 0.3mm of the solution. Since the dye tube has a radius of 2.5mm, the central portion of the solution is hardly excited at all. For the concentration series, the concentration was varied in ten steps starting from 9×10^{-5}M and increasing up to 1.0×10^{-3}M. At the lowest concentration, almost 20% of the incident light has not been absorbed after passing through 2.5mm of solution. For each concentration of dye solution, the laser was aligned, and lasing was attempted but not observed.

Pressure Detection System

To satisfy the size and responsivity requirements imposed on the opto-acoustic pressure detector, a Pitran pressure sensitive transducer (series PT-L, Stow Laboratories, Inc.) was chosen [77]. Basically the device is a silicon NPN planar transistor that has its emitter-base junction mechanically coupled to a metal diaphragm. Displacement of this diaphragm causes stress-induced variation in the transistor's gain. In a suitable circuit, this change in gain causes a change in voltage output which is linearly proportional to the pressure differential across the device.

The unit is small; the diaphragm is only 3/16" in diameter. Yet it is sensitive. In its standard circuit (figure 21), it provides a linear 2 volt output over a 0.1 psi differential pressure range. This converts to a sensitivity of almost 400mV/torr. Pressure equivalent noise is usually less than 10^{-3} torr, and the device has a typical rise time of 10^{-5} seconds.

The device does show a considerable temperature coefficient; for a fixed bias voltage and zero pressure differential across the Pitran, the output voltage will vary with temperature up to 400mV/^{o}C for some models. This drift can be minimized by constructing a suitable temperature-compensation circuit. However, we have found that such a circuit causes a significant increase in noise at the output. In practice, since the temperature drift is of

Figure 21. Schematic of standard Pitran circuit.
All resistors are 10kΩ.

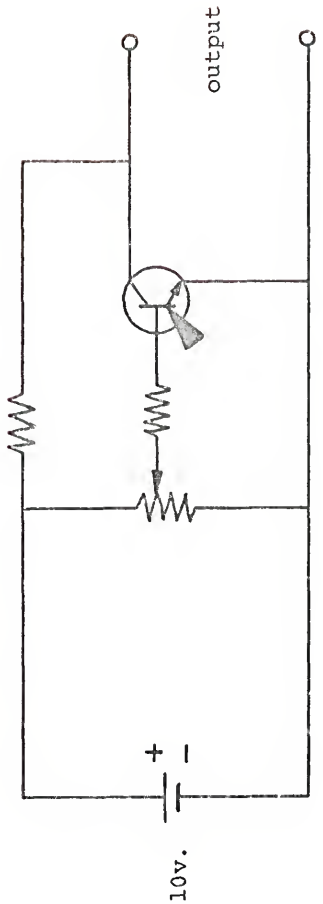
output
+
-
10v.

such low frequency, it is sufficient to monitor the zero-pressure output and adjust it manually just prior to a run. The actual data-gathering period of a pulsed opto-acoustic experiment is so short that temperature drift during this time is insignificant.

In mounting the Pitran in the opto-acoustic cell, precautions must be taken to avoid exerting mechanical strain on the device and at the same time properly shielding the electrical connections against electromagnetic interference. A cross-sectional view of the Pitran mounted in the opto-acoustic cell is given in Figure 22. Mounting begins by carefully applying a thin layer of soft-cure epoxy (Eccobond 45, Emerson and Cuming, Inc.) around the rim of the head of the Pitran. It is then set into a Teflon seat and the epoxy is room-temperature cured overnight. (The Teflon seat is used to electrically insulate the Pitran case (=collector) from the grounded cell.) The seat is then carefully attached to the Pitran holder by means of six small counter-sunk screws. An airtight connection is provided by a rubber gasket. A Teflon sleeve with four small diameter holes drilled parallel to its axis is now slid into the bottom of the Pitran holder. Three of the channels in the sleeve fit loosely over the Pitran leads, the fourth insures airflow to the reference (rear) side of the Pitran. With the sleeve in positon, three small set screws are now tightened to hold the sleeve in place. A

Figure 22. Cross-section of Pitran mounted on opto-acoustic cell.

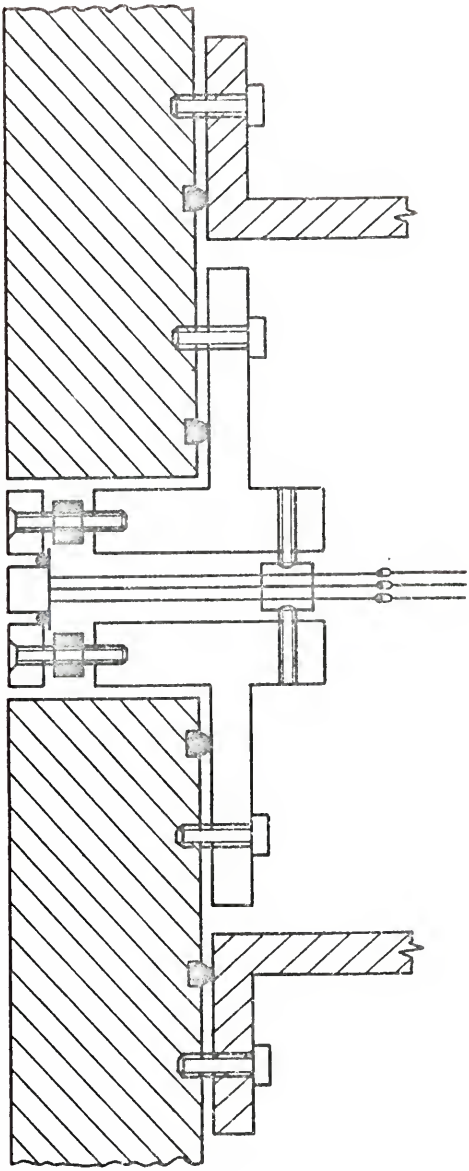

single drop of hard-cure epoxy (Shell Epon Resin 828) is then put into each of the three holes in the Teflon sleeve which encompass a Pitran head. After room-temperature curing, this epoxy helps to absorb any stress put on to the exposed Pitran leads and keeps it from transferring to the Pitran itself.

The Pitran holder is now mounted to the opto-acoustic cell with six screws, vacuum-tightness insured by the use of an "O"-ring. Socketed flexible wires are then slipped over the Pitran leads. These wires are permanently soldered to vacuum tight coaxial cable connectors (Amphenol, #82-843) mounted in the aluminum cup which can now be attached to the cell.

Coaxial BNC cables are used to connect the Pitran to its control electronics in order to minimize electromagnetic pickup. The control electronics for this device (basically the circuit of Figure 21) were purchased from Stow Laboratories (Model 850) and modified to minimize line and background noise. The output of this circuit is then fed into a second circuit, schematically shown in Figure 23. For biasing, the Pitran output is switched into a long time constant RC filter which presents a stable DC output level to be read with a voltmeter. The bias adjust potentiometer is used to set this level to 2.000 volts. During a run, the Pitran signal is switched into an AC amplifier with selectable voltage gains of 1, 2.5,

Figure 23. Block diagram of Pitran bias monitor and signal amplification circuit.

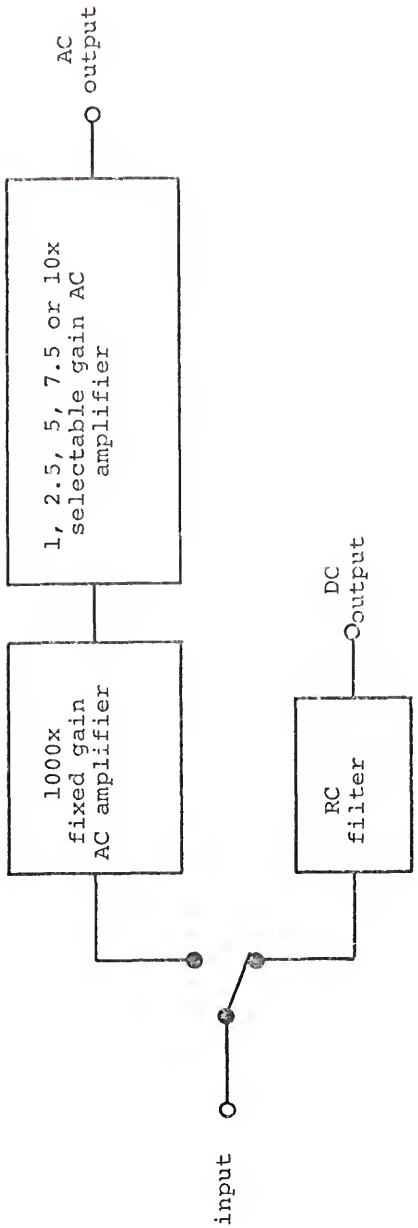
AC
output
1, 2.5, 5, 7.5 or 10x
selectable gain AC
amplifier
1000x
fixed gain
AC amplifier
DC
output
RC
filter
input

5, 7.5 or 10 thousand. This degree of amplification is necessary in order to provide the high level signal required by the data logging instruments.

The other pressure measuring device used in the opto-acoustic experiments is a capacitance manometer (Datametrics Barocel Model 1173 Electronic Manometer + Model 523-10 pressure sensor). As mentioned in a previous section, this instrument is used to measure static pressure differences between the experimental and reference cells. The manometer is capable of full scale measurement of pressures from 10 torr down to 10^{-3} torr, with an accuracy of 0.1% of reading + 2% of full scale. Such accurate measurement of static pressure can be of use in determining the presence and extent of any decomposition or photochemical reaction which changes the number of gaseous molecules in the experimental chamber relative to the reference chamber.

Pressure readings are taken directly from the analog panel meter on the manometer, or a digital voltmeter is used to monitor the high level analog output available at the rear of the manometer electronics. This output varies from 0 to 1 volt full scale and is linear with the panel meter reading. Because of these characteristics, it can also be used as input to the data logging equipment when a static or slowly varying pressure is to be monitored for a long period of time.

Data Gathering and Processing System

The instrument used to capture and accumulate the analog signals generated in the course of the opto-acoustic experiments is a CAT (Computer of Averaged Transients). This instrument consists of a Model CN-1024 Pulse Analyzer System (Technical Measurements Corporation) equipped with a Model 202 Logic Unit which provides signal averaging capability. The CAT has 1024 channels which it scans sequentially at the onset of a trigger pulse. Each channel accumulates data in the form of counts which are stored in a nonvolatile magnetic core memory which has a capacity of 17 binary bits (131, 071 counts) per channel.

As a repetitive waveform is generated for a number of times, at each occurrence it is sampled 1024 times and each sample is added to the appropriate channel in the CAT's memory. When sufficient signal is accumulated, scanning is stopped and the stored signal is divided by the number of sweeps N_s to obtain the average waveform. The benefit of this averaging procedure is that any random noise which was present in the original signal tends to cancel itself out. This leads to the signal-to-noise ratio in the averaged signal being greater than in a single signal by a factor of $N_s^{1/2}$.

The CAT provides for selection of the dwell time per channel, t_{dwell}, from one of the 16 values given by the expression

$$t_o \times 2^m \times 10^n$$

where both m and n range from 0 to 3 and t_o is the minimum dwell time. Using a Time-Mark Generator (Tetronix) t_o was determined as 30.61μsec, only 2% below its nominal value of 31.25μsec. During CAT operation as each channel is addressed, the current count must be transferred from memory to an arithmetic register in the CAT, then the contents of this register returned to memory before the cycle repeats for the next channel. Thus, a fixed portion of the dwell time, t_{dead}, is used for internal data manipulation so that the actual time for which a channel is active is slightly less than the dwell time.

During the active channel time, while the count is in the arithmetic register, pulses generated by a voltage controlled oscillator (VCO) in the logic unit are added to it. The frequency of the VCO is dependent in a linear fashion on the instantaneous input voltage. Thus, in the course of one sweep, a number of counts C is added to each channel which is directly related to the average voltage, $\bar{V}$, applied to the CAT input during the period for which the channel is active. This relationship can be expressed in a mathematical form as

$$C = (f_o + f_v \cdot \bar{V})(t_{dwell} - t_{dead}) \tag{23}$$

where f_o is the zero voltage frequency of the VCO and f_v is the change in VCO frequency per volt change in input signal.

To determine the values of the parameters f_o, f_v and t_{dead}, a pulse generator was used to provide 1 volt square wave input pulses as the CAT was synchronously triggered for a pre-determined number of sweeps. This was repeated for the ten shortest dwell times. After each set of sweeps the average channel reading for the low (0 volts) and high (1 volt) level of the square wave was determined. These data are plotted in Figure 24. A least squares fit of the data to equation (23) provide the following values: $t_{dead} = 13.3\mu sec$, $f_o = 3.42 \times 10^5$ sec^{-1} and $f_v = -5.79 \times 10^4$ $sec^{-1}v^{-1}$. The sign of f_v indicates that the signal is inverted as stored.

The input to the CAT is limited to $\pm$ 3 volts. It is advantageous to amplify the input signal so that its maximum peak-to-peak excursion covers this input range since conversion accuracy is fixed by the linearity of the VCO as $\pm$ 0.5% of full scale, or $\pm$ 15 millivolts. For very small dwell times, uncertainty is also introduced by the possible error of $\pm$ 1 count always present in digital counting schemes. This becomes clear when C is calculated from equation (23) for $t_{dwell} = t_o$. The average count per channel for zero voltage input is just under six counts. Conversely, an error of $\pm$ 1 count converts to an uncertainty of $\pm$ 1 volt. This latter source of inaccuracy is overcome by increasing the final count, either by increasing t_{dwell} or by running many sweeps. The number of

Figure 24. Plots of average channel counts versus channel dwell time for 0 volts (upper line) and 1 volt (lower line) inputs.

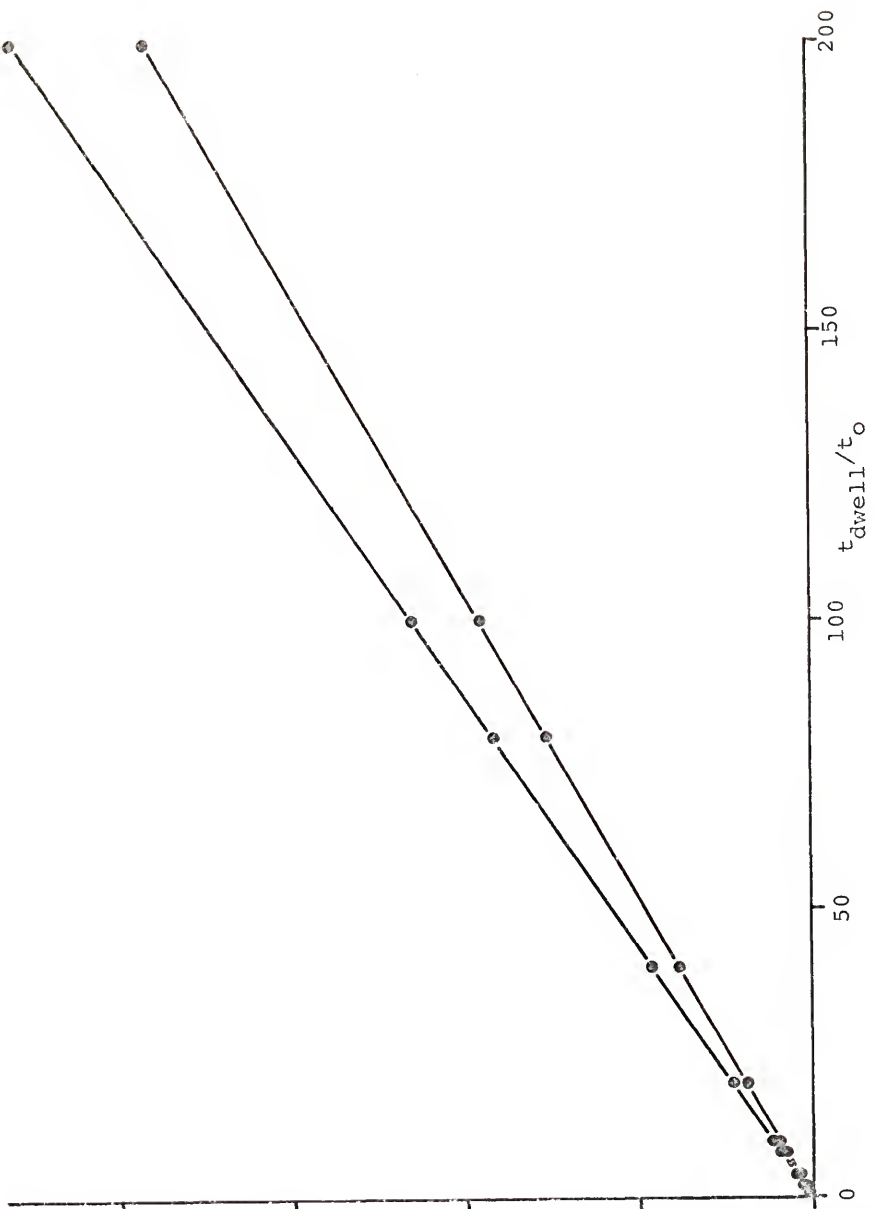
1800
1350
C/N$_s$
900
450
0
50
100
150
200
t_{dwell}/t_o

sweeps required to reduce the digital counting uncertainty to equal that of the converter is given by 1.15 msec/(t_{dwell} -t_{dead}), which for $t_{dwell} = t_o$ comes out to 67 sweeps.

Once the averaged signal is in the CAT, it must be transferred out to be processed. The Wang 700C Programmable Calculator which was used to generate the simulation plots was also available to process the CAT data and to control its plotting. The 700C is equipped with a Wang 705-1 Microface for remote data entry. However, the Microface accepts only TTL level, parallel binary-coded-decimal (BCD) data whereas the CAT output is either parallel binary (-12v level) or in the form of a pulse train (-20v level).

To interface the CAT output to the Microface, a device given the name of Picoface (from Practical Interface for CAT Output) was designed and built. The principle operations of the Microface-Picoface-CAT system during data readout are as follows. With the CAT manually set in the decimal readout mode, the programmable calculator instructs the Microface to initiate data transfer. The Microface unit sends out a pulse (execute command) through the Picoface to the CAT, signalling it to begin readout. The CAT responds by sending a pulse train into the Picoface where it is level shifted and counted by a series of one binary and five decimal counting units. The number of pulses in the train is equal to the count in the channel being interrogated; the address of this channel is indicated by a series of

light-emitting diodes on the front panel of the Picoface. As the pulse train ends, the CAT sends a signal (print command) back to the Microface through the Picoface signifying that counting is complete. After the Microface accepts the BCD count data, the counting units are automatically reset, the CAT is advanced to the next channel and the system is ready for another counting sequence. Data transferred in this fashion can now be digitally plotted, stored on magnetic tape or processed in a number of ways by the programmable calculator to extract pertinent information.

One additional element which should be considered in this section is a device called Diamux (for dual input analog multiplexer). This is a device which was designed and built to provide the capability of recording two simultaneous analog signals in the CAT. It would be useful, for example, for simultaneously recording the transient signals generated by both the Pitran and a photomultiplier tube. The Diamux does this by alternately gating two field-effect transitors which connect the two signals to the CAT input. By synchronizing this gating with the CAT channel advance, one signal is averaged in the 512 even-numbered channels and the other in the 512 odd-numbered channels. Though the signals are intermixed in this fashion, it is quite simple to program the calculator to process just one at a time. Thus both can be individually plotted, stored, etc.

Operating Procedure

A block diagram of all the elements involved in the pulsed opto-acoustic experiments discussed in this work is shown in Figure 25. The solid arrows connecting the blocks represent signal flow in the basic experimental setup. Dotted lines are used to show possible additional elements and alternate connections.

Before initiating an experiment, the following conditions must be satisfied. The sample vapor is present in the opto-acoustic cell at the desired pressure. The dye laser is aligned, its grating turned to the desired wavelength, its spark gap pressurized and its flash capacitor charged to the proper voltage. The Pitran is biased at 2.000v and is switched to the amplification circuit. The CAT is cleared and in the count mode. The oscilloscope is set to single-sweep and armed to accept a trigger pulse.

A single opto-acoustic experiment can now begin by manually firing pulse generator #1. This triggers both the CAT and pulse generator #2. This second generator delays firing for a set period to allow the CAT to establish a "baseline." When it does fire, it triggers both the dye laser and the oscilloscope. The latter is used to display the output of the photodiode monitoring the laser. The scope display can be photographed or its peak value can simply be observed and recorded. The pressure variation in the cell induced by the laser pulse is picked up by the Pitran, amplified and directed to the CAT where it is

Figure 25. Block diagram of elements involved in pulsed opto-acoustic experiments.

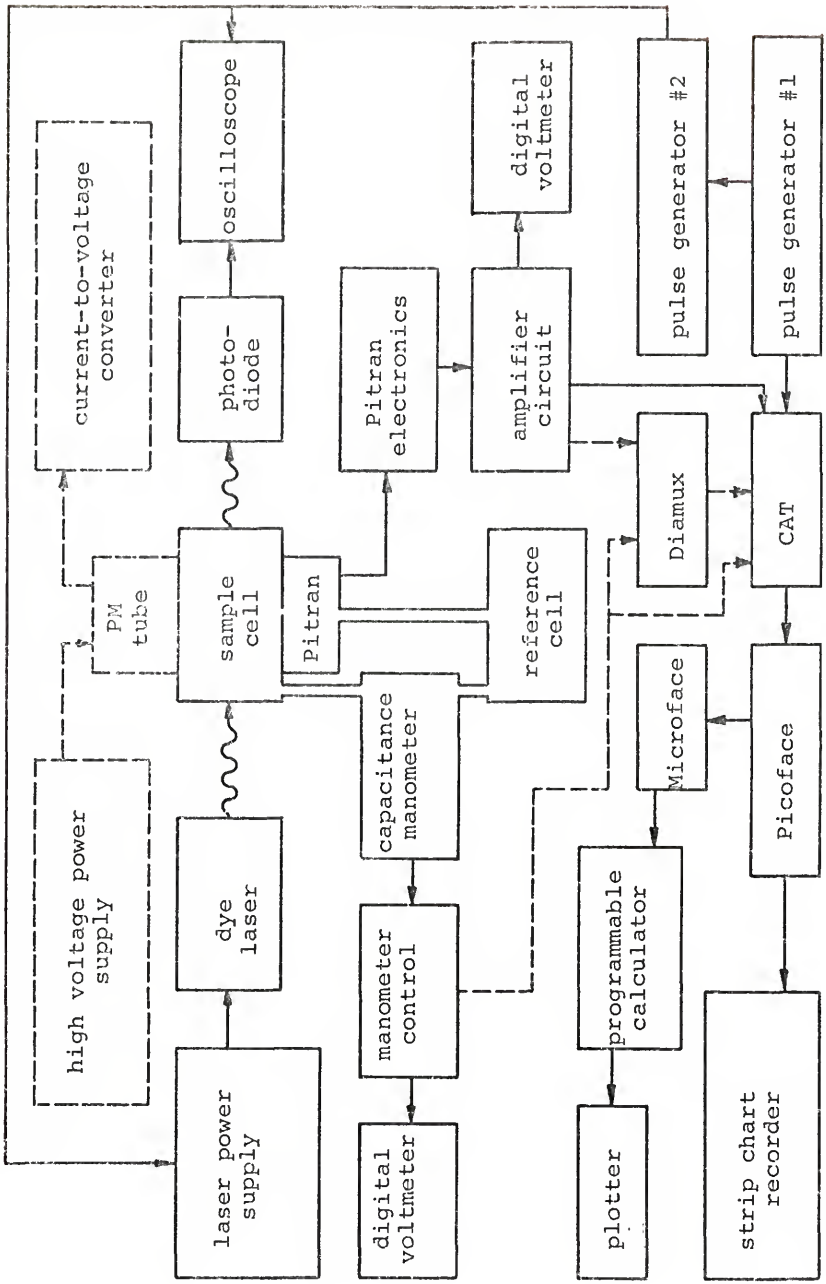
oscilloscope
current-to-voltage converter
photo-diode
Pitran electronics
digital voltmeter
amplifier circuit
pulse generator #2
pulse generator #1
high voltage power supply
PM tube
sample cell
Pitran
reference cell
Diamux
CAT
dye laser
capacitance manometer
Microface
Picoface
laser power supply
manometer control
programmable calculator
digital voltmeter
plotter
strip chart recorder

digitized and accumulated.

Before beginning another sequence, sufficient time must be allowed for the turbulence in the laser dye cavity to diminish. During this time the Pitran DC bias can be checked and re-adjusted if necessary. The run can then be repeated by re-arming the oscilloscope and again firing pulse generator #1. As long as there is no decomposition of the sample vapor, as would be indicated by a rise in the capacitance manometer reading with time, data accumulation can continue indefinitely. The practical restriction on the number of runs made is the number of shots of reasonably high pulse energy which the laser can deliver from a single dye solution.

CHAPTER FOUR
OBSERVATIONS

Flashlamp Experiments

Before the laser experiments were begun, a small xenon flashlamp apparatus in conjunction with an early version of the opto-acoustic cell was used to determine whether our pressure detection system was indeed sensitive enough to detect minute pressure signals. Acetone was used as the sample vapor because of its availability and high vapor pressure. With regards to signal strength, the high room temperature vapor concentration obtainable with acetone is offset by the very low extinction coefficient for acetone absorption ($\sim$14 lit mole^{-1}cm^{-1} at λ_{max} = 280 nm) [76,p. 377] and the small fraction of flashlamp radiation available in this wavelength region.

Experiments were run with 50 to 100 torr of acetone in the sample cell. The flashlamp radiation was passed through a filter before entering the cell to remove infrared radiation. The pressure variations were detected by the Pitran, amplified and either displayed on an oscilloscope or averaged in the CAT. The observed signals showed a very fast rise (<0.3 msec) independent of pressure followed by a slow return to the pre-flash level. The rate at which the signals decayed

varied inversely with pressure as expected. The averaged signal (25 flashes) shows a signal-to-noise of 1 for voltages corresponding to peak-to-peak pressure changes of 1 mtorr.

The "bumps" expected in the pressure signal due to the logitudinal acoustic wave are quite evident. They do not appear equally spaced as in Figures 6-8, because the version of the cell used does not have the Pitran mounted at the center of the cell. It is situated instead 3.8 cm from the front cell window and 8.9 cm from the rear. As the wave resonates in the cell, it thus takes a shorter time to pass the detector, reflect off the near window, and return than it does for the similar trip to the far window. Thus, the acoustic bumps appear grouped in pairs where the ratio of the time between the occurrence of two paired bumps and the time between successive pairs equals the ratios of the two trip distances [64].

With time, as the signal decreases, the bumps tend to broaden so that after several milliseconds the paired-bump structure is no longer present. At this point, the time between successive maxima in the signal is the round-trip travel time of the acoustic wave in the cell. For 100 torr of acetone this time is measured as 1.17 ms in the 5" cell. From this measurement the speed of sound in the vapor can be calculated as 2.17×10^4 cm/s. With this value γ can now be calculated from equation (19) as 1.10 which is in good agreement with reported data on acetone vapor [78].

Laser Experiments

Choice of Sample

In choosing a sample to which the pulsed opto-acoustic technique could be applied, several points had to be considered. Since the technique itself is new, it was felt that it should be applied to a molecular system about which there already existed a reasonable amount of knowledge. In this way results could be at least partially verified by previous data while opto-acoustic spectroscopy, by virtue of its unique approach, would certainly provide added insight. On the practical side, to be suitable a sample has to satisfy certain criteria with regard to vapor pressure, extinction coefficient and wavelength of absorption. Based on the latter many otherwise suitable samples were ruled out because their absorption bands lay outside the region accessible to our dye laser. This criterion grew even more restrictive as the narrowed lasing band of our laser became apparent. On the basis of the above criteria, two molecules were examined for suitability.

Pyridazine

Pyridazine belongs to a class of compounds, the diazines, whose excited state characteristics have been the object of numerous investigations [79]. Of the diazines, pyridazine alone has an allowed electronic transition which appeared to be excitable by the dye laser. The transition, which is actually to the second excited singlet state, is $n \rightarrow \pi^*$ in nature and has its origin at 375 nm [80]. The deactivation of this state is known to be dominated by

radiationless processes, so that it is an efficient "heat producer" [81]. The major question concerning pyridazine's suitability was its absorptivity.

A 5g sample of pyridazine (Aldrich Chemical Co.) was obtained and trap-to-trap distilled twice under vacuum using liquid nitrogen. It was then distilled a third time from potassium hydroxide pellets, as suggested by Cohen and Goodman [81]. The first two distillations removed some solid residue; the third removed an impurity which gave the sample its original reddish-orange color. The sample was then put through five freeze-pump-thaw cycles. The distilled and degassed sample is not colorless but is slightly yellowish. A gas chromatograph indicated the presence of only a single component in the sample.

A fraction of the sample was distilled into a 10cm gas absorption cell and its spectrum taken on the Cary 14 spectrophotometer using the 0.2 slidewire. The absorption was too small to be detected. For this reason, a selectable path length multipass gas cell (Beckman Instruments) was employed. A modified sample compartment was attached to the spectrophotometer which allowed the cell to be introduced into the sample beam from the side. Since the cell is intended for use in the infrared, it is fitted with KBr windows. These windows cause no problem, although the front surface mirrors in the cell do introduce some background absorption, evidently due to contamination. This absorption is structureless, however, and equivalent to a sloping

baseline. Figure 26 shows the absorption spectrum of pyridazine at its room temperature vapor pressure (subsequently measured as ∿0.3 torr) over a 4.6 m path. The small peak at 375nm corresponds to the origin of the $S_0 \rightarrow S_2$ transition. Other prominent peaks in the spectrum are also observed and their assignments [80] noted in the figure.

The strongest transition, the band at 357.5nm, has an optical density of at most 0.03. This corresponds to an absorptivity of 6.5×10^{-5} cm^{-1}. Even with a pulse energy of 10mJ, absorption into this "peak" would produce a maximum pressure rise of less than 1m torr. For this reason, pyridazine was ruled out as a prospect for experimentation.

Oxalyl chloride

Oxalyl chloride is also a member of a well-studied class of molecules, the α-dicarbonyls. Though not studied in nearly as much detail as some other members of the class, e.g. glyoxal, biacetyl, the absorption spectrum of oxalyl chloride has been reported and some things are known of its excited state behavior. In particular, both the $S_0 \rightarrow S_1$ [82] and $S_0 \rightarrow T_1$ [83] bands have been analyzed. Since oxalyl chloride has a relatively high vapor pressure at 25°C (89 torr), it was hoped that both the singlet and triplet absorption systems would be suitable for opto-acoustic study.

The singlet system has its origin at 368nm. The transition, though formally allowed ($^1A_g \rightarrow {}^1A_u$) is weak, as expected for an $n \rightarrow \pi^*$ transition. As also expected of a $n \rightarrow \pi^*$ transition, a progression in the carbonyl stretching mode

Figure 26. Absorption spectrum of pyridazine vapor over 4.6 m path, 320 to 400 nm.

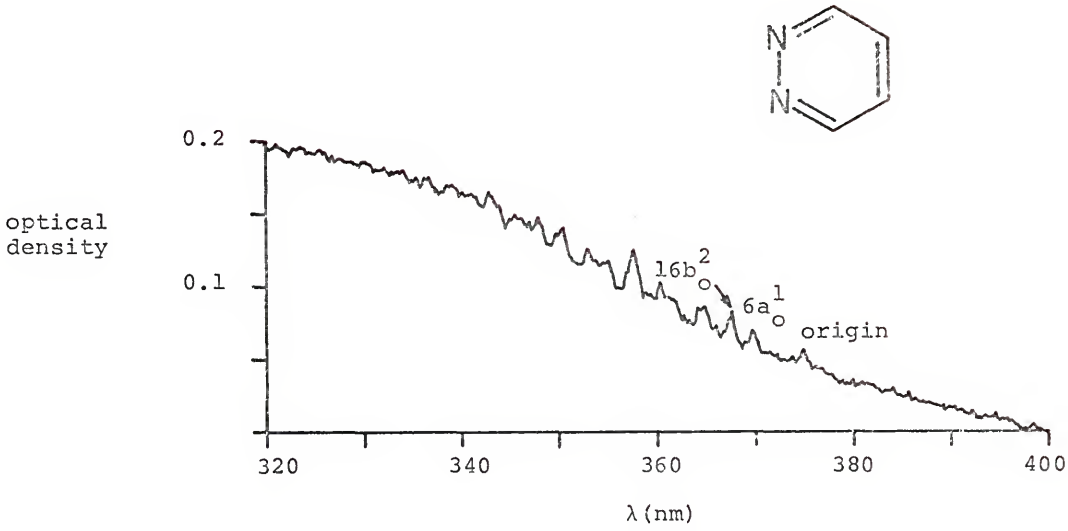
optical
density
0.2
0.1
16b^2_o
6a^1_o
origin
320
340
360
380
400
λ(nm)

($\sim$1450 cm^{-1}) is quite evident with each member of the progression acting as a pseudo-origin for other vibrational bands.

The origin of the triplet system is at 410nm. This transition too is $A_g \rightarrow A_u$ ($n \rightarrow \pi^*$), however, because it is spin-forbidden, it is considerably less intense than its singlet counterpart. The triplet system shows much vibrational structure and extends upward in energy to the onset of the singlet system. Triplet emission has been observed both in the crystal at 4.2K and in a cyclohexane matrix at 77K with lifetimes of 7.4 and 13 ms, respectively [84].

A 12.7g sample of oxalyl chloride (Aldrich Chemical Co.) was obtained. The sample was carefully transferred to a special sample container which was fitted with a Teflon stopcock due to oxalyl chloride's reportedly high reactivity towards stopcock greases [85]. Purification was accomplished via trap-to-trap distillation. After two such distillations the sample lost its original reddish-orange tint leaving behind a reddish residue. After degassing, the purified sample was stored in the dark.

To measure the absorptivity of the singlet vibronic bands, a room temperature spectrum was taken of oxalyl chloride vapor in a 10 cm gas cell. The spectrum is shown in Figure 27 from 310 to 390nm. The prominent bands are marked with the assignments of Balfour and King [82]. The diffuseness of the spectra at shorter wavelengths has previously been reported and tentatively ascribed to the presence of a higher-lying dissociative $^1A_u(n\pi^*)$ state. The proposed explanation for

Figure 27. Oxalyl chloride vapor absorption spectrum in 10 cm gas cell, 310 to 390 nm.

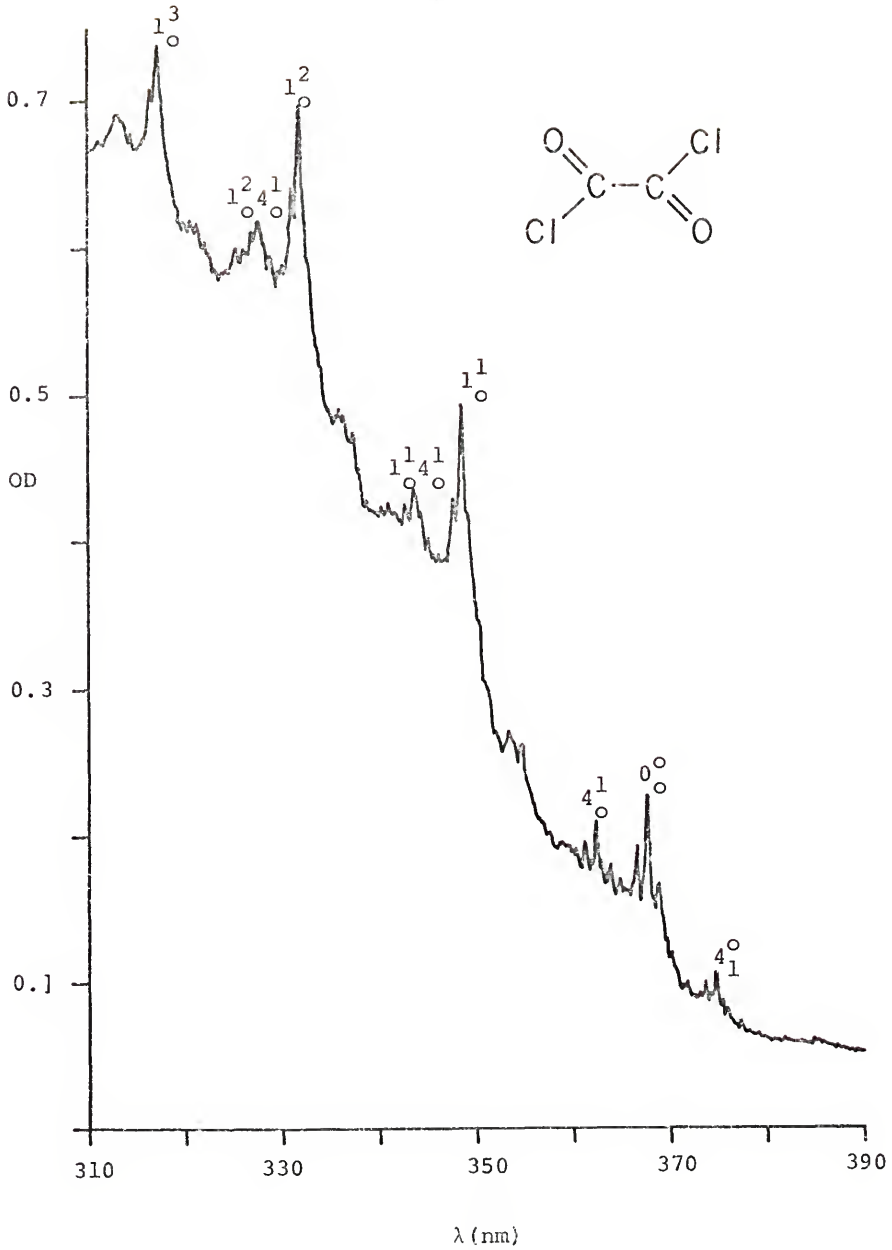
0.7
0.5
OD
0.3
0.1
310
330
350
370
390
λ (nm)
1^3_0
1^2_0
$1^2_0 4^1_0$
1^1_0
$1^1_0 4^1_0$
4^1_0
0^0_0
4^0_1
O
Cl
C
C
Cl
O

the continuum underlying the spectral peaks is absorption due to ·COCl radicals produced during exposure to light [86]. The absorptivity of the 0-0 transition at 368nm can be estimated from Figure 27 as 2.3×10^{-2} cm^{-1}. This transition is certainly sufficiently strong to be examined by the opto-acoustic approach, however because of the narrow tuning range of our laser, it is inaccessible. The same applies to the other bands of the singlet spectrum.

To examine the region of oxalyl chloride triplet absorption, the multipass cell was again utilized. This time, however, the KBr windows were replaced with quartz windows. A spectrum was taken of the evacuated cell from 360 to 420nm using the one meter path which showed a rather linear increase in absorbance over this range of about 0.1. The degassed sample was then allowed to enter the evacuated cell and come to equilibrium. The triplet spectrum oxalyl chloride vapor from 380 to 420nm is shown in Figure 28 for a 6.4 m absorption path. All the prominent peaks have been previously assigned [83].

Sample absorbance in the triplet region is sizable, but it cannot be read directly because of the cell mirror absorption. For this reason, all optical densities were measured with respect to the absorption at 420nm where oxalyl chloride is transparent. The absorbance of the $S_0 \rightarrow T_1$ origin band (410nm) was measured in this fashion for several path lengths and this data plotted in Figure 29. The plot is linear as expected from Beer's law and has a

Figure 28. Oxalyl chloride vapor absorption spectrum over 6.4 m path, 380 to 420 nm.

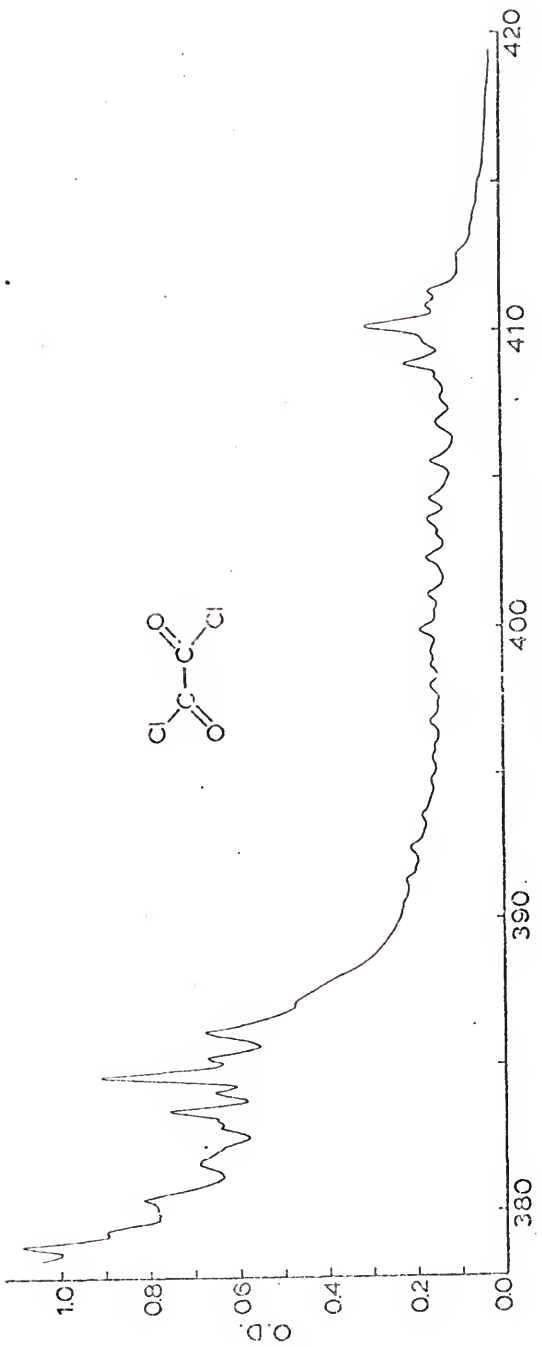
O.D.
1.0
0.8
0.6
0.4
0.2
0.0
380
390
400
410
420
WAVELENGTH(nm)
Cl
O
C
C
Cl
O

Figure 29. Plot of absorbance of the $S_o \rightarrow T_1$ origin band of oxalyl chloride vapor relative to the background absorbance at 420 nm versus path length.

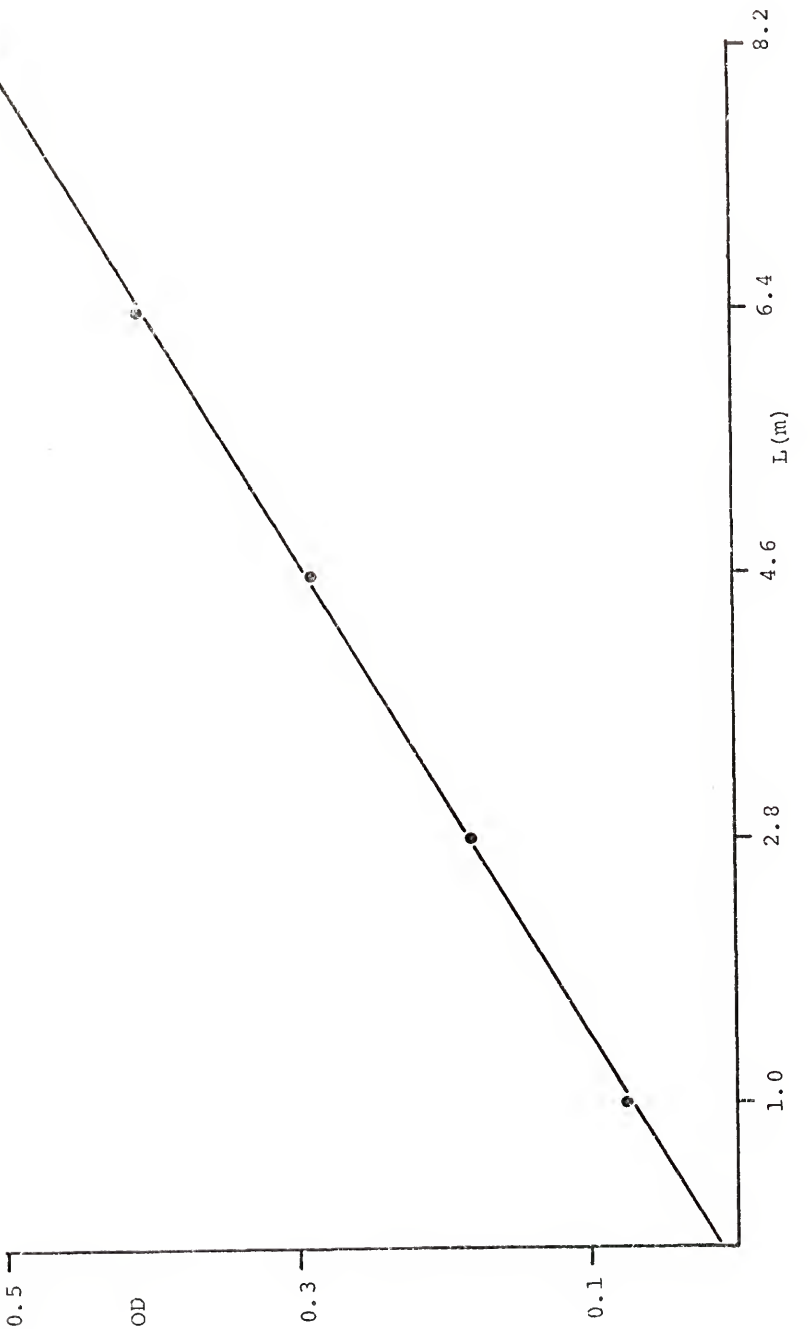
0.5
OD
0.3
0.1
1.0
2.8
4.6
L(m)
6.4
8.2

slope of 6.12×10^{-4} cm^{-1} which is the absorptivity of oxalyl chloride at 410nm. The intercept of this plot is not zero and apparently arises from the increased absorbance of the mirrors at the lower wavelength. Even accounting for this effect, the bands around 385nm are more intense than the origin band by a factor of two or three. One can calculate that in the experimental cell these bands will absorb approximately 5% of the incident radiation. Being positioned directly in the region where the dye laser is active, these bands appeared to make oxalyl chloride an excellent candidate for opto-acoustic examination.

Results

The experimental equipment was arranged as diagrammed in Figure 25. The Diamux unit was not used and the amplified Pitran output was connected to the CAT input. With the sample cell evacuated, the sequence of steps which would be followed in an actual run were carried out. It was found that the firing of the laser caused sufficient electromagnetic interference (EMI) to cause a "spike" to be inserted in the otherwise flat signal being sampled by the CAT. This artifact, though of significant magnitude, affected the input for only 0.1 ms or so and thus was a minor problem.

A second effect of the laser interference on the CAT was quite more troublesome and involved the read/write cycle of the signal averager. When this problem occurred, laser firing caused the CAT to either retrigger, i.e. immediately

begin a new sweep, or cease operation in mid-sweep. Several steps were taken to reduce this interference. A number of grounding schemes were used in an attempt to avoid ground loops. An aluminum box was built to house the laser and was grounded to hinder transmission of EMI. The CAT was moved to an adjacent room and connected to the other equipment solely by shielded cables which were fed through the common wall. All these approaches did not restrain the CAT from sporadically being affected by the laser firing.

One measure which did provide a definite improvement, though not a complete solution, was to insert a reed switch in the CAT's trigger line. Output from the second pulse generator was connected both to the reed coil and to one reed switch contact; the other contact led to the CAT trigger input. Approximately 3 ms after the first pulse generator is fired, the second delivers a 1 ms 7v positive pulse which serves the dual purpose of both closing the reed switch and triggering the CAT. Ten milliseconds later, the pulse from the first generator makes its positive transition and fires the laser. This sequence causes the trigger input of the CAT to be totally unconnected during laser firing and avoids any spurious signal being coupled to it.

Once the equipment appeared to be working as planned, a sample of oxalyl chloride was allowed into the cell. It was noted that whenever the valve separating the two chambers of the cell was closed, the pressure in the experimental

chamber would slowly begin to rise relative to that of the reference chamber at a rate far exceeding that of the leak rate of the cell. Since this pressure rise occurred in the dark and even when an hour was allowed for sample equilibration, it appeared that some form of thermal decomposition of the sample was taking place. To determine the nature of this reaction and the rate at which it was occurring, it was examined more closely. Approximately 1.5 torr of oxalyl chloride was allowed to enter the cell, valve (B)was closed, the reference chamber was evacuated and the variation of the pressure in the experimental chamber was followed using the capacitance manometer. A plot of pressure versus time is given in Figure 30. The straight line drawn at the bottom of the figure represents the pressure rise which occurs under similar circumstances in an evacuated cell due to the leak rate of the cell. One observes that (1) the pressure rise in the presence of oxalyl chloride is far greater than could be ascribed to a leak, (2) the rise is at first linear then asympototically approaches the final pressure and (3) the final pressure (attained after 137 minutes and marked by the arrow in the figure) is very close to twice the initial pressure.

The conclusion to be reached from these observations is that the oxalyl chloride undoubtedly decomposes in the aluminum cell to produce two moles of volatile product per mole of reactant. The shape of the pressure versus time plot is indicative of a surface reaction [87], showing at

Figure 30. Plot of pressure rise due to oxalyl chloride decomposition in experimental cell versus time.

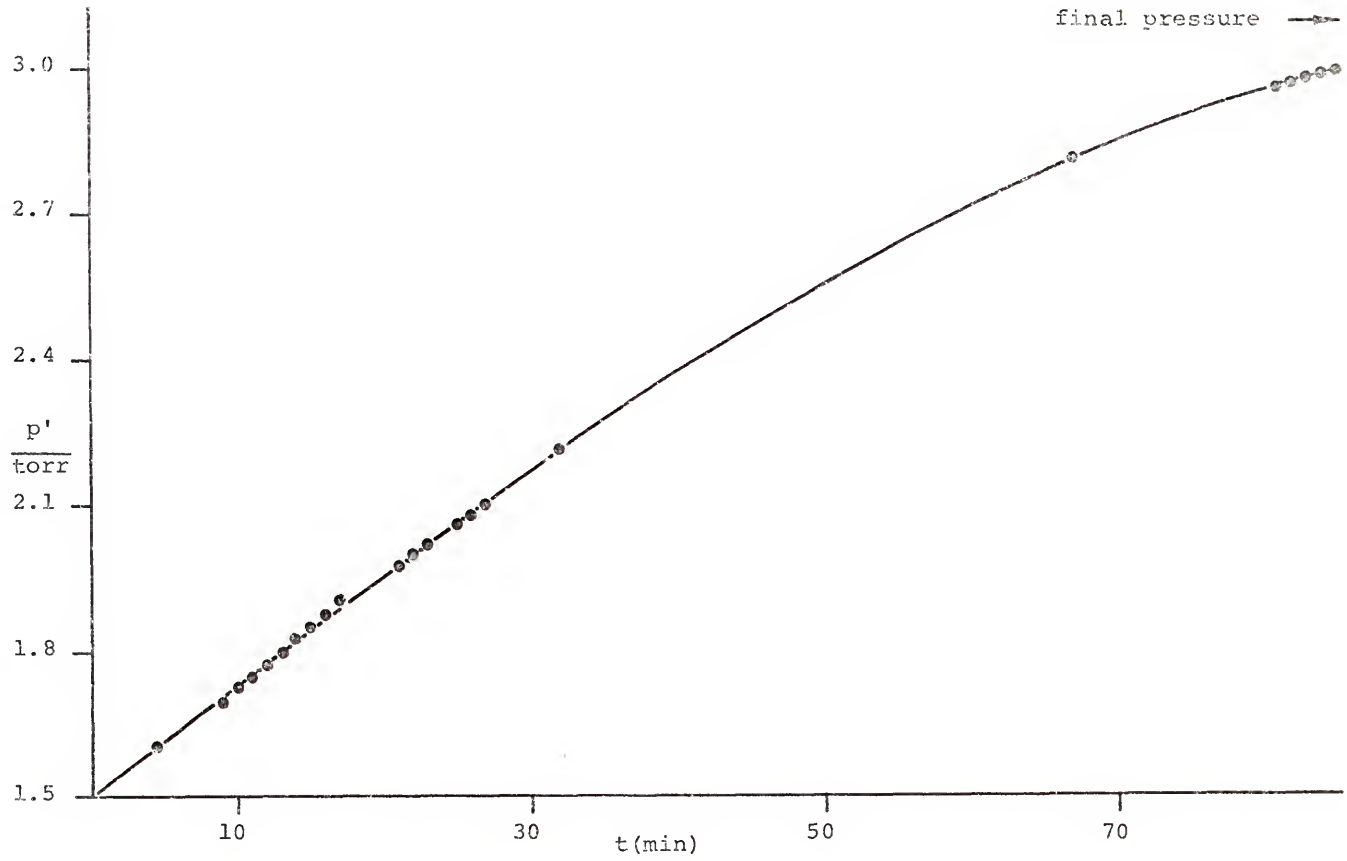
final pressure
3.0
2.7
2.4
p'
torr
2.1
1.8
1.5
10
30
50
70
t(min)

first zero-order, then first-order reaction. From the linear portion of the plot, a value of 22.3 mtorr/min is extracted for the rate of depletion of the oxalyl chloride.

After reaction, the product vapor is transferred to an infrared gas cell and its spectrum recorded on an infrared spectrophotometer (Perkin-Elmer, Model 237B). Only the absorption characteristic of carbon monoxide is observed. The thermal decomposition of oxalyl chloride has been studied [88] at elevated temperature. The decomposition is found to be predominantly decarbonylation with one molecule each of carbon monoxide and phosgene ($COCl_2$) being formed per molecule of oxalyl chloride. Evidently, in the aluminum cell the reaction proceeds further with the chlorines apparently being lost to the walls and a second molecule of carbon monoxide forming.

Before the means was available for measuring the laser output, several actual opto-acoustic experiments were performed using oxalyl chloride and exciting into the 386.4nm band. These were all done in the dark to avoid photochemical decomposition. Also, laser firing took place within minutes of the sample being introduced into the cell so little thermal decomposition could occur. In general, no response to the excitation could be obtained from the Pitran. However, the capacitance manometer when set to 10 mtorr full scale was found to produce a signal, the general form of which is shown in Figure 31. The shape of the signal was found to vary only slightly from run-to-run although

Figure 31. CAT-averaged capacitance manometer signal generated by laser firing.

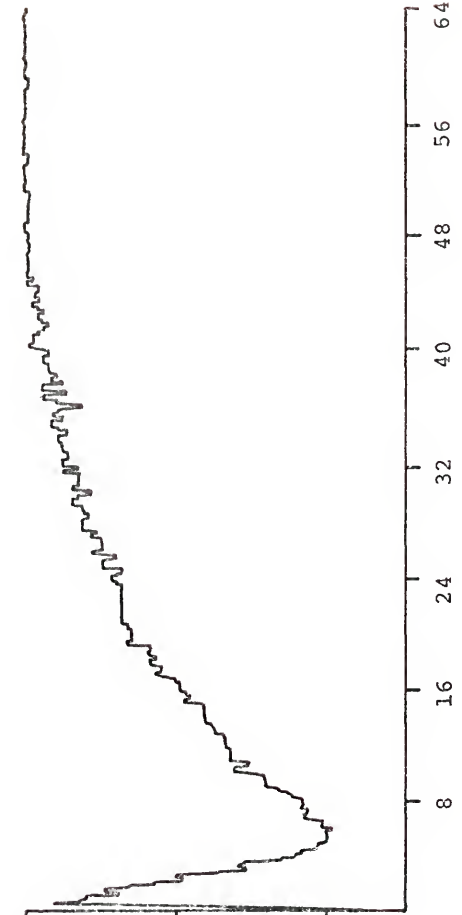
780
750
720
count
8
16
24
32
40
48
56
64
t(ms)

different initial pressures of oxalyl chloride were used. When data on laser pulse energy became available, it was realized that the signal was an artifact. It could be produced, it was found, even with the laser beam blocked as long as the manometer was on a sensitive scale. This check for an artifact signal had been run previously, but for that test the manometer had been set on its least sensitive (10 torr) scale.

CHAPTER FIVE
COMMENTS

In the previous chapters the ground work has been set for a useful new approach to the study of excited state rate processes. A theoretical foundation has been derived for pulsed opto-acoustic spectroscopy and the application of the technique to real molecular systems has been discussed. An experimental system was designed and assembled, and preliminary experiments run.

The failure of the attempted experiments to produce any new information on molecular excited states or, indeed, to even experimentally establish the feasibility of the time-resolved opto-acoustic technique is greatly disappointing. It would be more disappointing by far, however, if the usefulness of the technique described in this work was dismissed on the basis of the present results. Even a cursory analysis of the experimental facts makes it quite obvious that the experimental approach undertaken to observe the opto-acoustic signals failed because of the uniquely poor performance of the dye laser system, which fell far short of its expected capabilities in every critical area, although hundreds of man-days were spent attempting to improve its performance. The dozens of conversations held

with the manufacturer plus the visit by their representative to our laboratory were helpful, but the improvements they affected allowed us only to achieve the performance characteristics previously outlined in Table 4.

The most important failing of the laser was that insufficient optical energy was supplied to the experimental cell. Even if the most energetic laser pulse observed (150μJ) were completely converted to thermal energy in the cell, a pressure rise of only 5.6 mtorr would result. This would produce a signal not significantly above the overall single-shot noise. Of course, not all the impinging light is absorbed and converted to heat. The role of the sample is of central importance in heat generation. But, here too, laser performance played an important role since its narrow active band greatly limited the choice of sample.

Further work employing the present detection system will certainly require pulses significantly more energetic than 150μJ being delivered to the cell. Even with the present laser system, this has been achieved in the visible region (150mJ, Rhodamine 6G) [89]. So for these larger wavelengths, attaining sufficient pulse energies appears to be problem. However, at shorter wavelengths the laser dyes tend to be less efficient. For this region, one must either obtain one of the existing dye lasers which can provide the pulse energies required [90] or resort to frequency doubling of the laser output. This latter technique is somewhat inefficient, but with energetic pumping it could provide

ultraviolet pulses with energies several times the maximum observed in this work [91]. A final alternative would be to use a fixed frequency laser as the pump beam, but this would sacrifice wavelength tunability.

With regards to the pressure detector employed, although in our hands it did appear rather short-lived, it is hard to fault the Pitran on its performance. However, another type of detector has appeared which exhibits an order of magnitude greater sensitivity and significantly less output noise, though with a reduced frequency response [92]. This general type of detector is known as a capacitance microphone and consists of a thin layer of a pliable dielectric material sandwiched between two electrodes, one being typically a metal foil. Pressure variations across the dielectric cause it to deform and hence change the overall capacitance of the microphone. In a constant voltage system, the change in capacitance causes a current to flow which is detected by a low-noise, high-sensitivity charge amplifier. For the foil electret variety of condenser microphone, an external voltage source is not even required since polarization charges in the dielectric maintain a bias in the device [93].

The condenser microphones are not "point" detectors as is the Pitran, and because of this equation (17) does not accurately describe the surface-averaged signal they would produce. It is easy to show, however, that if a condenser microphone of length Δ is placed at the outer surface of a cylindrical cell with its center at L/2, the pressure

signal it "sees" is given by a modification of equation (17) with the term $\sin(m\pi\Delta/L)/(m\pi\Delta/L)$ introduced into the summation for $m>0$. This added factor tends to smooth out the acoustic bumps as Δ increases. An interesting result is with $\Delta=L$; no acoustic bumps should be observed, but rather just the gross pressure rise.

With improvements in laser performance and detector response, the application of pulsed opto-acoustic spectroscopy to the study of excited states can become a rather important technique. For the study of molecules which show either a very high or very low luminescence yield, the approach offers some unique advantages. A molecule with a very low level of luminescence is quite difficult to study by light emission. However, this molecule necessarily has a high radiationless yield so it is a good object of study for the opto-acoustic technique. For a molecule with a high level of luminescence, it is in general very difficult to determine radiationless yields accurately, since they are calculated indirectly from luminescence yields. Yet in some cases, evaluation of laser dyes for example, it is important to know these quantities accurately. In this case, opto-acoustic spectroscopy is a means of measuring this small quantity directly as opposed to estimating it as a difference of two larger quantities. Also, it possesses the capability of distinguishing between the different pathways of radiationless decay.

LIST OF REFERENCES

1. M. Gouterman, J. Chem. Phys. 36, 2846(1962).

2. G. W. Robinson, J. Chem. Phys. 47, 1967(1967).

3. S. Fischer, J. Chem. Phys. 53, 3195(1970).

4. C. Tric, J. Chem. Phys. 55, 4303(1971).

5. W. Siebrand, J. Chem. Phys. 54, 363(1971).

6. D. F. Heller, K. F. Freed and W. M. Gelbart, J. Chem. Phys. 56, 2309(1972).

7. A. Nitzan and J. Jortner, J. Chem. Phys. 56, 3360(1972).

8. S. H. Lin, J. Chem. Phys. 56, 2648(1972).

9. W. Siebrand, J. Chem. Phys. 50, 1040(1969).

10. S. H. Lin, Trans. Faraday Soc. 66, 1879(1970).

11. B. Sharf, J. Chem. Phys. 55, 320(1971).

12. A. Nitzan, J. Jortner and P. M. Rentzepis, Chem. Phys. Lett. 8, 445(1971).

13. D. F. Heller and K. F. Freed, Int. J. Quantum Chem., Symp. No. 6, 267(1972).

14. R. Englman and J. Jortner, Mol. Phys. 18, 145(1970).

15. S. H. Lin, J. Chem. Phys. 53, 3766(1970).

16. K. Takahashi and M. Yokota, Mol. Phys. 20, 663(1971).

17. G. R. Fleming, O. L. J. Gijzeman and S. H. Lin, Chem. Phys. Lett. 21, 527(1973).

18. J. O. Uy and E. C. Lim, Chem. Phys. Lett. 7, 306(1970).

19. U. Laor and P. K. Ludwig, J. Chem. Phys. 54, 1054(1971).

20. K. G. Spears and S. A. Rice, J. Chem. Phys. 55, 5561 (1971).

21. J. K. Burdett and M. Poliakoff, Chem. Soc. Rev. 3, 293 (1974).

22. C. Holzapfel, Rev. Sci. Instrum. 45, 894(1974).

23. G. A. Crosby, J. N. Demas and J. B. Callis, J. Res. Nat. Bur. Stand., Sect. A 76, 561(1972).

24. A. G. Bell, Proc. Am. Assoc. Advance. Sci. 29, 115 (1880) and J. Soc. Telegraph Eng. 9, 404(1880).

25. A. G. Bell, Philos. Mag. 11, 510(1881).

26. E. Mercadier, C. R. Acad. Sci. 91, 929(1880).

27. W. H. Preece, Proc. R. Soc. London 31, 506(1881).

28. W. H. Preece, A. G. Bell and J. Tyndall, J. Soc. Telegraph Eng. 9, 363(1880).

29. W. C. Röntgen, Ann. Phys. Chem. 12, 155(1881).

30. J. Tyndall, Proc. R. Soc. London 31, 307(1881).

31. M. L. Veingerov, Dokl. Akad. Nauk SSSR 19, 687(1938).

32. A. H. Pfund, Science 90, 326(1939).

33. K. F. Luft, Z. Tech. Phys. 24, 97(1943).

34. M. J. E. Golay, Rev. Sci. Instrum. 20, 816(1949).

35. V. N. Smith, Instruments 26, 421(1953).

36. W. D. Hershberger, E. T. Bush and G. W. Leck, RCA Rev. 7, 442(1946).

37. Y. I. Gerlovin, Opt. Spectrosc. 7, 352(1959).

38. S. P. Belov, A. V. Burenin, L. I. Gershtein, V. V. Korolikhin and A. F. Krupnov, Opt. Spectrosc. 35, 172(1973).

39. V. L. Rudin, Opt. Spectrosc. 24, 316(1968).

40. E. L. Kerr and J. G. Atwood, Appl. Opt. 7, 915(1968).

41. L. B. Kreuzer, N. D. Kenyon and C. K. N. Patel, Science 177, 347(1972).

42. L.-G. Rosengren, E. Max and S. T. Eng, J. Phys. E 7, 125(1974).

43. A. Rosencwaig, Science 181, 657(1973) and Opt. Commun. 7, 305(1973).

44. G. Gorelik, Dokl. Akad. Nauk SSSR 54, 779(1946).

45. P. V. Slobodskaya, Izvest. Akad. Nauk SSSR, Ser. Fiz. 12, 656(1948).

46. B. I. Stepanov and O. P. Girrin, J. Exp. Theor. Phys. 20, 947(1950).

47. For a review of this early work see R. Kaiser, Can J. Phys. 37, 1499(1959) and M. E. Delaney, Sci. Prog. (Oxford) 47, 459(1959).

48. W. R. Harshbarger and M. B. Robin, Acc. Chem. Res. 6, 329(1973).

49. E. Hey, Ph. D. Thesis, Univeristy of Heidelberg (1967).

50. P. G. Seybold, M. Gouterman and J. Callis, Photochem. Photobiol. 9, 229(1969).

51. J. B. Callis, M. Gouterman and J. D. S. Danielson, Rev. Sci. Instrum. 40, 1599(1969).

52. M. S. deGroot, C. A. Emeis, I. A. M. Hesselman, E. Drent and E. Farenhorst, Chem. Phys. Lett. 17, 332(1972) and Chem. Phys. Lett. 27, 17(1974).

53. W. R. Harshbarger and M. B. Robin, Chem. Phys. Lett. 21, 462(1973).

54. J. G. Parker and D. N. Ritke, J. Chem. Phys. 59, 3713 (1973).

55. J. G. Parker and D. N. Ritke, J. Chem. Phys. 61, 3408 (1974).

56. J. G. Parker, J. Chem. Phys. 62, 2235(1975).

57. K. Kaya, W. R. Harshbarger and M. B. Robin, J. Chem. Phys. 60, 4231(1974).

58. K. Kaya, C. L. Chatelain, M. B. Robin and N. A. Kuebler, J. Am. Chem. Soc. 97, 2153(1975).

59. T. F. Hunter, D. Rumbles and M. G. Stock, J. Chem. Soc.,Faraday Trans. 2 70, 1010(1974).

60. T. F. Hunter and M. G. Stock, J. Chem. Soc., Faraday Trans. 2 70, 1022(1974) and Chem. Phys. Lett. 22, 368(1973).

61. T. F. Hunter and M. G. Stock, J. Chem. Soc., Faraday Trans. 2 70, 1028(1974).

62. J. O. Hirschfelder, C. F. Curtiss and R. B. Bird,

"Molecular Theory of Gases and Liquids," John Wiley & Sons, Inc., N. Y. (1967).

63. P. R. Longaker and M. M. Litvak, J. Appl. Phys. 40, 4033(1969).

64. R. D. Bates, Jr., G. W. Flynn, J. T. Knudtson and A. M. Ronn, J. Chem. Phys. 53, 3621(1970).

65. T. Aoki and M. Katayama, Jpn. J. Appl. Phys. 10, 1303(1971).

66. D. R. Siebert, F. R. Grabiner and G. W. Flynn, J. Chem. Phys. 60, 1564(1974).

67. P. W. Berg and J. L. McGregor, "Elementary Partial Differential Equations," Holden-Day, Inc., San Francisco, 1966, p. 376, and J. B. Marion, "Classical Electromagnetic Radiation," Academic Press, New York, 1965, p. 86.

68. G. Shortley and D. Williams, "Elements of Physics," Prentice-Hall, Inc., New Jersey, 1965, p. 448.

69. R. D. Present, "Kinetic Theory of Gases," McGraw-Hill Book Company, Inc., New York, 1958, pp. 66-69.

70. J. G. Parker, Appl. Opt. 12, 2974(1973).

71. P. P. Sorokin, J. R. Lankard, V. L. Moruzzi and E. C. Hammond, J. Chem. Phys. 48, 4726(1968).

72. G. Büttenbender and G. Herzberg, Ann. Phys. 21, 577 (1934).

73. J. E. Bjorkholm, T. C. Damen and J. Shah, Opt. Commun. 4, 283(1971).

74. N. Carbone, Los Alamos Research Laboratory, private communication.

75. C. G. Hatchard and C. A. Parker, Proc. R. Soc. London, Ser. A 235, 518(1956).

76. J. G. Calvert and J. N. Pitts, Jr., "Photochemistry," John Wiley and Sons, Inc., New York, 1967.

77. D. J. Curran and S. J. Swarin, Anal. Chem. 43, 1338 (1971).

78. B. T. Collins, C. F. Coleman and T. DeVries, J. Am. Chem. Soc. 71, 2929(1949).

79. K. K. Innes, J. P. Byrne and I. G. Ross, J. Mol. Spectrosc. 22, 125(1967).

80. K. K. Innes, W. C. Tincher and E. F. Pearson, J. Mol. Spectrosc. 36, 114(1970).

81. B. J. Cohen and L. Goodman, J. Chem. Phys. 46, 713 (1967).

82. W. J. Balfour and G. W. King, J. Mol. Spectrosc. 26, 384(1968).

83. W. J. Balfour and G. W. King. J. Mol. Spectrosc. 27, 432(1968).

84. H. Shimada, R. Shimada and Y. Kanda, Spectrochim. Acta, Part A 23, 2821(1967).

85. K. B. Krauskopf and G. K. Rollefson, J. Am. Chem. Soc. 58, 443(1936).

86. B. D. Saksena and G. S. Jauhri, J. Chem. Phys. 36, 2233(1962).

87. K. J. Laidler, "Chemical Kinetics," McGraw-Hill Book Company, Inc., New York, 1965, pp. 267-8.

88. Z. G. Szabo, D. Kiraly and I. Bardi, Z. Phys. Chem. (Frankfurt am Main) 27, 127(1961).

89. J. Eyler, University of Florida, private communication.

90. Anon., Electro-Optical Systems Design 7(12), 25(1975).

91. F. M. Johnson and M. W. Swagel, Appl. Opt. 10, 1624 (1971).

92. L.-G. Rosengren, Appl. Opt. 14, 1960(1975).

93. G. M. Sessler and J. E. West, J. Acoust. Soc. Am. 40, 1433(1966).

BIOGRAPHICAL SKETCH

Joseph J. Wrobel was born March 18, 1947 in Chicago, Illinois. In 1968 he received a Bachelor of Science degree in Chemistry (cum laude) from Loyola University of Chicago and in the fall of that year entered the Graduate School of the University of Florida. In December, 1974, he accepted his current position as Research Physicist at the Eastman Kodak Research Laboratories in Rochester, New York.

Dr. Wrobel was married in September, 1970, and has one child. He was the recipient of a National Science Foundation Traineeship from 1968 to 1972 and a Graduate Council Fellowship for 1972-73. He is currently a member of the American Chemical Society.

I certify that I have read this study and that in my opinion it conforms to acceptable standards of scholarly presentation and is fully adequate, in scope and quality, as a dissertation for the degree of Doctor of Philosophy.

Martin T. Vala, Chairman
Associate Professor of Chemistry

I certify that I have read this study and that in my opinion it conforms to acceptable standards of scholarly presentation and is fully adequate, in scope and quality, as a dissertation for the degree of Doctor of Philosophy.

William Weltner, Jr.
Professor of Chemistry

I certify that I have read this study and that in my opinion it conforms to acceptable standards of scholarly presentation and is fully adequate, in scope and quality, as a dissertation for the degree of Doctor of Philosophy.

Gardiner H. Myers
Associate Professor of Chemistry

I certify that I have read this study and that in my opinion it conforms to acceptable standards of scholarly presentation and is fully adequate, in scope and quality, as a dissertation for the degree of Doctor of Philosophy.

Raymond Pepinsky

Raymond Pepinsky
Professor of Physics

I certify that I have read this study and that in my opinion it conforms to acceptable standards of scholarly presentation and is fully adequate, in scope and quality, as a dissertation for the degree of Doctor of Philosophy.

Mark L. Teply

Mark L. Teply
Associate Professor of
Mathematics

This dissertation was submitted to the Graduate Faculty of the Department of Chemistry in the College of Arts and Sciences and to the Graduate Council, and was accepted as partial fulfillment of the requirements for the degree of Doctor of Philosophy.

August, 1976

Dean, Graduate School

"What's that you're in again, Joe?"

"Chemical Physics, Ma."

"I've got to write that down."

1972

UNIVERSITY OF FLORIDA
3 1262 08553 3080